Effect of Fly Ash Particles on the Mechanical Properties and Microstructure of Aluminium Casting Alloy A535

A Thesis Submitted to the College of Graduate Studies and Research

in Partial Fulfilment of the Requirements for the Degree of

Master of Science

in the Department of Mechanical Engineering

University of Saskatchewan

Saskatoon, Saskatchewan

Canada

By

Emmanuel Gikunoo

PERMISSION TO USE

In presenting this thesis in partial fulfilment of the requirements for the Masters degree from the University of Saskatchewan, I agree that the Libraries of this University may make it freely available for inspection. I further agree that permission for copying of this thesis in any manner, in whole or in part, for scholarly purposes may be granted by the professor or professors who supervised my thesis work or, in their absence, by the Head of the Department or the Dean of the College in which my thesis work was done. It is understood that any copying or publication or use of this thesis or parts thereof for financial gain shall not be allowed without my written permission. It is also understood that due recognition shall be given to me and to the University of Saskatchewan in any scholarly use which may be made of any material in my thesis.

Requests for permission to copy or to make other use of material in this thesis in whole or part should be addressed to:

Head of the Department of Mechanical Engineering

57 Campus Drive

University of Saskatchewan

Saskatoon, Canada, S7N 5A9

ABSTRACT

Fly ash is a lightweight coal combustion by-product (CCB) separated from the exhaust gases of power generating plants using suspension-fired furnaces in which pulverized coal is used as the fuel. Its physical and chemical properties make it useful in construction and industrial materials, especially in cement manufacturing, concrete, liquid waste stabilization, and hydraulic mine backfill. The addition of fly ash into aluminium alloys has the potential to reduce the cost and density of aluminium castings while improving other physical and mechanical properties of the resulting metal matrix composites (MMCs).

This study investigated the effect of fly ash addition on the mechanical properties and microstructural behaviour of aluminium casting alloy A535. The unreinforced A535 alloy and its MMCs containing a mixture of 5 wt.% fly ash and 5 wt.% silicon carbide, 10 wt.% fly ash and 15 wt.% fly ash were investigated in the as-cast and solution heat treated conditions. Microhardness measurements, Charpy impact testing, tensile testing, optical microscopy, scanning electron microscopy (SEM), energy dispersive X-ray spectrometry (EDS), inductively coupled plasma/mass spectrometry (ICP/MS), X-ray diffractometry (XRD), and X-ray fluorescence spectroscopy (XRF) were used to evaluate these effects.

The results of this study show that increasing the fly ash content of the melt increased the porosity of the castings, which ultimately affected the density, tensile and impact properties of the MMCs. The density, microhardness, tensile strength and Charpy impact

energy of the composites decreased with increasing fly ash content. The decline in density of the MMCs was due to extensive porosity developed with fly ash addition. Depletion of solid solution strengthening magnesium in the matrix was the reason observed for the decline in hardness. The loss in Charpy impact energy and tensile properties of the MMCs are also attributed partly to the depletion of solid solution strengthening magnesium atoms from the matrix and partly to porosity.

Microstructural studies revealed non-uniform distribution of reinforcement particles in the composites. The fly ash particles were found to congregate at the boundaries of α-aluminium dendrites in the castings. Mg content of A535 alloy decreased with increasing weight fraction of fly ash. Mg was found to be tied up in a complex network of Mg_2Si thereby reducing its availability in the matrix for solid solution strengthening.

ACKNOWLEDGEMENT

I would like to express my sincere appreciation to my supervisor, Professor I. N. A. Oguocha, for his thoughtful insights, guidance and advice throughout this research. My appreciation goes to Dr. Jason Lo of CANMET, Ottawa, Ontario for the supply of test materials. Special thanks also go to the members of my supervisory committee, Prof. S. Yannacopoulos and Prof. R. Fotouhi, for their useful suggestions. Technical assistance provided by Mr. Dave Crone, Mr. Hans Steinmetz, Christopher James (Mechanical Engineering Department), Dr. O. Omotoso (CANMET Energy Technology Centre, Devon, Alberta), Mr. Tom Bonli (Geology Department) and Prof. R. O. Idem and his staff (Lauren Erickson and Robyn Fahlman) at University of Regina is gratefully acknowledged..

I am especially gratefully to my colleagues in the Materials Science Group whose contributions and encouragements have taken me this far. The informal support and encouragement of many friends has been indispensable. I cannot end without thanking my family, on whose constant encouragement and love I have relied on throughout my studies.

Financial assistance from the NSERC grant to my supervisor and scholarship from Mechanical Engineering are highly acknowledged.

TABLE OF CONTENTS

LIST OF TABLES

LIST OF FIGURES

NOMENCLATURE

Abbreviations

ρ_c	density of the composite
ρ_m	density of the unreinforced A535 alloy
ρ_r	density of fly ash
A535 hybrid	A535 alloy + 5 wt.% fly ash + 5 wt.% SiC
A535+10	A535 alloy + 10 wt.% fly ash
A535+15	A535 alloy + 15 wt.% fly ash
EDS	Energy dispersive X-ray spectrometry
EPMA	Electron probe microanalysis
FA	Raw fly ash used in fabricating the composite
FA-1	Raw fly ash used in fabricating the composite dissolved in Aqua Regia
FA-2	Fly ash particles recovered from A535+10
FA-3	Fly ash particles recovered from A535+15
Hybrid-1	SiC and fly ash particles recovered from A535 hybrid
ICP/MS	Inductively coupled plasma/mass spectrometry
ICP/OES	Inductively Coupled Plasma/Optical Emission Spectroscopy
SEM	Scanning electron microscopy
V_r	weight ratio of fly ash
VHN	Vickers Hardness Number
XRD	X-ray diffractometry
XRF	X-ray fluorescence spectroscopy

1. INTRODUCTION

1.1 Background

Metal Matrix composites (MMCs) are advanced engineered materials resulting from a combination of two or more materials (one of which is a metal) in which tailored properties are achieved. As current functional materials reach their performance limits, designers are looking to MMCs to provide the extra strength, stiffness, and higher temperature capabilities required for advanced applications. Compared with unreinforced metal alloys, MMCs generally offer the following advantages: higher specific strength and stiffness, weight reduction, better resistance to wear and impact damage, a lower thermal coefficient of expansion (CTEs), tailorable thermal conductivity, and better vibration damping [1,2]. Potential application areas for these types of materials include aerospace, defence, automotive, sporting goods, and marine.

In recent years, several research efforts have been directed at developing aluminium alloy MMCs [1-42]. Most conventional discontinuous aluminium alloy MMCs are expensive thereby limiting their utilization in the manufacture of many structural and non-structural components. As such, research is being intensified to produce inexpensive aluminium alloy MMCs with similar, or possibly better, engineering application bases. To achieve this goal, low-cost and low-density fly ash particulate reinforcements are

being investigated as replacements for the relatively more expensive reinforcements [3-20].

Fly ash is a lightweight coal combustion by-product (CCB) produced in upwards of five million tons annually in Canada. It is separated from the exhaust gases of coal-fired thermal power plants using electrostatic or mechanical precipitators and is generally finer than Portland cement, with a relative density that varies from 1.3 to 4.8 depending on the mineralogy of the coal burnt [43]. It consists mainly of small glassy spheres of varying sizes (ranging from less than 1 μm to more than 100 μm) [43-45]. The constituents of fly ash are based on the mineral content of the coals used. The major constituents are oxides and mixed metal oxides of silicon, aluminium, iron, and calcium thereby making them ceramic in nature.

The disposal of fly ash from coal-fired power stations causes significant economic and environmental problems [46]. A relatively small percent of fly ash is consumed worldwide. Although the utilization level varies from a minimum of 3% to a maximum of 57%, the world average only amounts to about 16% of the total ash [43]. Canada utilizes about 25% of its fly ash production in cement, concrete, mining applications and road construction [47] while the remaining amount is disposed off in landfills, ash dams and lagoons at a significant cost to the utility companies and their customers [43]. This unproductive use of land and lagoons and the associated long-term financial burden of maintenance and environmental pollution has led to the realization that alternative uses for fly ash as a value-added product beyond the aforementioned uses are needed.

The physical and chemical properties of fly ash make it a useful construction and industrial material, especially in cement manufacturing, concrete, liquid waste stabilization, and hydraulic mine backfill [43-45]. Utilization of fly ash in producing novel materials, waste management, recovery of metals and agriculture are the new areas that will expand the positive reuse of this abundant material, thereby helping to reduce the environmental and economic impacts of its disposal. Currently, research on the use of fly ash as a filler and reinforcement in both MMCs [3-20] and polymer matrix composites (PMCs) [48-54] has been growing. Prior studies show that fly ash can be used in forming inexpensive aluminium alloy MMCs with improved mechanical properties that can compete favourably with other available composites [3-20]. Using fly ash to reinforce aluminium alloy MMCs offers advantages of reducing disposal volumes for coal-powered utility plants [14]. This provides a high value-added use of fly ash in producing composites with improved material properties, such as wear resistance and low density, and at a reduced cost [15]. These composites can find useful applications in machine parts, sporting goods, electronic packaging, automotive and aerospace components. These will, as a result, help in reducing the discharge of greenhouse gases thereby fulfilling some of the key objectives of the Kyoto Protocol.

Aluminium casting alloy A535 is a non-heat treatable Al-Mg alloy with the highest combination of strength, shock resistance, ductility, and corrosion resistance than any other casting aluminium alloy. Its machinability is excellent and possible immediately following casting. It develops its strength through solid solution strengthening. The fairly high Mg content gives it protection from mild alkalis, salt spray, seawater and mild acids such as fruit juices. Due to its high corrosion resistance, castings produced

from A535 alloy do not require any further surface treatment for most applications. Its industrial application is very diverse. It is used for parts in instruments and computing devices where dimensional stability is of major importance. It is typically used in brackets and machine parts that need strength as well as impellers, optical equipment and similar applications requiring a high polish or anodized finish [55,56].

1.2 Research Objectives

The present study is motivated by the limited knowledge of and technology bases for fly ash-reinforced aluminium alloy MMCs. Non-uniformity in fly ash (e.g. particle size and chemical composition) is the major problem in fly ash-reinforced aluminium MMCs research. Processing for specific properties with variable particulates, compiling property database, and addressing machinability and recyclability issues need to be addressed.

Studies on A356.2, AK12, A360 and 443 fly ash-reinforced aluminium MMCs have shown great promise especially in automotive applications [3-20]. There is, therefore, a reasonable ground to carry out more research on other aluminium alloy series in order to improve our understanding of fly ash-reinforced aluminium MMCs.

The main objectives of this study were:

1. To determine the effect of fly ash addition on the mechanical and physical properties of A535 alloy.

2. To investigate the microstructural changes caused by fly ash addition in A535 alloy.
3. To complement the existing database and improve knowledge of fly ash-reinforced aluminium MMCs.

1.3 Thesis Outline

This thesis is divided into five chapters. Chapter 1 provides a general overview of current research efforts to produce inexpensive aluminium alloy MMCs with possibly better engineering application bases. Chapter 2 presents a comprehensive literature review on fly ash, its production, properties and uses. It also discusses aluminium alloys and fly ash-reinforced aluminium metal matrix composites (MMCs). Materials and experimental procedures are presented in Chapter 3. Chapter 4 discusses the experimental results obtained from this work. Chapter 5 summarizes the conclusions emanating from the results presented in Chapter 4 and offers recommendations for future work.

2. LITERATURE REVIEW

2.1 Fly Ash Sources

Fly ash is a lightweight coal combustion by-product (CCB) separated from the exhaust gases of coal-fired thermal power plants using electrostatic or mechanical precipitators. It is made up of very fine, predominantly spherical glassy particles. The major chemical constituents in fly ash are silica, alumina and oxides of iron and calcium. Because of its fineness, pozzolanic and sometimes self cementitious nature, fly ash is widely accepted and specified as mineral admixture in cement and concrete [43-45]. Fly ash has also been successfully used in many other applications in civil engineering construction and other specialty materials.

Coal, the material from which fly ash is derived, is used as fuel for about 40% to 50% of electric power generation all over the world [43]. Figure 2.1 shows a schematic diagram of fly ash production and collection system in modern thermal power plants. During the combustion of pulverized coal in suspension-fired furnaces of modern thermal power plants, the volatile matter is vaporized and the majority of the carbon is burned off. The mineral matter associated with the coal, such as clay, quartz and feldspar disintegrate to varying degrees. The slagged particles and unburned carbon are collected as either bottom ash, fly ash or economizer ash [57]. In the past three decades, flue gas desulphurisation equipment has been mandated to capture SO_x from the flue gases. The

flue gases along with the fly ash are treated using lime with majority of the fly ash collected with calcium sulphate powder [58].

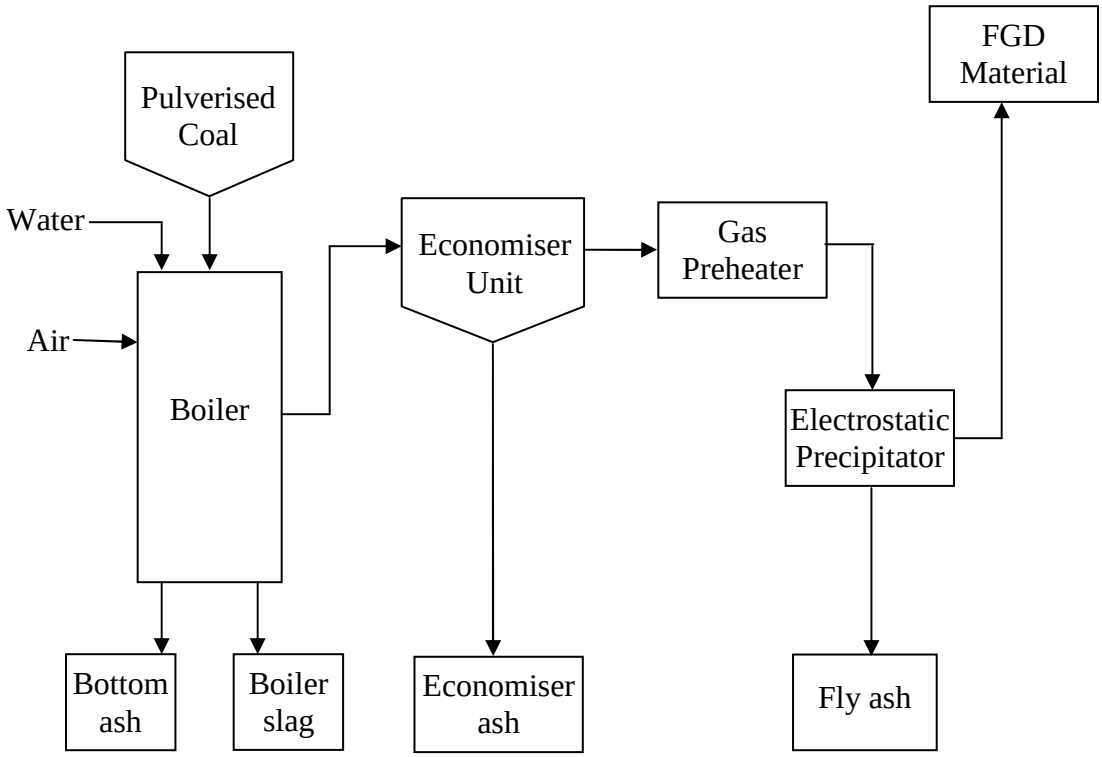

Figure 2.1. Flow diagram of a coal-fired thermal power plant showing its combustion by-products [58].

Coal combustion not only results in a residue consisting primarily of mineral matter in the coal, but also of organic matter, which is not fully burned. Different types of coal produce different quantities of ash, depending on the concentration of the inorganic mineral constituents in that type of coal [59]. Depending on the collection system, varying from mechanical to electrical precipitators, about 85% to 99.9% of the ash from the flue gases is retrieved in the form of fly ash. Fly ash accounts for 75% to 85% of the total coal ash and the remainder collected as dry bottom ash, wet bottom boiler slag, economizer ash and flue gas desulphurization (FGD). Because of its mineralogical

composition, fine particle size and amorphous character, fly ash is generally pozzolanic and in some cases also self-cementitious. Pozzolans are siliceous and aluminous materials, which in themselves possess little or no cementitious value but will, in finely divided form and in the presence of moisture, chemically react with calcium hydroxide at ordinary temperatures to form compounds possessing cementitious properties [60]. The bottom ashes are much coarser than fly ash and are therefore not pozzolanic. It is thus important to recognize that not all coal ash is fly ash and the fly ashes produced by different power plants are not equally pozzolanic. Therefore, not all coal ash is suitable for use as mineral admixture in concrete and other specialty materials [61]. The following categories of coal ash can be distinguished.

2.1.1 Fly Ash

It is the material separated from the exhaust gases of power plants with suspension-fired furnace in which pulverized coal is used as fuel. It is collected from the flue gases using electrostatic, mechanical precipitators or bag houses. Fly ash generated in coal burning power plants is an inherently variable material because of several factors. Among these are the type and mineralogical composition of the coal, degree of coal pulverisation, type of furnace and oxidation conditions including air-to-fuel ratio, and the manner in which fly ash is collected, handled and stored before use. Since no two plants may have all of these factors in common, fly ash from various power plants is likely to be different [62]. The fly ash properties may also vary within the same plant because of load conditions over a twenty-four hour period. Non-uniformity of fly ash is a serious disadvantage and sometimes the main hurdle in the effective and wide scale utilization of fly ash as an

additive in any large scale production [63]. The major components of fly ash reported in oxide form are silica (SiO_2), alumina (Al_2O_3), and oxides of calcium and iron (CaO and Fe_2O_3). Because of its fineness and mineralogy including amorphous nature, fly ash is generally pozzolanic and sometimes also self cementitious [58]. The density of fly ash depends on the proportion of its chemical constituents and on its porosity. Its density ranges between 1.3 g/cm^3 and 4.8 g/cm^3. The densities of some of the constituents of fly ash are shown in Table 2.1

2.1.2 Dry Bottom Ash

This is the residue from coal burned in dry bottom furnaces and is the product that falls through open grates. It generally consists of fused ash particles varying in size from 19 μm to 75 μm. Some of the aggregated fused particles can be easily crushed between fingers, others are hard to break and need mechanical equipment to pulverize further. Since many of the particles are spongy and porous, they are, therefore, susceptible to deterioration under loading and compaction. The specific gravity of bottom fly ash particles ranges between 2.08 and 2.73. The major chemical compounds present reported in oxide form are silica (SiO_2), hematite (Fe_2O_3) and alumina (Al_2O_3) in varying proportions depending upon the source of coal burned. It is not pozzolanic and mostly used as replacement of fine aggregate in concrete products and other civil engineering applications [64].

Table 2.1 Densities of some constituents of fly ash [64].

Constituent	Density
SiO_2	2.65
Al_2O_3	3.4 – 3.6
CaO	3.3 – 3.4
Fe_2O_3	5.3 – 5.4
$Al_6Si_2O_{13}$	2.8 – 3.0
Fe_3O_4	5.1 – 5.2
Coal	0.64 – 0.93

2.1.3 Wet Bottom Boiler Slag

This is the molten residue in a wet-bottom boiler discharged into water filled hopper. The particle size is smaller than that of dry bottom ash and the particles are glossy, very hard and brittle. Its colour is uniformly black and specific gravity lies in the range of 2.60 to 3.85 depending on the iron oxide (Fe_2O_3) content. The chemical composition of the wet bottom boiler slag is generally the same as that of the dry bottom ash, with the amount of ash depending on the source of coal. Like dry bottom ash, it is not pozzolanic and is generally used as replacement of fine aggregate in concrete products and other civil engineering applications [65].

2.1.4 Economizer Ash

It consists of coarse particles very similar to fly ash collected from the gases escaping from the boiler using electrostatic precipitators and hoppers below the economizer unit. It is much finer than the bottom ash as well as wet bottom boiler slag. The economizer ash is generally not suitable for use as a pozzolan and needs to be disposed of [65].

2.1.5 Flue Gas Desulphurization

It is the residue resulting from flue gas desulphurization (FGD), usually called waste gypsum. Limestone powder or slurry is used to capture SO_x from the flue gases. Fly ash may or may not be separated prior to desulphurization. The characteristics of desulphurization ashes depend on their sulphate, sulphite and lime content. The fixated FGD sludge has a great potential for use as construction material in combination with fly ash, lime and cement. Research is underway to develop use for FGD so that surface subsidence which is caused by abandoned deep coalmines is not only reduced but also, control the acid mine drainage [65].

2.2 World Production and Utilization of Fly Ash

In 2002, the Energy Information Administration indicated that the total coal production worldwide was 5.6 billion metric tons [66]. The major coal producing countries and their total productions in 2002 is shown in Figure 2.2. Canada's production of coal in that same year was 66.6 million metric tons with 61.9 million metric tons being consumed domestically [47]. Canada's production comes mainly from Alberta, British Columbia and Saskatchewan [47]. The two major uses for coal are in electricity generation and steel production. To date, these uses have continued to be at the heart of development by most countries seeking economic growth. About 60% of the world's coal production is consumed in the electric generation industry [46].

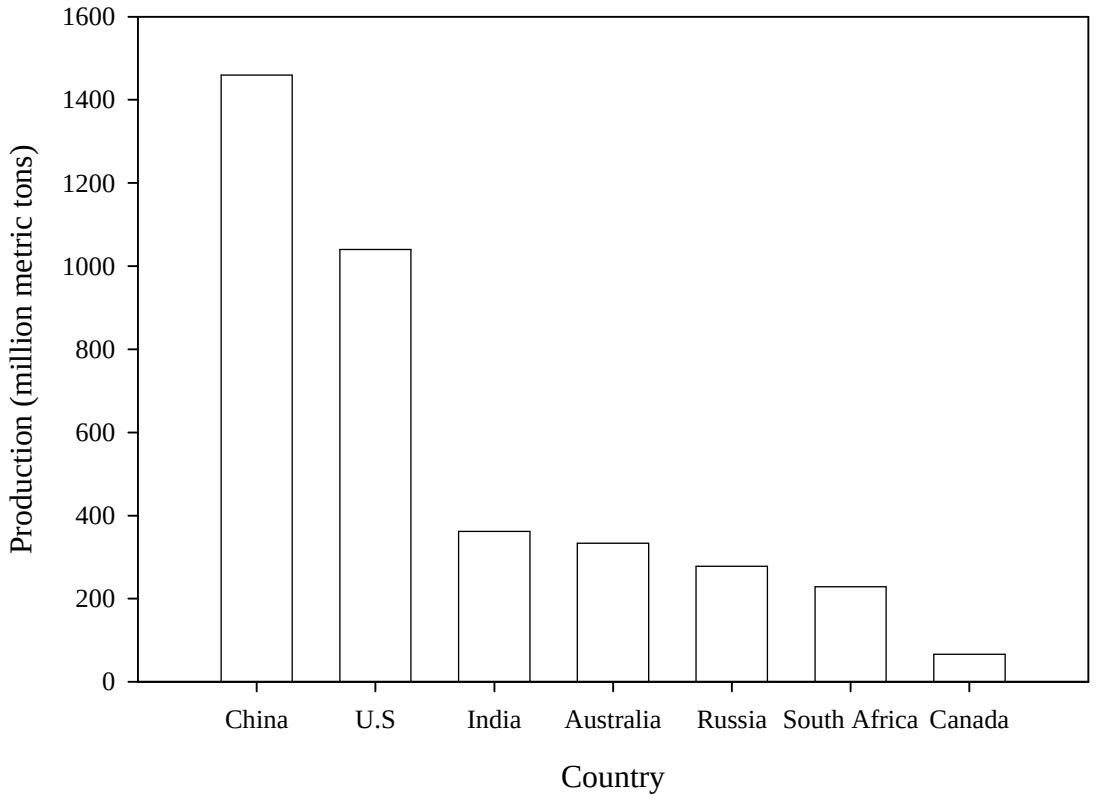

Figure 2.2. Major coal producing countries and their productions in 2002 [65].

Of the various industrial wastes, coal ash is perhaps the most abundant world over. In 2002, the world's CCBs production from coal was around 544.3 million metric tons, with fly ash constituting about 453.6 million metric tons [66]. Canada generated 7.1 million metric tons of CCBs that year out of which 4.7 million metric tons was fly ash [47]. Table 2.2 shows Canada's production and use of CCBs in 2002.

The best method of disposing a waste is to re-use it in one form or the other. Re-use of CCBs is therefore becoming an increasingly attractive alternative to disposal all over the world for the following reasons:

1. Costs and problems associated with the disposal in an environmentally sound manner are minimized or eliminated.

2. Less land area is required for disposal, thus enabling other uses of the land which also decreases permit requirements.
3. There may be financial returns from the fly ash sales, which may be used to at least offset the cost of processing.
4. Use of fly ash can replace some scarce or expensive natural resources such as aluminium.

Table 2.2. Canada's production and use of CCBs in 2002 in thousand tons [47].

Production	Fly Ash	Bottom Ash	FGD Gypsum*	Others	Total CCPs
Produced	4744	1886	354	133	7116
Disposed/Stored	3851	1664	-	133	5648
Removed from Disposal	10	3	-	-	13
USE (DOMESTIC)					
Cement	382	161	-	-	543
Concrete/grout	423	-	-	-	423
Mining applications	115	-	-	-	115
Roadbase/subbase	8	23	-	-	31
Wallboard	-	-	504	-	504
Others	90	52	-	-	142
Total use	1017	236	504	-	1757
Individual use percentage	21	13	142	-	n.a.
Cumulative use percentage	21	19	25	25	25

* Anomaly in the data obtained from Natural Resources of Canada shows that total use is greater than the annual production.

Though the utilization of fly ash on worldwide basis varies widely from a minimum of 3% to a maximum of 57%, the world average only amounts to about 16% of the total ash [43]. Canada utilizes about 25% of its fly ash production in cement, concrete, mining applications and road construction [47]. The remaining amount is disposed off in landfills and lagoons at a significant cost to the utility companies and thus to their consumers [43]. All those responsible for the disposal of and/or utilization of fly ash are

constantly seeking potential utilization options for fly ash. With the effective utilization of increased volumes of fly ash as construction material in civil engineering applications and as fillers in other specialty materials, the problems and costs associated with the ash disposal in an environmentally sound manner will be appreciably reduced or, in some cases, possibly eliminated.

Many of the uses of fly ash are directly related to its pozzolanic properties. Its utilization can be classified as follows [67-69]:

1. Structural fills in embankments, dams, dikes and levees, and as sub-base and base courses in roadway construction. This includes its use as raw material in cement production, as an admixture in blended cements and as replacement of cement or as a mineral admixture in concrete. It is also used for producing lightweight aggregates for concrete and many other applications.
2. They are employed in high value-added applications such as metal extractions. High value metal recovery of aluminium, gold, silver, vanadium and strontium fall in this category. Fly ash has potential use for producing lightweight refractory materials and exotic high temperature resistant tiles. It is also used as specialty refractory material as well as additives to forging in order to produce high strength alloys. Lightweight and high strength aluminium metal matrix composites (MMCs) prepared by blending fly ash with aluminium melt have been developed [3-20]. These composites are mainly employed in the automobile and aircraft industries.
3. Based upon its physical properties, fly ash is used as landfill for land reclamations for residential, commercial and recreational development projects.

It also finds use as filler material in asphalt, plastics, paints and rubber products. Fly ash has been successfully used in water treatment and as absorbent for oil and chemical spills.

2.3 Classification of Fly Ash

Fly ash, like volcanic ash a natural pozzolan, has been established and successfully used as a pozzolanic material in cement concrete and other related products for more than half a century. When fly ash is used in combination with Portland cement, calcium hydroxide liberated from the hydration of Portland cement reacts with the alumino-silicates present in the fly ash to form the cementitious calcium alumino-silicate hydrate compounds, which possess cohesive and adhesive properties [70]. Two categorizes of fly ash exist: Classes C and F. Table 2.3 shows the ASTM requirement for the chemical composition of Classes C and F fly ashes.

Class C fly ash is normally produced from the burning of lignite or sub-bituminous coal. They have both pozzolanic and varying degrees of self cementitious properties. Most Class C fly ashes contain more than 15 wt.% CaO but some may contain as little as 10 wt.% CaO. When mixed with water, these ashes hydrate almost in the same way as Portland cement does. The degree of self-hardening generally varies with the calcium oxide content of the fly ash. Higher CaO content generally denotes higher self-cementitious value. They have very little unburned carbon with loss on ignition (LOI) being less than 1 wt.%. The typical crystalline phases of these ashes are anhydrite

($CaSO_4$), tricalcium aluminate ($Ca_3Al_2O_6$), lime (CaO), quartz (SiO_2), periclase (MgO), mullite ($Al_6Si_2O_{13}$), merwinite ($Ca_3Mg(SiO_4)_2$)and ferrite ($(Mg,Fe)(Fe_3Al)_2O_4$) [71-73].

Class F fly ash is usually produced from burning anthracite or bituminous coal. Presently, no appreciable amount of anthracite coal is used for power generation. Therefore, essentially all Class F ashes used nowadays are derived from bituminous coal found in some of the eastern provinces of Canada and the midwestern and eastern states of the United States. This class of fly ashes with calcium oxide content less than 6 wt.%, designated as low calcium ashes, are not self-hardening but generally exhibit pozzolanic property. These ashes contain more than 2 wt.% unburned carbon determined by LOI test. Quartz (SiO_2), mullite ($Al_6Si_2O_{13}$) and hematite (Fe_2O_3) are the major crystalline phases identified in fly ashes derived from eastern bituminous coal. In the presence of water, the fly ash particles produced from a bituminous coal react with lime or calcium hydroxide to form cementing compounds similar to those generated by Class C fly ash [71-73].

Table 2.3. Chemical compositional requirements of Classes C and F fly ashes [71].

	Class	
	F	C
$SiO_2 + Al_2O_3 + Fe_2O_3$, min. wt.%	70.0	50.0
SO_3, max. wt.%	5.0	5.0
LOI, max. wt.%	6.0	6.0
Moisture content, max. wt.%	3.0	5.0

2.4 Characteristics of Fly Ash

The effective utilization or disposal of fly ashes requires adequate knowledge of their physical, chemical and mineralogical properties. Coal particles are burned at high temperatures (between 1400°C and 1800°C) in the furnace where volatile matter is vaporized and the carbon is burned off [43]. However, the inorganic matter in coal, present in the form of impurities, is converted into ash. Up to 95 wt.% of this mineral matter may be composed of clays, pyrite, quartz and calcite [43]. During combustion, these mineral particles undergo physical and chemical changes in the presence of excess air at high temperatures. As a result, several crystalline and glassy phases are formed. The pyrites (FeS_2) change to iron oxide, whereas the clay and mica particles slag and partially vitrify to form small glassy spheres composed of amorphous aluminosilicates. Calcination of calcite gives rise to oxide and hydroxide of calcium and carbon dioxide. Intermixed particles of clay and calcite and gaseous matter produce some calcium silicate ($CaSiO_3$), calcium aluminate ($CaAl_2O_4$) and calcium sulphate ($CaSO_4$). Other carbonates and some chlorides, if present in coal, undergo volatilization and sulphation to produce sulphates, carbon dioxide (CO_2) and hydrochloric acid (HCl). Quartz particles are rather unaffected and pass through the flame zone without much change in shape [74].

The thermally altered mineral matter produced from coal combustion in a furnace is quenched as it leaves the flame zone. Due to the quenching, spherical to rounded fly ash particles that result have glassy exterior surface. Some of the gases evolved during combustion are trapped in the fly ash particles, producing low specific gravity

cenospheres which float on water and are, therefore, also called floaters. The glass fraction in fly ashes usually varies between 70% and 89% depending on the type and coal source, degree of pulverisation, combustion conditions in the furnace, and the rate of cooling of the combustion residue [75].

Fly ash disposal and utilization methods also alter the ash characteristics and affect the properties of the materials in which the ash is used. Leachates from ash deposits, compacted fill and concrete may contain heavy metals such As, Pb, and Hg. Thus for utilization or disposal of fly ash, the characterization of fly ash for its physical properties, chemistry, microstructure including morphology, and mineralogy is essential [43].

2.4.1 Physical Properties

In the majority of studies conducted for classification and/or characterization of fly ashes, physical properties such as particle shape, size and distribution, fineness, specific gravity, and pozzolanic activity index are considered as the main parameters [76-88]. A brief description of the physical properties of fly ash is presented in this section.

2.4.1.1 Particle Morphology

Morphological studies on particle shape and surface characteristics of various types of fly ashes have been conducted using scanning electron microscope (SEM) [76-80]. Microscopic examination reveals that the inorganic portion of fly ash samples consist

predominantly of glassy spheres. Most of the carbon present is in the form of distinct, fused particles with an extensive macro porous structure, many appearing to be fragments or shells of swollen, nearly spherical or rectangular char particles. The inorganic rich particles, primarily fine particles, are generally distinguishable from the low-atomic-weight carbonaceous material. Significant amount of fully or little fused ash particles are generally seen on the residual carbon particles. The ash and carbon particles can easily be differentiated because the brightness in SEM images is related to the local atomic weight (heavy elements appear brighter) [79]. Figure 2.3 shows the typical micrograph of fly ash particles. The morphology of the fly ash particles is seen to depend on size. Smaller fly ash particles are more spherical in shape than the larger ones.

2.4.1.2 Fineness

Fineness is one of the primary physical characteristics of fly ash that relates to its pozzolanic activity [81]. ASTM C618 sets the limit for a maximum amount of fly ash retained on the 45 μm mesh sieve at 34% as quality control measure [89]. A large fraction of fly ash particles are smaller than 10 μm in size. Fineness of fly ash particles is also defined by specific surface area determined by the Blaine air permeability method or by nitrogen adsorption method. Joshi *et al.* [82] determined the physical properties of 14 Canadian fly ashes and their results shown in Table 2.4. For most Canadian fly ashes, surface area ranges from 0.17 m^2/g to 0.59 m^2/g. The large difference in specific surface area can be due to either grain size distribution, large amounts of spongy minerallic particles in fly ash, or a significant amount of porous carbon particles [83].

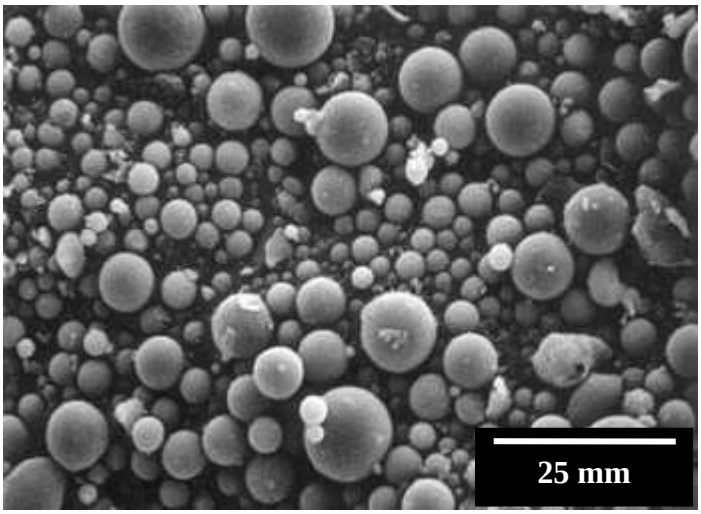

Figure 2.3. SEM micrograph of fly ash particles [75].

Table 2.4. Physical properties of typical Canadian fly ashes [82].

Coal Type	Source	Overall Apparent Specific Gravity	% Retained on 45 μm Sieve	Specific Surface Area (m^2/g)
Sub-bituminous	Alberta	2.19	32.0	0.42
Sub-bituminous	Alberta	1.92	26.0	0.46
Sub-bituminous	Alberta	1.91	22.0	0.43
Sub-bituminous	Alberta	2.03	9.8	0.59
Lignite	Saskatchewan	2.54	2.8	0.50
Sub-bituminous	Saskatchewan	2.15	20.4	0.22
Lignite	Saskatchewan	2.37	44.8	0.17
Lignite	Saskatchewan	2.39	26.6	0.22
Bituminous	Ontario	2.46	24.0	0.28
Bituminous	Ontario	2.31	27.0	0.25
Bituminous	New Brunswick	2.94	21.4	0.31
Bituminous	New Brunswick	2.87	26.4	0.18
Bituminous	Nova Scotia	2.53	28.2	0.36
Sub-bituminous	Nova Scotia	2.44	34.4	0.38

Several studies suggest that in addition to particle size, gradation is an important performance parameter, which can be related to the reactivity of different fly ashes [82-88]. Gradation is the separation of the particles into different size fractions by means of sieve analysis. A large percentage of fly ash particles larger than the 45 μm have been

reported to have a negative effect on the 28 day and 90 day strengths of normally cured Portland cement-fly ash mortars. At the same time, a large percentage of particles less than 10 μm had a positive influence on mortar strengths [82].

2.4.1.3 Specific Gravity

The specific gravity of fly ash is reported to be related to its shape, colour as well as chemical composition of fly ash particle. In general, specific gravity of fly ash may vary from 1.3 to 4.8 [43]. The Canadian fly ashes have specific gravity ranging from 1.91 to 2.94, as can be seen from Table 2.4. Fly ash particles with some minerallic impurities have specific gravity between 1.3 and 1.6. Opaque spherical magnetite and hematite particles, light brown to black in colour, when present in sufficient quantity in fly ash increase the specific gravity to about 3.6 to 4.8. As the amount of quartz and mullite increases, the specific gravity decreases. Fly ash pulverisation also releases some of the gases trapped during quenching inside the large hollow spherical particles and increases the bulk specific gravity of the fly ash [88].

2.4.1.4 Pozzolanic Activity

Fly ash particles are produced almost in the same way as ash is produced from a volcano. Both types of ashes fall under the same group of finely divided admixtures as per American Concrete Institute (ACI) committee 212 and exhibit pozzolanic activity [90]. All commercial fly ashes react with calcium hydroxide in the presence of water to produce highly cementitious water insoluble products. This property of the ashes is

known as pozzolanic activity. The pozzolanic activity depends on many parameters, most important of which are fineness, amorphous matter, chemical and mineralogical composition and the unburned carbon content or LOI of the fly ash. Several investigators [80-87] have reported that when fly ash is pulverized to increase fineness, its pozzolanic activity increases significantly. However, the effect of increase in specific surface beyond 0.6 m^2/g is reported to be insignificant [83].

Chemical composition of fly ash does not reflect the form in which various compounds are present. Yet the two governing parameters indicative of the reactivity are its calcium oxide and carbon content. The carbon content is generally determined by the standard LOI test. Carbon also acts as diluent of the active pozzolanic matter in the fly ash and contributes to size fractions larger than 45 mm. Because of the undesirable effect of carbon on the pozzolanic activity, different organisations specifying the use of fly ash as pozzolan limit the LOI in fly ash from 3 to 6%. The effect of iron oxide on the pozzolanic activity of fly ash is not that significant when high amount of silica is present [89].

2.4.2 Chemical Properties

Chemical constituents of fly ash reported in terms of oxides include silica (SiO_2), alumina (Al_2O_3), and oxides of calcium (CaO), iron (Fe_2O_3), magnesium (MgO), titanium (TiO_2), sulphur (SO_3), sodium (Na_2O) and potassium (K_2O). Unburned carbon is another major constituent in all the ashes. For fly ash to act as a pozzolan, it is necessary to have chemical constituents (e.g. SiO_2 and Al_2O_3) capable of reacting with

lime in the presence of water. For Class F ashes, the ASTM C618 standard states that the sum of silica, alumina and iron oxide (SiO_2 + Al_2O_3 + Fe_2O_3), must be at least 70% whereas for Class C the required minimum is 50% [91]. The lower requirement for Class C fly ashes recognizes that considerable amount of CaO will be present in self-hardening cementitious materials and thus the percentage of the pozzolanic components may therefore be lower [91].

The range of various constituents in fly ashes from major producing countries is presented in Table 2.5. Fly ashes from sub-bituminous and lignite coals contain relatively large proportion of CaO and MgO. Such ashes are characterized as Class C ashes in ASTM C618. On the other hand, the ashes produced from bituminous coal are characterized as Class F. They are relatively rich in Fe_2O_3 and contain less than 5% calcium oxide [91]. Table 2.6 presents ranges of CaO content in some North American fly ashes derived from various classes of coal. Canadian fly ashes have CaO contents ranging from 0.76% to 20.05% compared to 1.10 to 30.53% in United States fly ashes [43].

2.4.3 Mineralogical Characteristics

Mineralogical analysis of fly ash is the X-ray diffraction (XRD) study of its crystalline and glassy phases. Different X-ray diffraction studies [82-86] indicate that fly ash mineralogy varies significantly, particularly in Class C fly ashes. Each fly ash is unique and may itself vary with time due to the differences in chemical composition and mineralogy of the coal source as well as due to the combustion conditions in the furnace.

Table 2.5. Average chemical composition (wt.%) of some fly ashes from leading producing countries [43].

Country		#	LOI	SiO_2	Al_2O_3	Fe_2O_3	CaO	MgO	SO_3	Na_2O	K_2O
Japan	Av.		0.73	57.96	25.86	4.31	3.98	1.58	0.34	1.49	2.15
	Max	12	1.23	63.27	28.35	5.90	6.74	2.09	0.81	2.36	3.15
	Min		0.06	53.41	22.88	2.82	1.04	1.00	0.02	0.88	1.73
USA	Av.		7.83	44.11	20.81	17.49	14.75	1.12	1.19	0.73	1.97
	Max	34	18.00	51.09	28.03	31.30	30.53	1.40	2.80	2.10	2.98
	Min		1.00	32.70	14.60	8.50	1.10	0.70	0.30	0.22	1.28
Canada	Av.		1.62	47.86	20.34	12.90	9.47	1.26	0.34	1.52	1.62
	Max	14	6.25	57.90	23.70	42.20	20.05	3.96	0.99	5.80	2.93
	Min		0.10	31.70	13.60	3.50	0.76	0.06	0.10	0.09	1.02
Great Britain	Av.		3.86	46.16	26.99	10.44	3.06	1.99	1.59	0.90	3.26
	Max	14	11.70	50.70	34.10	13.50	7.70	2.90	6.80	1.90	4.20
	Min		0.60	41.40	23.90	6.40	1.70	1.40	0.60	0.20	1.80
France	Av.		3.72	48.45	25.89	8.70	5.95	2.36	1.01	0.64	3.94
	Max	17	15.15	54.05	33.40	15.30	38.75	4.45	7.00	0.85	6.00
	Min		0.30	29.90	10.80	5.80	1.48	1.10	0.10	0.15	0.703
Germany	Av.		9.65	41.13	24.39	13.93	5.06	1.83	0.77	-	-
	Max	9	20.10	49.54	29.35	20.88	11.81	4.26	2.10	-	-
	Min		1.48	34.10	21.06	8.37	2.18	0.75	0.12	-	-

where # = number of samples

Table 2.6. Range of CaO content in North American fly ashes derived from various classes of coal [43].

Type of Coal	CaO content (wt.%) in fly ash
Eastern bituminous	1-6
Colorado bituminous	4-8
Utah and Alberta sub-bituminous	6-12
Texas lignite	7-12
Saskatchewan lignite	10-15
North Dakota lignite	18-25
Montana and Wyoming sub-bituminous	22-32

Fly ashes, generally, have 15 wt.% to 45 wt.% crystalline matter. The high calcium ashes, derived from sub-bituminous and lignite coals, contain larger amounts of crystalline matter ranging between 25% and 45%. The glassy particles in Class C fly

ashes seem to contain large amount of calcium, which also makes their surface highly strained. It is possibly for this reason that the Class C fly ashes are highly reactive [43].

Table 2.7 presents crystalline phases in North American fly ashes identified by a semi-qualitative X-ray powder diffraction analysis. These data indicate that Class F fly ash consists typically of the crystalline phases of quartz, mullite, hematite and magnetite in a matrix of alumino-silicate glass. Class C fly ashes, on the other hand, have a much more complex assemblage of crystalline phases that typically contain the four phases present in Class F ashes plus several other phases as given in Table 2.7. For Class C ashes, glass composition among the particles is more heterogeneous and ranges from calcium aluminate to sodium calcium alumino-silicate [92].

Ghosal *et al.* [85] reported that the surface of the fly ash particles are the most reactive portions due to the maximum influence of quenching on these surfaces. Also, as the fly ash particle size increases, the amount of crystalline silica (SiO_2) in the ash increases and the proportion of calcium containing compounds decreases. Therefore, large size particles are less reactive.

Mineralogical characterization is valuable in determining the crystalline phases that contain the major constituents of fly ash. However, fly ash mineralogy is mostly dependent on the type and composition of the source coal. It is generally believed that the pozzolanic activity of the fly ash is influenced by calcium in the glass, and not by the free calcium oxide or crystalline CaO [93]. The most variable phases identified in fly ash are anhydrite ($CaSO_4$), periclase (MgO), ferrite spinel or magnetite (Fe_3O_4), hematite

(Fe_2O_3), melinite ($Ca_2Al_3O_7$) and lime (CaO). Ferrite spinel refers to the ferromagnetic spinel phase in fly ash, which manifests the common tendency for solid substitution of Al, Mg and Ti for Fe [94]. Anhydrite and the non-oxides are largely controlled by the pyrite and clay content of the coal. It is reported [43] that melinite forms from crystallization of fly ash particles, which is dependent on the ash cooling rate in the furnace and flue, and thus could reflect variable furnace operating conditions.

Table 2.7. Mineralogical classification of crystalline phases in North American fly ashes [92].

Class	Constituents	
	Name	Nominal Composition
F	Hematite	Fe_2O_3
	Mullite	$Al_6Si_2O_{13}$
	Quartz	SiO_2
	Ferrite spinel	$(Mg,Fe)(Fe,Al)_2O_4$
C	Anhydrite	$CaSO_4$
	Alkali sulphate	$(Na,K)_2SO_4$
	Dicalcium silicate	Ca_2SiO_4
	Tricalcium aluminate	$Ca_3Al_2O_6$
	Hematite	Fe_2O_3
	Lime	CaO
	Melinite	$Ca_2(Mg,Al)(Al,Si)_2O_7$
	Mullite	$Al_6Si_2O_{13}$
	Merwinite	$Ca_3Mg(SiO_4)_2$
	Periclase	MgO
	Quartz	SiO_2
	Sodalite structure	$Ca_2(Ca,Na)_6(Al,Si)_{12}O_{24}(SO_4)_{1-2}$
	Ferrite spinel	$(Mg,Fe)(Fe,Al)_2O_4$

2.4.3.1 Anhydrite ($CaSO_4$)

It forms from reactions involving CaO, SO_2 and O_2 in the furnace or flue. The amount of anhydrite increases with increasing SO_3 and CaO content of the ash. Anhydrite is a characteristic phase in Class C fly ashes and has also been detected in some Class F

ashes. For most ashes, only about half of the SO_3 is present as anhydrite. The rest ends up in the formation of alkali sulphates. In the case of high SO_3 ashes, alkali sulphates and calcium sulpho-aluminate are also identified as crystalline phases.

Anhydrite plays a significant role in fly ash hydration behaviour because it participates with tricalcium aluminate and other soluble aluminates to produce ettringite, calcium sulpho-aluminate hydrate ($Ca_6Al_2(SO_4)_3(OH)_{12}.26H_2O$). The formation of ettringite immediately on adding water to fly ash contributes significantly to the self-hardening characteristics of fly ash. Ettringite may also precipitate and control the leachability of potentially hazardous trace elements from the fly ash (e.g. As, Pb, and Hg) thus affecting the geochemical behaviour of the disposed ash in landfills or disposal ponds [94].

2.4.3.2 Ferrite Spinel and Hematite (XY_2O_4)

Crystalline ferrite spinel and hematite are present in all the fly ashes. For most ashes, only one third to one half of the iron is present as crystalline oxide. The reactivity of a fly ash is however dependent on the glassy phases of Fe_2O_3. There is at least a small amount, from 0.1 to 1%, of iron present as hematite in almost all the fly ashes. Class C fly ashes however have lower amounts of hematite as well as total Fe_2O_3 than Class F fly ashes.

In the ASTM C618 standard [91], the pozzolanic activity of a fly ash is assumed to be related to the chemical composition as is evident from the limitations on the sum of SiO_2 and Al_2O_3 present as non-reactive quartz, mullite and other silicates and alumino-

silicates. Only the glassy phases of SiO_2 and Al_2O_3 are reported to be pozzolanic [89]. The more glassy oxides an ash contains, the greater is its potential for pozzolanic activity although the composition and structure of the glassy phases are also important [43].

2.4.3.3 Tricalcium Aluminate ($Ca_3Al_2O_6$)

Class C fly ashes invariably contain tricalcium aluminate ($Ca_3Al_2O_6$) with its relative content increasing with increase in CaO content of the ash. Sometimes, intermediate calcium ashes, with CaO content of 8% to 15%, have also been found to contain this compound. Tricalcium aluminate is one of the most important crystalline phases usually identified in fly ash because it contributes to ettringite formation, and also in self-hardening reactions as well as disruptive sulphate reactions [42].

2.5 Aluminium Alloys

Aluminium is a silvery-white-coloured metal having high reflectivity for light and heat. The alloys of aluminium are generally of a similar colour, some with a bluish tinge. Its density is 2.7 g/cm^3 and this falls to 2.6 g/cm^3 for the solid at 660°C, just below the melting point, and 2.4 g/cm^3 for the molten metal at this temperature. Fusion is accompanied by an increase in volume of 6.5 – 6.7% depending on the metal purity, the lower value corresponding to 99.5% aluminium. The melting point of 99.99% aluminium is 660.2°C and the heat of fusion is 387 J/g. Its thermal conductivity is 209 W/mK. Small amounts of impurities have a deleterious effect on conductivity. The

reflectivity of pure aluminium is 80% to 85% of incident visible radiation. The reflective power of aluminium is of importance in the construction of various types of light or heat reflectors as it takes up less heat in sunshine compared to those of other metals. Aluminium and its alloys are slightly paramagnetic [95].

Pure aluminium has low strength and this limits its commercial usefulness. As such, strength improvement is a major objective in the design of aluminium alloy systems. Table 2.8 shows that small percentage of impurities present in commercially pure aluminium raises the tensile strength from the 31 MPa of the zone refined metal to 80 MPa. The hardness also shows a similar dependence [96]. Most metallic elements readily alloy with aluminium, however, only a few are important major ingredients in aluminium alloys. Nevertheless, an appreciable number of other elements serve as supplementary alloying additions for improving alloy properties and characteristics.

Aluminium alloys can be grouped into two categories: *cast* and *wrought* aluminium alloys. Wrought grades are designed for formability, cast grades for castability. Wrought alloys undergo mechanical working by processes such as rolling, extrusion and forging during fabrication. Cast alloys, on the other hand, results in shapes produced by introducing molten aluminium into moulds by processes such as sand, permanent mould and die castings. The striking difference, therefore, is in their structure. These result in wrought grades being textured with cast grades having equal properties in all directions [97].

Table 2.8. Mechanical properties of aluminium of various purities [96].

Purity	Zone Refined	99.9%	99.8%	99.5%	99.0%
Tensile Strength, MPa	31	52	61	72	80
Brinell Hardness	11	15	19	21	22

Cast aluminium alloys have been developed for casting qualities such as fluidity and feeding ability, as well as for properties such as strength, ductility and corrosion resistance. Thus their chemical composition differs widely from those of the wrought aluminium alloys. The various cast aluminium alloy groups is shown in Appendix A1. Favoured for being lightweight and durable, these aluminium castings are typically used for producing castings for engine parts, components and casings for the automotive and aerospace industries [98]. Wrought aluminium alloys are available primarily in the form of worked products such as sheet, foil, plate, extrusions, tube, forgings, rod, bar, and wire. They also find widespread application in the automobile and aerospace industries. The various wrought aluminium alloy groups are shown in Appendix A2.

Both cast and wrought aluminium alloys can further be divided into two main classes, the heat-treatable and the non-heat-treatable. Heat treatable aluminium alloys are those alloys that gain strength from subjecting the material to a sequence of processing steps of solution heat treatment, quenching and age hardening. These results in the development of sub-micron sized particles, precipitates, in the matrix, which in turn influences the material properties of the alloy. Non-heat treatable alloys obtain no significant strengthening by heating and cooling. They obtain higher strength either by strain-hardening or by solid solution. Both classes depend for their properties on the

existence of a range of solid solutions in which the alloying elements are dissolved in the aluminium matrix [99,100].

2.5.1 Non-Heat-Treatable Aluminium Alloys

2.5.1.1 Aluminium – Manganese Alloys

Maximum solubility of manganese in aluminium is 1.82%. This solubility is further reduced by the inevitable presence of iron as an impurity, so that the maximum amount of manganese, which can be safely used, is 1.25%. If more is added there is the danger of large primary particles of the intermetallic compound $MnAl_6$ being formed with disastrous effects on the local ductility. The presence of manganese raises the tensile strength in the annealed condition appreciable with corresponding increases in the work-hardened tempers. It also provides excellent corrosion resistance [100].

The presence of manganese not only confers increased strength but also raises the recrystallization temperature by some 50 to 60°C without impairing the resistance to corrosion. The alloy is rather prone to coarse grain on annealing, but this is normally taken care of by using special processing conditions such as flash annealing [96].

2.5.1.2 Aluminium – Magnesium Alloys

Magnesium has substantial solubility compared to other alloying elements and up to 7% can be used in the wrought condition and up to 10% in the casting alloys. In the alloys with higher magnesium content, due to the diminished solubility of magnesium at low

temperatures, there is a tendency for the β-phase, Mg_2Al_3, to precipitate along the grain boundaries leading to some susceptibility to stress or intergranular corrosion. This precipitation is extremely slow at room temperature, but more rapid at 70 or 100 °C. It is therefore, not advisable to use the alloys with over 3% magnesium for high temperature service in corrosive environments [96].

These alloys work-harden rapidly and the higher the magnesium content the more rapidly they work harden [100]. The magnesium alloys are readily welded by the argon arc process and posses good ductility. In general, magnesium increases the strength of aluminium alloys. In the cold worked condition, these alloys exhibit a phenomenon known as age-softening. Age-softening is a phenomenon resulting in the spontaneous decrease of strength and hardness in certain strain hardened alloys containing magnesium at room temperature.

2.5.2 Heat–Treatable Aluminium Alloys

The heat-treatable alloys of aluminium belong to three main alloy systems. These systems, Al–Cu–Mg, Al–Mg–Si and Al–Zn–Mg, have one property in common, the solid solubility relations change markedly with temperature [96,100]. The significance of this is that if the alloys are heated to the solution treatment temperature a large proportion, in some cases all, of the alloying elements is taken into solid solution. If the metal is then rapidly cooled, for example, by quenching in cold water, the alloying elements are retained in supersaturated solid solution and are only precipitated slowly at room temperature or at the moderate temperatures used for artificial ageing. This

precipitation is accompanied by a marked increase in properties. Silicon is also present in all the alloys, sometimes as an incidental impurity and sometimes as a deliberate additive with a definite effect on the response to thermal treatment.

2.5.2.1 Aluminium–Copper–Magnesium Alloys

These alloys were the original heat-treatable aluminium alloys discovered by Wilm in 1906. In addition to the main alloying elements, they contain iron as an incidental impurity and manganese added to raise the recrystallization temperature and to increase strength [96].

Copper has appreciable solubility and high strengthening effect when added to aluminium alloys. 0.1% to 0.2% chromium must however be added to counteract the adverse effect on corrosion resistance of the copper addition. These alloys are mostly used in aircraft and other heavy engineering construction where high strength and good ductility are required. Immediately after quenching these alloys, they are very ductile and in this condition forming of any kind is relatively easy to carry out [101].

2.5.2.2 Aluminium–Magnesium–Silicon Alloys

The alloys in this system may be regarded as general purpose alloys for structural engineering, and are usually produced in the form of extrusion, sheet or plate. These alloys, of which there are numerous variations, may be divided into two main groups. The first comprises those alloys having between 0.8% and 1.2% of magnesium plus

silicon. These alloys are readily extruded, have moderate strength, good corrosion resistance and for thin sections may be quenched to give satisfactory properties.

The second type, which is much stronger, contains between 1.4% and 1.8% of magnesium plus silicon and fall into two distinct categories. The first category has a balanced composition with the magnesium and silicon contents in the proportions required for the formation of Mg_2Si. To this basic composition, 0.25% copper is added to improve mechanical properties and about 0.1% chromium to counteract the adverse effect on corrosion resistance of the copper addition. The second category has excess silicon compared to the first. This type gives high mechanical properties together with excellent corrosion resistance. They however show intercrystalline brittleness when heat-treated to maximum properties. Up to 0.5% weight manganese is added to eliminate this effect. This alloy is used, without the manganese addition, for some decorative architectural purposes where a good finish for anodizing and a high surface hardness are important, and any slight brittle tendency can be safely ignored [96].

2.5.2.3 Aluminium–Zinc–Magnesium Alloys

The alloys of this system yield the highest strength for aluminium alloys and are therefore employed in aircraft and space vehicle applications, where specialized methods of construction can be used, and proper precautions taken to minimize stress corrosion problems. They are readily weldable and are comparatively insensitive to rates of cooling from the solution temperature, so that welds made in them recover their full properties within a short period of welding.

They are susceptible to serious stress corrosion, particularly in the vicinity of welds. When designing structures with this type of alloys, it is therefore important to provide adequate surface protection mostly by cladding. The extruded form of this alloy is generally used in the clad condition to minimize corrosion hazard. Clad sheet has a sandwich type of structure with a thin layer of pure aluminium or a 1% zinc alloy on each surface and a core of the strong alloy. This is carried out at the rolling stage, with the thin protective layer in contact with the top and bottom faces of the rolling ingot before it enters the rolls [96,99,100].

2.5.3 Aluminium Casting Alloy A535

Aluminium casting alloy A535 is an aluminium-magnesium alloy with the highest combination of strength, shock resistance and ductility of any as-cast (non-heat treated) aluminium alloy. Maximum properties are available immediately after casting without the aid of heat treatment or natural aging. These properties are not affected by stress relieving (T2 condition) and remain the same for the life of the casting [55]. Some physical and mechanical properties of A535 alloy is shown in Table 2.9. Its liquidus temperature is 630°C and the solidus 550 °C with a solution heat treatment of 400°C for 5 hours [102].

A535 has the highest resistance to corrosion of any of the common aluminium alloys. This is due to the almost complete absence of heavy metal contaminants, the primary cause of electrolytic corrosion. Also, the fairly high content of magnesium gives it protection from mild alkalis, salt spray, seawater and mild acids such as fruit juices.

Even when exposed to these corrosive elements, it retains its original colour and appearance [55].

The dimensional stability of aluminium casting alloys is affected by internal stresses. These stresses are due to differential cooling within a casting after pouring or during quenching after solution heat treatment. Generally, the faster the cooling rate the higher the stresses. Because these stresses are concentrated at the surface of a casting, when a surface is machined they become unbalanced and the casting distorts. However, since A535 develops few stresses during cooling, the majority of its castings can be successfully machined in the as-cast (F) condition. This gives A535 a superior machinability and can be milled at speeds four times faster than other aluminium casting alloys. High microfinishes can be achieved at high speeds. It takes a very high mirror polish and it is normally used for sand and permanent mould castings, but can also be used for die casting. They can be welded by any inert gas shielded-arc systems [55].

Table 2.9. Typical physical and mechanical properties of A535 alloy [55,56].

Density	2.62 g/cm^3
Electrical conductivity	23 % IACS
Thermal conductivity at 25 °C	0.23 CGS
Tensile strength	241.3 MPa
Yield strength	124.1 MPa
Percent elongation in 51 mm	9.0%
Brinell Hardness	60-90
Charpy Impact Energy	13.6 J
Fatigue strength	68.9 MPa

A535 has a Charpy Impact rating of 13.6 J and therefore ideally suited for applications encountering high vibrational shock loads. It is often used in aircraft landing gears,

rocket launchers and lightweight armoured vehicles. It is also used in computing devices and electric equipment where dimensional stability is essential and highly useful in marine and other corrosive-prone applications [55].

A535 is slightly (about 10%) more expensive and slightly more difficult to cast than the more common aluminium casting alloys. However, these cost disadvantages are often offset by the elimination of heat treatment, easier straightening (when necessary) and easier finishing operations. Because of its low silicon content, molten A535 is less fluid than the more common aluminium casting alloys. Large but extremely thin sections are thus difficult to cast [55].

2.6 Metal Matrix Composites

A metal matrix composite is a material that satisfies the following conditions [103-106]:

(i) It must be artificially manufactured

(ii) It must be a combination of at least two chemically distinct materials with a distinct interface separating the constituents

(iii) The separate materials forming the composite must be combined three-dimensionally. (Laminates such as clad metals or honeycomb sandwiches are not considered basic composite materials if the same metal is used throughout).

(iv) It should be created to obtain properties, which would not otherwise be achieved, by any of the individual constituents.

MMCs consist of at least two components: one is the metal matrix and the second, a reinforcement. In the production of the composite, the matrix and the reinforcement are

mixed together and can be physically distinguished. This distinguishes a composite from a two or more phase alloy, where the second phase forms a particulate with a definite chemical formula. Compared with monolithic metals, MMCs offer the advantage of better high temperature properties, high specific strength and modulus, better wear resistance, lower thermal expansion and excellent thermal conductivity. They however have lower toughness and higher cost of fabrication. Based on these properties, MMCs find applications in the electrical, automotive and aerospace industries.

MMCs are classified based on the type of reinforcement. Ceramics are the most common type of reinforcements used in MMCs. The primary role of the reinforcement is to carry the load. It increases the strength, stiffness, and high temperature resistance but lowers the density of MMCs [107]. These properties make them very useful in both room and elevated temperature applications. The reinforcements can be divided into four major categories: continuous fibres, short fibres, whiskers, and particulates.

2.6.1 Continuous Fibre Reinforcement

The main continuous fibres used are boron, graphite, alumina and silicon carbide. The fibre is unique for unidirectional load when it is oriented in the same direction of loading, but it has low strength in the direction perpendicular to the fibre orientation. MMC materials reinforced with Tyranno (silicon-carbide fibre containing titanium additions) exhibit high transverse strength and are used mainly in the aerospace industry. They offer the best combination of strength and stiffness. However, the cost of these

systems is very high, mainly because of the high cost of the continuous fibres and of the production [108,109].

2.6.2 Short Fibres

There is a higher ratio of length to diameter in fibres and hence their high strength in composites, considering aligned fibres. Nevertheless, disoriented short fibres have been used with some success as aluminium matrix composite reinforcement. The oxide fibres are used mainly for reinforcement of automobile engine components. Short fibres are still used mainly for refractory insulation purposes due to their low strength compared with others, but they are cheaper than both fibres and whiskers [109,110].

2.6.3 Whiskers

Whiskers are characterized by their fibrous, single-crystal structures, which have almost no crystalline defects. Numerous materials, including metals, oxides, carbides, halides and organic compounds, have been prepared under controlled conditions in the form of whiskers. Generally, a whisker has a single dislocation, which runs along the central axis. This relative freedom from dislocations means that the yield strength of a whisker is close to the theoretical strength of the materials. This type is more costly than the particulates, but offer higher strength [105,111]. Silicon carbide is the most widely used whisker reinforcement. Silicon carbide-reinforced aluminium has been used widely in aerospace vehicles with Japan leading the world in whisker production.

2.6.4 Particulates

Particulates are the most common and cheapest reinforcement. They produce isotropic MMCs, which show promise for structural applications. Initially, attempts were made to produce reinforced aluminium alloys with graphite powder, but only low volume fractions of reinforcement has been incorporated (<10%) [111]. Presently, higher volume fractions of reinforcements have been achieved for various kinds of ceramic particles (oxide, carbide, nitride) [112-114]. The USA leads the world in particulate production with ALCAN having made the greatest progress in research on particulates [115]. A number of particulate reinforced systems have been in use industrially for many years, with cermets, used in the electronics industry for the tracks of precision variable resistors, and high-speed cutting-tool tips, as the most widely used.

2.7 Fly Ash-Reinforced Aluminium MMCs

Fly ash-reinforced MMCs is a type of MMCs in which a metal alloy is the matrix and fly ash the particulate reinforcement. Fly ash has recently been combined with aluminium alloys to produce a class of MMCs called fly ash-reinforced aluminium MMCs or Ashalloys [3-20]. The use of fly ash in aluminium MMCs offer the advantages of reducing its disposal volumes for the electric utility industry, while providing a high-value-added use of fly ash. They also provide improved material properties at a reduced cost. Since the production of aluminium is energy-intensive, the replacement of part of aluminium by fly ash promises significant energy savings [7,12].

2.7.1 Fabrication of Fly Ash-Reinforced Aluminium MMCs

MMCs in general are difficult to fabricate by the conventional metal fabrication methods. There are several fabrication techniques available to manufacture MMCs. The choice depends on the types of matrix and reinforcement materials and on the form of the reinforcement [9,104]. However, there are generally three main routes for fabricating fly ash-reinforced aluminium MMCs: stir casting, powder metallurgy and pressure infiltration technique. The following sub-sections describe the common fabrication methods for fly ash-reinforced aluminium MMCs.

2.7.1.1 Stir Casting

Stir casting is a primary process of composite production whereby the reinforcement material is incorporated into the molten metal by stirring [116]. It has the advantages of being relatively low in cost and capable of producing large complex shapes. Rohatgi *et al.* [7] have developed inexpensive stir casting technique to produce fly ash-reinforced aluminium MMCs containing various amounts of fly ash particles due to their high fluidity.

In order to produce high-quality castings from composites, studies have shown that several modifications must be made to the normal melting and casting practice [15,117,118]. The most obvious modification involves the continuous stirring of the molten composite in order to keep the reinforcement particles in suspension. The alloy should be melted at a controlled temperature and the desired quantity of fly ash added to

the molten aluminium alloy. The temperature of the melt should also be controlled and kept below the critical temperature so as to avoid the formation of other compounds, which can have a disastrous impact on the fluidity of the melt. Continuously stirring creates a vortex which forces the slightly lighter fly ash particles into the melt dispersing the fly ash particles as uniformly as possible till all the material is transferred into a pre-heated and pre-coated transfer ladle and finally poured into preheated permanent moulds. Cooling, cutting to shape, and surface cleaning produces composites with fly ash particles that tend to segregate along the aluminium dendrite boundary due to particle pushing [11].

2.7.1.2 Powder Metallurgy

Powder metallurgy is a process involving the consolidation of powdered samples of the metal and reinforcement at higher temperatures by means of a forging press. Rohatgi and co-workers [8,9,11] have fabricated fly ash-reinforced aluminium MMCs by powder metallurgy technique. Oven dried at 110°C, aluminium and fly ash powders were well blended by using a rotary drum. They varied the amount of fly ash from 5% to 10% by weight in the mixtures. Compaction of the aluminium fly ash samples was achieved at different pressures (138 MPa to 414 MPa) using a uniaxial hydraulic press. Aluminium and aluminium fly ash compacts were sealed in a transparent silica tube under pure nitrogen and sintered at 625°C and 645°C for 2.5 and 6 hours at both temperatures [9,11].

Green density of the aluminium fly ash powder compacts increased with increase in compacting pressure and a decrease in fly ash content. This produced fly ash particles without any significant shape changes even when sintered at 625°C for 2.5 hours. The morphology of aluminium powders however, changes during compaction due to plastic deformation. Rohatgi and co-workers [8,9,11] found that, when the quantity of fly ash in the composite increased above 10% by weight, the hardness significantly decreased, and thus it was concluded that powder metallurgy did not seem very promising for producing fly ash-reinforced aluminium MMCs.

2.7.1.3 Pressure Infiltration

Pressure infiltration is a process in which hydrostatic pressure is applied onto the molten matrix surface to drive the liquid into a perform [116]. Rohatgi and co-workers also fabricated fly ash-reinforced aluminium MMCs by pressure infiltration technique [11,18, 119]. They prepared preforms by mixing fly ash particles with mono-aluminium phosphate (MAP). A356.2 aluminium alloy was then poured into a mould, dried at 204°C for 24 hours and then cured at 815°C for 5 hours. The preforms were placed in a graphite die followed by preheating at 815°C for 2 hours. The aluminium alloy was poured into the die at 840°C and a pressure of 10 to 17 MPa applied on top of the molten alloy for a period of 10 minutes. This resulted in a uniform distribution of fly ash particles in the pressure-infiltrated casting.

Rohatgi and co-workers [11,18,119] concluded from their study that the pressure infiltration technique favours castings with higher volume percent fly. They were able to control the volume percent fly ash in the composite by controlling the porosity in the fly

ash preform. This they did by adjusting the quantity of foaming agent in the preform. [11,18].

2.7.2 Reactions at the Matrix-Reinforcement Interface

Interfaces are considered to be particularly important in the mechanical behaviour of MMCs since they control the load transfer between the matrix and reinforcement. Their nature have been found to depend on the matrix composition, the nature of the surface of the reinforcement, the fabrication method, and the thermal treatments applied to the composite [22,25,120]. Reactions occurring at these interfaces involving the matrix and the reinforcement have also been reported in the literature [18-29,120-125]. Reaction products are known to weaken the reinforcement-matrix interface depending on the temperature, environment, and other parameters [23,125].

In fly ash-reinforced aluminium MMCs fabricated by molten-metal methods, ceramic reinforcements can affect their eventual mechanical properties by reacting with molten aluminium and solid solution forming elements in the matrix alloy during fabrication. The main constituents of fly ash (i.e., SiO_2, Al_2O_3 and Fe_2O_3) have the thermodynamic propensity to react with aluminium and magnesium in Mg-containing aluminium alloys to form various reaction products as shown in Equations (2.1) to (2.7) [126,127] and this has been widely reported in the literature.

$$4Al_{(l)} + 3SiO_{2(s)} \leftrightarrow 3Si_{(s)} + 2Al_2O_{3(s)} \qquad (\Delta G^\circ = -532.2kJ/mol \text{ at } 1000K) \qquad (2.1)$$

$$2Al_{(l)} + Fe_2O_{3(s)} \leftrightarrow 2Fe_{(s)} + Al_2O_{3(s)} \qquad (\Delta G^\circ = -799.6kJ/mol \text{ at } 1000K) \qquad (2.2)$$

$$3Mg_{(l)} + 4Al_2O_{3(s)} \leftrightarrow 2Al_{(s)} + 3MgAl_2O_{4(s)} \qquad (\Delta G^\circ = -215.1kJ/mol \text{ at } 1000K) \qquad (2.3)$$

$SiO_{2(s)} + 2Mg_{(l)} \leftrightarrow 2MgO_{(s)} + Si_{(s)}$ (ΔG° = -255.6kJ/mol at 1000K) (2.4)

$2SiO_{2(s)} + 2Al_{(l)} + Mg_{(l)} \leftrightarrow MgAl_2O_{4(s)} + 2Si_{(s)}$ (ΔG° = -426.4kJ/mol at 1000K) (2.5)

$Fe_2O_{3(s)} + 3Mg_{(l)} \leftrightarrow 3MgO_{(s)} + 2Fe_{(s)}$ (ΔG° = -917.0kJ/mol at 1000K) (2.6)

$MgAl_2O_{4(s)} + 3Mg_{(l)} = 4MgO_{(s)} + 2Al_{(s)}$ (ΔG° =-84.9 kJ/mol at 1000K) (2.7)

The Al_2O_3 formed in Equations (2.1) and (2.2) has been reported to be unstable in Al-Mg alloys by Lloyd [120] and reacts with the magnesium to form spinel ($MgAl_2O_4$) as shown in Equation (2.3). At high magnesium levels and lower temperatures, MgO may form while the formation of spinel is favoured at higher temperatures. The released Si and Fe from Equations (2.1), (2.2), (2.4)-(2.6) can also migrate diffusively or convectively from the fly ash- aluminium matrix interface and alter the matrix chemistry [19]. Depending on the prevailing processing conditions, the excess Si, for example, may combine with Mg to form Mg_2Si as shown in Equation (2.8).

$2Mg + Si = Mg_2Si$ (ΔG° = ~73 kJ/mol at 1000K) (2.8)

Several workers have reported the precipitation of the Mg_2Si phase in the microstructure of particle-reinforced aluminium alloy MMCs [36-39,125,128,129]. Kobashi and Choh [38] have reported that Mg_2Si precipitates form when 5 wt.% Mg is added to pure aluminium whereas, in a more recent study, Ahlatci *et al*. [39] observed Mg_2Si precipitates in an aluminium alloy MMC containing more than 2 wt.% Mg. Liu *et al.* [129] have noted that there are two aspects to Mg_2Si formation in as-cast Al-Mg-Si alloy. One is via the binary eutectic reaction $L \rightarrow \alpha\text{-Al} + Mg_2Si$ that gives rise to Mg_2Si precipitates with lamellar or Chinese-script structure. The other is via the ternary

eutectic reaction L $\rightarrow$ α-Al + ($Al_8Si_6Mg_3Fe$) + Mg_2Si which yields block-like Mg_2Si particles.

The use of fly ash in Al-Mg alloys therefore results in the depletion of solid solution strengthening magnesium in the matrix thereby resulting in the decline in the mechanical properties of the resulting composites.

2.7.3 Physical and Mechanical Properties of Fly Ash-Reinforced Aluminium MMCs

The complex structure of fly ash particles makes its utilization in fly ash-reinforced aluminium MMCs very complex. However, the lowering of the density, improvement in elastic modulus, tensile strength and wear resistance of the resulting composites are properties which have led to an interest in research into fly ash-reinforced aluminium MMCs.

2.7.3.1 Density

The density of fly ash particles obtained from various sources [3,4,7] has been found to range between 1.6 and 2.7 g/cm^3. Their incorporation into aluminium alloys therefore leads to a significant reduction in the density of the composite. Low density fly ash-reinforced aluminium MMCs could be attractive for rotary parts in automobile and other transportation applications. Table 2.10 shows the effect of increasing fly ash content in

pure Al, A360 and A356 aluminium alloys. It can be seen that the measured densities increased with increasing weight fraction of fly ash for all the materials studied.

Table 2.10. Effect of fly ash addition on the density of some aluminium alloys [3,4,7].

Material	Density (g/cm^3)				
Wt.% fly ash →	0	5	10	15	20
Pure Al	2.70	2.55	2.45	2.40	2.34
A356	2.57	2.41	2.34	-	-
A360	2.70	2.64	2.60	2.55	2.50

2.7.3.2 Elastic Modulus

In particulate reinforced MMCs, elastic modulus is one of the properties that have been found to improve with increasing reinforcement content. Table 2.11 shows the effect of fly ash content on pure Al, A356 and A360 aluminium alloys obtained by Zhang *et al.* [3], Rohatgi *et al.* [7] and Kolukisa *et al.* [4] respectively. Zhang *et al.* [3] and Rohatgi *et al.* [7] performed studies with fly ash content ranging from 0 wt.% to 10 wt.% fractions. They initially observed a decline in elastic modulus as weight fraction of fly ash was increased. The elastic modulus however began to increase with increasing fly ash content after 3 wt.% fly ash. Kolukisa *et al.* [4] also performed similar tests with fly ash content ranging between 0 wt.% and 20 wt.% fractions. They however reported an increase in elastic modulus with increasing fly ash content till 15 wt.%. A higher elastic modulus was therefore reported between 5 wt.% and 15 wt.% fraction of fly ash for all the three samples. Higher elastic modulus, which indicates greater stiffness, means that in composite applications where stiffness is a major design criterion, fly ash-reinforced

aluminium MMCs of equivalent stiffness and with smaller cross sections can be used. This will ultimately lead to a reduced component mass.

Table 2.11. Effect of fly ash addition on the elastic modulus of some aluminium alloys [3,4,7].

Material	Elastic modulus (GPa)				
Wt.% fly ash →	0	5	10	15	20
Pure Al	75	74	81	-	-
A356	75	74	86	-	-
A360	58	61	64	65	62

2.7.3.3 Tensile Strength

Studies on the tensile strength of fly ash-reinforced aluminium MMCs have reported an increase with increasing weight percent fly ash. Table 2.12 shows the effect of fly ash addition on the tensile strength of A360 and 443 aluminium alloys. Kolukisa *et al.* [4] observed an increase in the tensile strength of A360 and 443 aluminium alloys with fly ash addition up to 15 wt.% fly ash. The microstructure has been reported to play a significant role in particulate reinforced composites with respect to tensile strength. Eliasson and Sandstrom [103] reported a decrease in grain size with increasing particulate reinforcement resulting in an increase in tensile strength. Differences in coefficient of thermal expansion (CTE) between the particulate reinforcement and the matrix also results in an increase in dislocation density which contributes to an increase in tensile strength.

2.7.3.4 Ductility

The ductility of discontinuous reinforced aluminium matrix composites involves a complex interaction of parameters. The primary factors are the reinforcement content and orientation of the matrix alloy. The fabrication process also affects the ductility of particulate reinforced MMCs. Composite ductility can be improved by reducing matrix porosity, breaking up inclusions and also making the dispersion of reinforced particles finer thereby increasing their uniformity [130]. Ductility however, decreases with increasing amount of reinforcement. Studies by Kolukisa *et al.* [4] on A360 and 443 aluminium alloys confirm this. Their results, shown in Table 2.13, reported a decline in percent elongation with increasing fly ash content.

Table 2.12. Effect of fly ash addition on the tensile strength of some aluminium alloys [4].

Material	Tensile strength (MPa)				
Wt.% fly ash →	0	5	10	15	20
A360	160	163	171	191	167
443	170	178	183	193	172

2.7.3.5 Wear Resistance

In MMCs, as in unreinforced alloys, it has been reported that abrasive wear involves gouging, grooving, and plastic deformation caused by the penetration of hard abrading particles [131]. The interaction of abrading particles with the dispersed hard particles, such as fly ash in the composite during the abrasion wear, is a feature which is not present during the abrasion of unreinforced alloys and, therefore, is expected to increase the wear resistance of the fly ash-reinforced aluminium MMCs. Rohatgi *et al.* [7] and

Kolukisa *et al.* [4] confirmed by observing a significant increase in abrasive wear resistance with increasing fly ash in the alloys they studied. Table 2.14 presents their findings. They attributed the increase in wear resistance to the presence of hard aluminosilicate fly ash particles.

Table 2.13. Effect of fly ash addition on the percent elongation of some aluminium alloys [4].

Material	Elongation (%)				
Wt.% fly ash →	0	5	10	15	20
A360	5.7	4.7	3.0	2.7	2.2
443	4.8	3.3	2.8	1.9	1.1

Table 2.14. Effect of fly ash addition on the wear of some aluminium alloys [4,7].

Material	Wear (10^{-6} cc/cm)				
Wt.% fly ash →	0	5	10	15	20
A356	6.0	3.9	3.2	-	-
A360	9.2	8.6	8.1	7.7	7.3
443	8.9	8.4	7.8	7.4	6.9

3. MATERIALS AND EXPERIMENTAL PROCEDURE

This chapter discusses the materials and the experimental methods employed in this study.

3.1 Materials

A535 alloy and its MMCs containing 5 wt.% fly ash + 5 wt.% SiC (A535 hybrid), 10 wt.% fly ash (A535+10), and 15 wt.% fly ash (A535+15) were used for this study. The MMCs were fabricated using a proprietary stir casting technique developed by CANMET, Ottawa, Canada. Table 3.1 shows the chemical compositional limits of A535 alloy as specified by ASTM B108. Table 3.2 shows the electron probe microanalysis (EPMA) for A535 alloy used for this study while Table 3.3 shows the chemical composition of fly ash used in fabricating the composites obtained in this study using X-ray fluorescence spectrometry (XRF). The fly ash was supplied by one of the power generating plants in the province of Ontario, Canada. The morphology of the fly ash particles is shown in Figure 3.1. It shows the typical spherical shape of most of the fly ash particles with generally smooth exterior surfaces. Their sizes range from less than 1 to more than 100 μm with their average surface area measured as 2.14 m^2/g.

Specimens for mechanical testing and microstructural studies were obtained by cutting from the as-cast samples. The level of difficulty in cutting increased with increasing fly

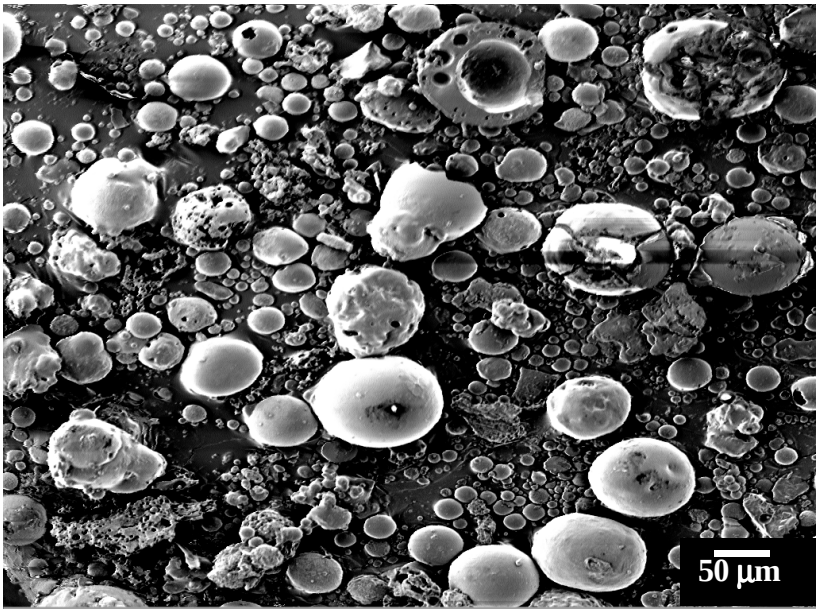

Figure 3.1. SEM micrograph showing the morphology of raw fly ash particles.

Table 3.1. Typical chemical compositional limits of alloying elements in A535 [56].

Element*	Mg	Cu	Si	Mn	Fe	Ti	Others
Weight %	6.2 – 7.5	0.05	0.15	0.10 – 0.25	0.15	0.10 – 0.25	0.15

* Balance = aluminium.

Table 3.2. Chemical composition of alloying elements in A535 alloy using EPMA.

Element*	Mg	Cu	Si	Fe	Ti
Weight %	6.17	0.01	0.01	0.02	0.04

* Balance = aluminium.

Table 3.3. Chemical composition of raw fly ash obtained using XRF.

Compound*	SiO_2	Al_2O_3	Fe_2O_3	MgO	CaO	TiO_2	K_2O	Na_2O	SO_3
Weight %	44.8	22.2	24.0	0.9	1.8	0.8	2.4	0.9	1.4

* Balance = oxides of other trace elements.

ash content. Thus, A535 was the easiest to cut with A535+15 being the most difficult. Wear resistance of the MMCs is, therefore, expected to improve with increasing fly ash content.

3.2 Chemical Analyses

3.2.1 X-ray Diffraction (XRD) and X-ray Fluorescence Analyses (XRF)

Reinforcement particles from all the composites were obtained by dissolving samples of these composites in Aqua Regia for 5 hours. The Aqua Regia was prepared by dissolving 4 parts of concentrated hydrochloric acid (HCl) in 1 part of concentrated nitric acid (HNO_3). The fly ash used in fabricating the composites was also dissolved in Aqua Regia as a control to determine the effect of Aqua Regia digestion on the fly ash particles. The dissolved particles were filtered, washed with de-ionized water and then dried at a temperature of 105°C for a day. Six samples were analyzed. These consisted of the fly ash and SiC used in fabricating the composites, the three sets of reinforcement particles obtained from Aqua Regia dissolution of the composites, and also the fly ash dissolved in Aqua Regia.

Diffraction data were collected with a Bruker D8 θ-θ X-ray diffractometer equipped with CoK_α monochromating multilayered mirrors on the incident and diffracted beam sides. The parallel beam configuration on the sample ensured that height variations in the samples did not result in a sample displacement error. The phases were quantified with TOPAS^{TM}, a Rietveld refinement software. Samples for XRF analysis were palletized with cellulose and analyzed with a 4 μm polypropylene film support under helium. Their chemical compositions were determined using Bruker S4 Explorer X-ray fluorescence spectrometer.

3.2.2 Inductively Coupled Plasma/Optical Emission Spectroscopy (ICP/OES)

The fly ash sample was totally digested by gently heating 0.25g of the sample in a mixture of $HF/HNO_3/HClO_4$ in a Teflon beaker on a hot plate until dry. The residue was then dissolved in 5% HNO_3 and topped to 15 ml with deionized water for analysis by Perkin Elmer Optima 3000 DV inductively coupled plasma/optical emission spectrometer (ICP/OES). This was used to determine the major element oxides, with the exception of SiO_2, and the larger suite of trace elements.

0.10 g of fly ash sample was also digested with 2.25 ml of a mixture of 9 parts HNO_3 with 1 part HCl for 1 hour at 95°C in a boiling water bath and topped to 15 ml with deionized water for analysis by the ICP/OES. This method was used to determine the smaller suite of trace elements. The SiO_2 portion was obtained by fusing 0.10 g of the fly ash sample with 1.00 g of lithium metaborate at 1000°C for 1 hour. The residue was dissolved in dilute HNO_3 topped to 100 ml with deionized water and then analyzed by the ICP/OES.

3.2.3 Inductively Coupled Plasma/Mass Spectroscopy (ICP/MS)

Powdered samples were scrapped from each of the four test materials. 100 mg of each powdered sample was weighed and poured into a Teflon screw capped jar (Savillex^R). 2 ml concentrated nitric acid (HNO_3) was added to each jar and the jars tightly capped. The jars were placed on a hot plate at a temperature of 150°C until the entire samples were dissolved. The solutions were then transferred into separate 125 ml bottles, their

jars rinsed thoroughly with water and transferred into appropriate bottles. About 15 ml of water was then added to fill each bottle.

The solutions were analyzed using Perkin Elmer Elan 5000 inductively coupled plasma/mass spectrometer (ICP/MS). Using the protocol of internal standardization, about 30 parts per billion (ppb) In, Tb and Bi were added into each sample solution so as to overcome instrumental drift and matrix effect. The high thermal energy and electron-rich environment of the ICP resulted in the conversion of most atoms into ions. A quadruple mass spectrometer permitted the detection of ions and each mass in rapid sequence, allowing signals of individual isotopes of an element to be scanned.

3.3 Physical and Mechanical Measurements

3.3.1 Density and Porosity

The density of raw fly ash used in fabricating the composites were determined. First, a measuring cylinder was filled with distilled water to within 0.5 cm of the 100 ml line. It was placed in a bell jar and evacuated to a pressure of between -86 kPa to -96 kPa until the water stopped bubbling. This removes any entrapped voids. The flask was then removed and filled to the 100 ml mark with distilled water. The weight of the water-filled flask was then recorded as WT_2.

15-30 g of fly ash (WT_1) was weighed into a flask. The sample was washed down in the flask with distilled water ensuring that the entire sample is under the water. The flask

was filled to within 1-2 cm of the 100 ml line. The setup was then placed under a bell jar and evacuated to a pressure of -86 kPa to -96 kPa until the sample stopped bubbling. It was removed and filled to the 100 ml mark with distilled water. The weight of the flask with sample and distilled water was then recorded as (WT_3). The density of the fly ash particles was then calculated from Equation 3.1 below. The same procedure was used in determining the bulk density of SiC particles.

$$\text{Density of fly ash} = \frac{WT_1}{(WT_2\text{-}(WT_3\text{-}WT_1))} \tag{3.1}$$

The densities of the composites were determined by means of Archimedes' principle. Archimedes' principle states that when a body is immersed in a fluid, there is a buoyant force acting upward on the body equal to the weight of the displaced fluid. The weight of the displaced fluid equals its volume when water is used (density of water = 1 g/cm^3). The volume of water displaced is equal to the volume of the body immersed. All weights were obtained by means of an Ohaus Scout^{TM} Pro Balance SP2001 equipped with a spring balance. The as-cast material was suspended in air on the spring by means of a thin thread and its weight determined as W_1. It was then completely submerged in a beaker of water and the new weight recorded as W_2. Its density was then calculated from Equation 3.2.

$$\text{Density of sample} = \frac{\text{Weight of sample}}{\text{Volume of sample}} = \frac{W_1}{W_1 - W_2} \tag{3.2}$$

Theoretical calculations, according to the rule of mixtures, was also used to determine the densities of the composites. This was obtained from Equation (3.3) [132].

$$\rho_c = V_r \rho_r + (1 - V_r)\rho_m \tag{3.3}$$

where V_r is the weight ratio of fly ash, ρ_c the density of the composite, ρ_r is the density of fly ash and ρ_m the density of the unreinforced A535 alloy.

The porosity of the test materials were also calculated from Equation (3.4) [133].

$$\text{Porosity (\%)} = \left(1 - \frac{\text{measured density}}{\text{calculated density}}\right) \times 100 \tag{3.4}$$

3.3.2 Hardness Measurements

Specimens of the unreinforced alloy and the three fly ash-reinforced A535 MMCs were tested in the as-cast and heat treated conditions. Solution heat treatment was carried out at 450±5°C for 5 hours, followed by water quenching. This temperature was chosen as a result of the position of the major constituents of A535 alloy in relation to the aluminium–magnesium binary phase diagram. Figure 3.2 shows a portion of the aluminium–magnesium binary phase diagram with the position marked X being the composition of the alloy and its equivalent solution heat treatment temperature. The samples used for hardness measurements were metallurgically polished to a high degree of smoothness. Hardness measurements were taken using a Buehler Micromet II Vickers Microhardness Tester with a load of 100g (resident time of 15s). The small load was chosen to produce indentations small enough to occur in the particle-free matrix. These indentations are pyramidal in shape. The two diagonals were measured using a focal scale on the microscope of the Vickers hardness tester. The Vickers Hardness Number (VHN) was computed from the average length of the diagonals by Equation (3.5).

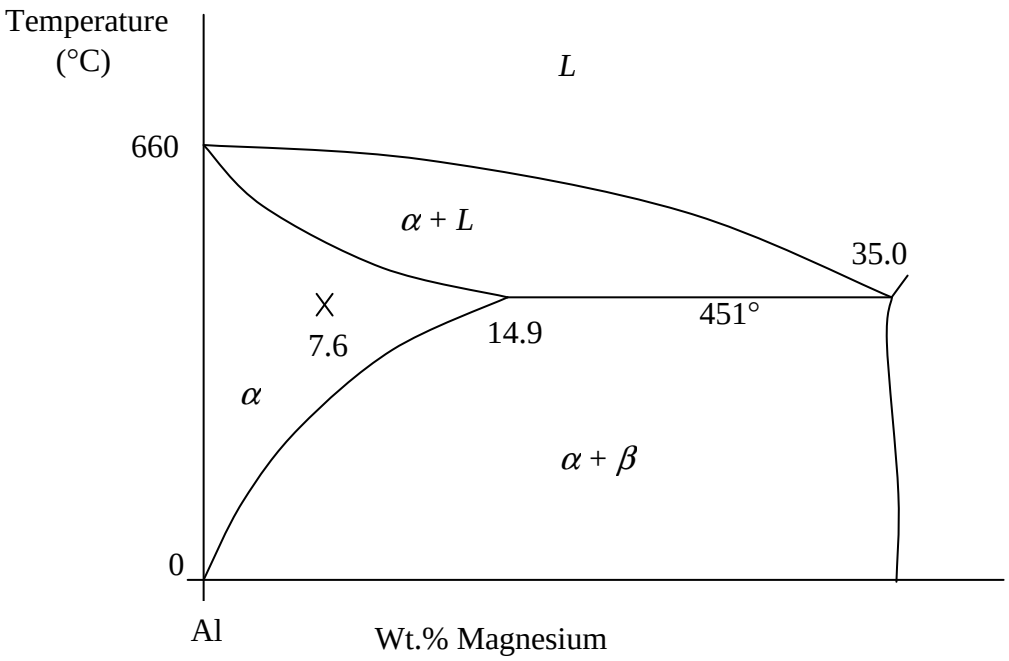

Figure 3.2. Portion of the aluminium – magnesium binary phase diagram.

$$VHN = 1854 \times \frac{F}{d^2} \tag{3.5}$$

where F is the applied load (gf), and d is the average length of the two diagonals (μm). For this study, F = 100 gf was used. All hardness results were based on an average of seven readings.

3.3.3 Charpy Testing

Standard ASTM E23 Charpy V-notch samples measuring 10 mm x 10 mm x 55 mm with a 45° V-notch (2 mm deep and 0.25 mm root radius) were used for the Charpy test. Solution heat treated samples were used for the tests. A Tinus Olsen Model 91310 Charpy tester was used for measuring the impact energy. The samples were supported as

a beam in a horizontal position and loaded behind the notch by the impact of a heavy swinging pendulum. The samples were forced to bend and fracture at a high strain rate. The Charpy tests results were based on an average of five tests.

3.3.4 Tensile Testing

Tensile specimens having a rectangular cross-section and a gauge length of 18 mm (see Figure 3.3) were tested in tension using an Instron® Model 1122 tensile testing machine with a crosshead speed of 0.1667 mm/s. The initial strain rate of 0.0093 s^{-1} was then obtained from Equation (3.6). All tensile tests were carried out using a 5.0 kN load cell. As-cast and solution heat treated samples were tested at room temperature. Solution heat treated samples were also tested at elevated temperatures of 150°C, 200°C, 250°C and 300°C. Custom-built pull-rods were used along with specimen grips in testing the samples. The pull rods were necessary in order to allow room for the furnace to be mounted for high temperature tests. Figure 3.4 shows the setup for the tensile test while Figure 3.5 shows a sample just after failing along with the furnace.

$$\text{Initial Strain Rate} = \frac{\text{cross head speed}}{\text{gauge length}} \tag{3.67}$$

The furnace was equipped with 6 heaters located in pairs, 180° apart, at the top, middle and bottom of the furnace. The heaters are labelled in Figure 3.5. The temperature of the furnace was controlled by adjusting the current to each heater by means of variacs until the required steady state was reached. The temperature within the furnace was measured via six Type K thermocouples located in the central opening of the furnace with two at

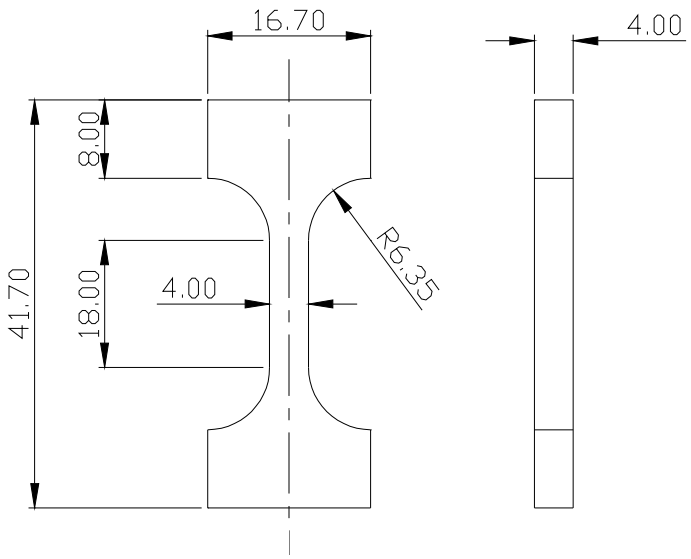

Figure 3.3. A typical tensile specimen. All dimensions in mm.

Figure 3.4. Tensile testing setup.

each of the three locations (i.e. top, middle and bottom) of the furnace. The thermocouples were connected to an output display box.

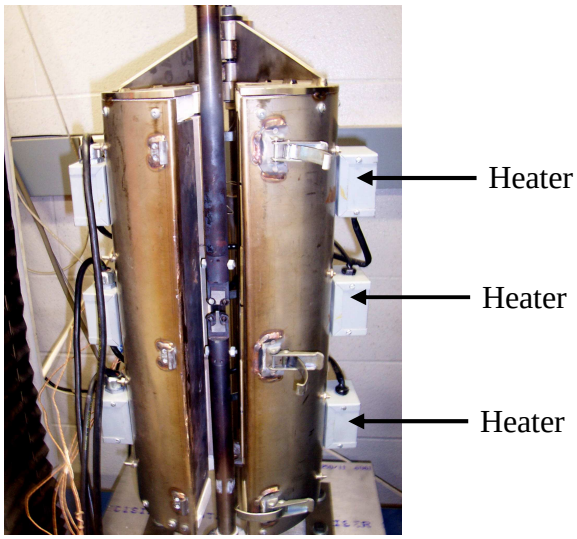

Figure 3.5. Tensile testing furnace.

The specimens were placed in the grips and the crosshead moved until the specimen is tightly in place. The test was then run until the specimen failed for the room temperature tests. For the high temperature tests, the furnace was closed and the heaters turned on to slowly heat up the test material. Once the required steady temperature was reached, the setup was left for 30 minutes to allow the material to achieve the uniform temperature throughout. The materials were then tested in the same fashion as the room temperature samples. Load-extension curves were recorded by means of an autographic device attached to the Instron Machine. Tensile strength, yield strength and percent elongation were calculated in accordance with ASTM E8M-91. The percent elongation was based on an initial gauge length of 18 mm marked on the undeformed specimens. The tensile testing results reported are based on the average of three tests.

3.4 Scanning Electron Microscopy and Energy Dispersive X-ray Spectroscopy

The SEM and energy dispersive X-ray spectroscopy (EDS) were used to study the microstructure and elemental compositions of all the test specimens. The raw fly ash sample was thoroughly mixed with isopropanol. The resulting paste was applied onto one side of a double-sided copper tape and allowed to dry. The dried powder, which was uniformly distributed on the copper tape, was lightly coated with gold for SEM analysis.

The same sample preparations were used for both SEM and EDS studies on the unreinforced A535 and its composites. Solution heat treatment was carried out at 450±5°C for 5 hours, followed by water quenching. The samples were metallurgically polished using a 240-320-400-600 grit cycle emery papers as well as a micropolishing cloth and a 1 μm diamond paste to a high degree of smoothness. The distribution and composition of the various phases present in these samples were obtained using a JEOL Model 5600 Scanning Electron Microscope equipped with an EDAX Genesis 7000 Energy Dispersive X-ray Spectrometer. The distribution of elemental Al, Ti, C, Fe, O, Si, Ca and Mg in the test materials were also determined. All the samples were examined at an acceleration voltage of 5-20 kV.

4. RESULTS AND DISCUSSION

4.1 Optical Studies

The optical micrographs of the unreinforced A535 alloys and its MMCs used for this study are shown in Figures 4.1(a) - (d), with the white arrows showing some of the pores that formed during fabrication. It can be seen that increasing the fly ash content increases the porosity in the MMCs, with the A535+15 composite having the highest porosity. This is consistent with results of other workers [27-30,64]. Porosity formation is often attributed to

(i) shrinkage coupled with interdentritic feeding during mushy zone solidification and

(ii) evolution of hydrogen gas bubbles due to sudden decrease in hydrogen solubility during solidification, which is a function of temperature, pressure and alloy composition [27,29,65].

Porosity is known to reduce the mechanical and fatigue properties of many MMCs and other engineering materials [27,66-68].

4.2 Distribution of Reinforcement Particles in the Matrix

The SEM micrograph of the fly ash particles used in fabricating the composites for this study is shown in Figure 3.1. It shows the typical spherical shape of most of the fly ash

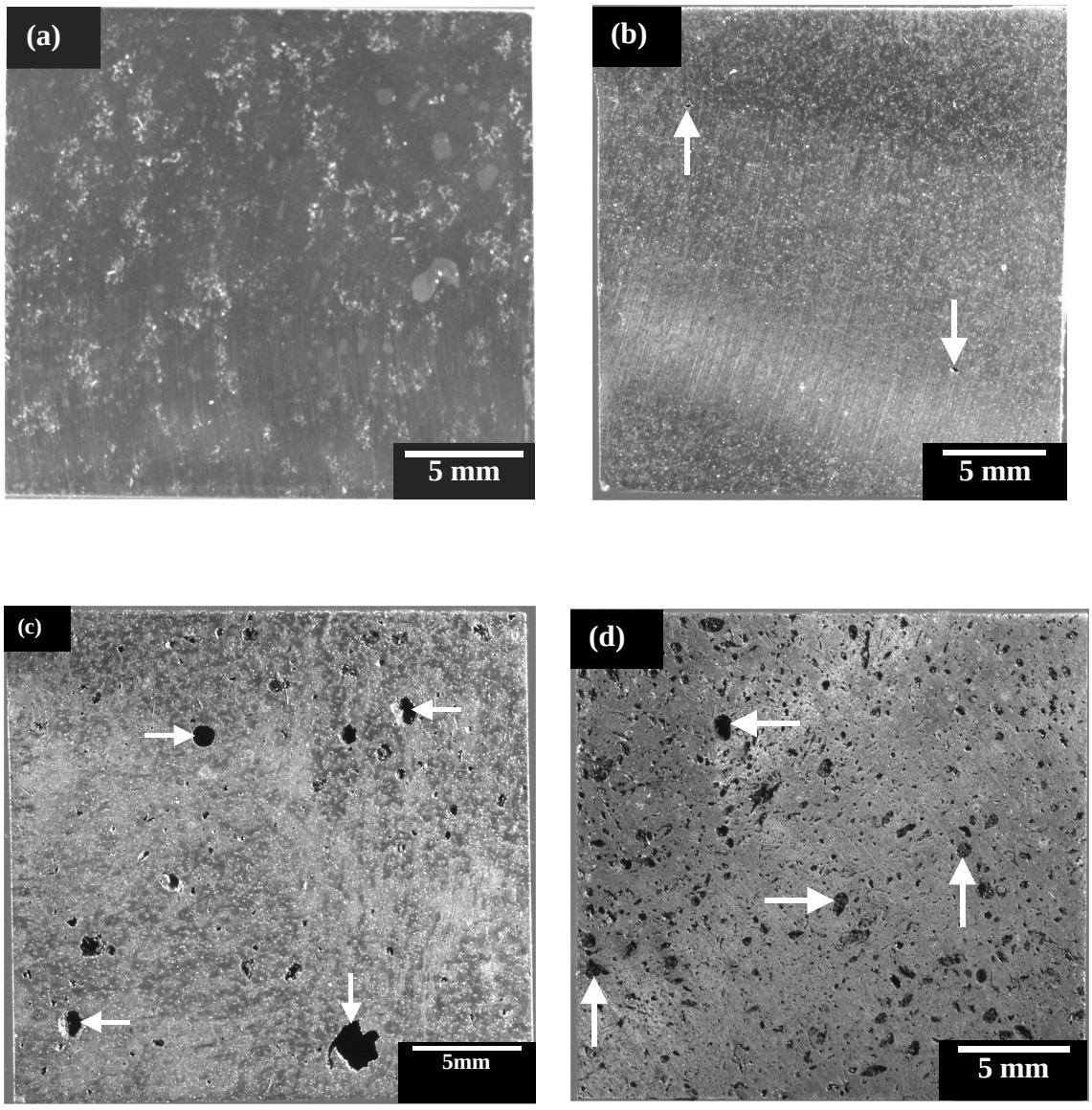

Figure 4.1. Optical micrographs of (a) A535 alloy, (b) A535 hybrid, (c) A535+10, and (d) A535+15 composites.

particles with generally smooth exterior surfaces. Their sizes range from less than 1 to more than 100 μm. Their average surface area was found to be 2.14 m^2/g compared to the surface area range of 0.17 to 0.59 m^2/g obtained by Joshi and Marsh [82] for some Canadian fly ashes. The large specific surface area shows that finer fly ash particles were used in fabricating the composites used in this study.

Figures 4.2(a) – (d) show the microstructure of typical as-cast samples of the unreinforced A535 alloy, A535 hybrid, A535+10 and A535+15 composites, respectively. There is non-uniform distribution of reinforcement particles in all the composites. The blisters shown in Figure 4.2(d) may be due to explosive rupture caused by hydrogen entrapment or explosive reaction between components of the fly ash during fabrication.

The reinforcement particles tend to congregate at the boundaries of α-aluminium dendrites in the castings as shown in Figures 4.2(c) – (d). Rohatgi and Guo [13] reported similar findings for particulate MMCs fabricated using the same stir casting technique used for the samples investigated in the present study. In their study, they found that fly ash particles occupied the interdendritic regions between α-aluminium dendrites partly due to lack of nucleation of α-aluminium dendrites on fly ash particles and partly due to pushing of fly ash particles by growing α-aluminium dendrites. They postulated that the pores developed within the composites were as a result of fly ash addition. This is understandable since in the general stir casting of particle-reinforced MMCs, any gas entrapment during particle incorporation or stirring will lead to poor particle distribution as particles attach to gas bubbles, and porosity is also increased [117].

Studies by Kolukisa *et al.* [4] using a proprietary stir mixing method however resulted in the homogeneous distribution of fly ash particles in A360 and 443 aluminium alloy composites. Bienias *et al.* [5] also obtained higher structural homogeneity with minimum possible porosity levels, good interfacial bonding and quite a uniform

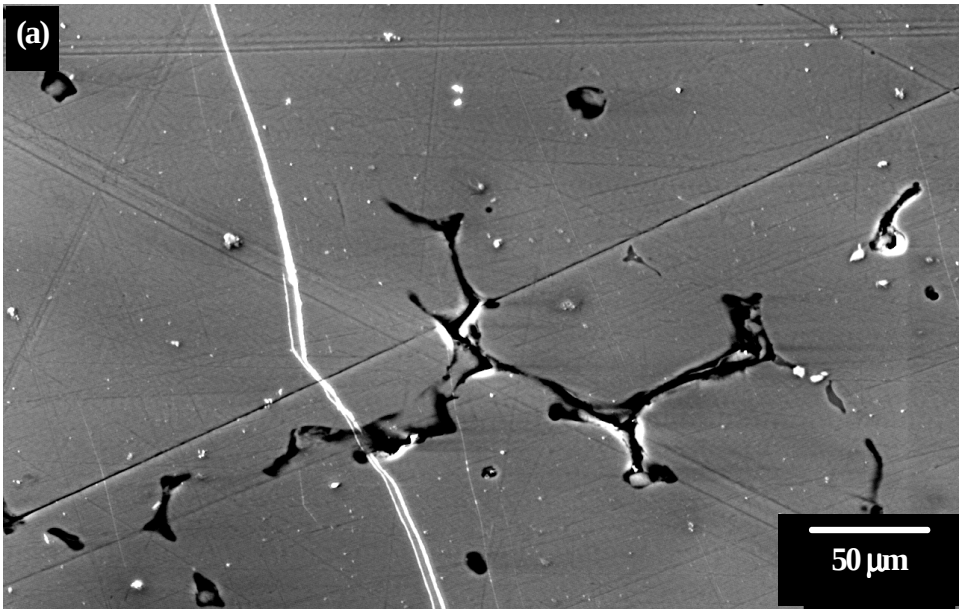
(a)
50 µm

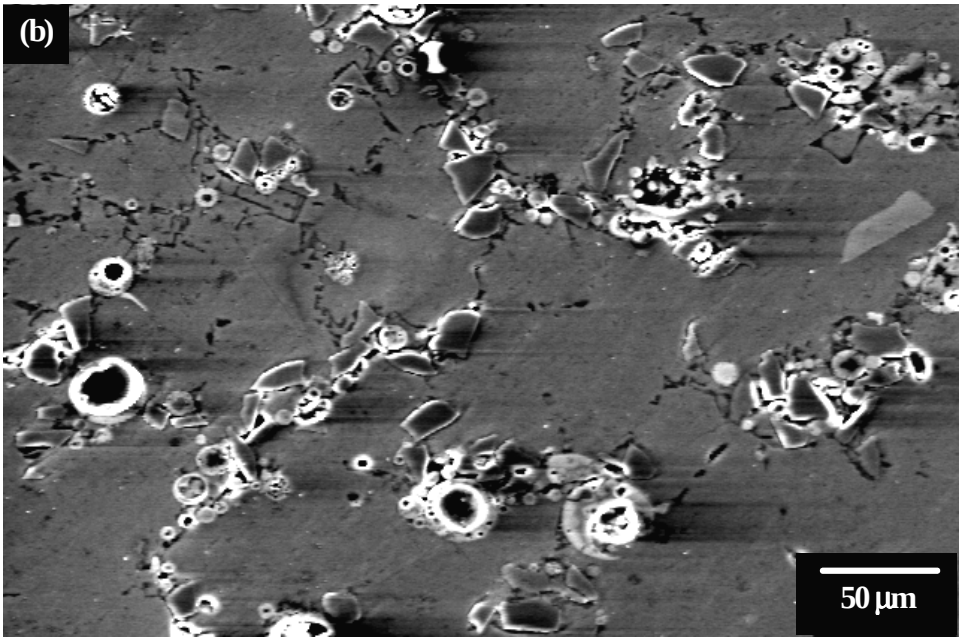
(b)
50 µm

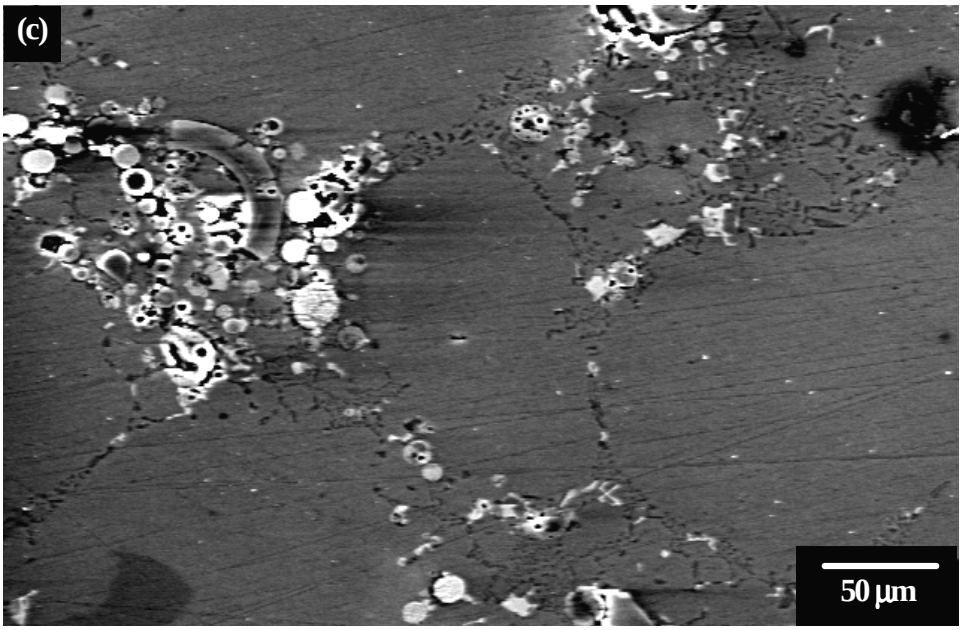

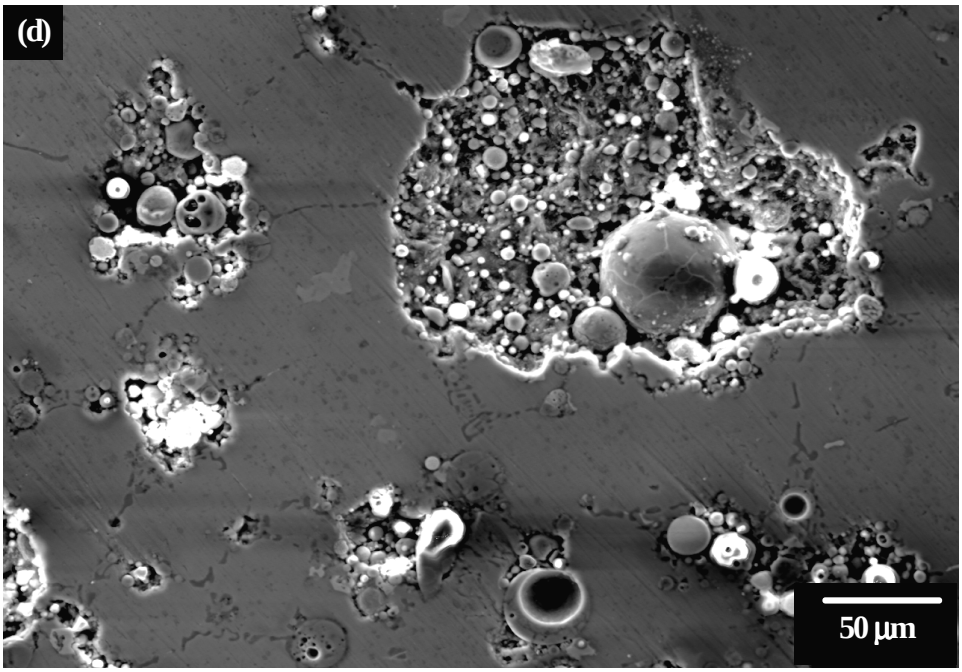

Figure 4.2. SEM micrographs showing the microstructure of as-cast samples of (a) A535 alloy, (b) A535 hybrid, (c) A535+10 and (c) A535+15.

distribution of fly ash particles when they synthesized fly ash-reinforced AK12 (aluminium-silicon base) alloy composite by squeeze casting technology.

4.3 Chemical Analyses

4.3.1 XRD Studies

Fly ashes consist largely of the inorganic residue of coal after the combustion process. They have a complex microstructure, with a mixture of amorphous (usually predominant) and crystalline phases. The X-ray patterns of the raw fly ash used in fabricating the composites (FA), raw fly ash dissolved in Aqua Regia (FA-1), SiC and fly ash particles recovered from A535 hybrid (Hybrid-1), and fly ash particles recovered from A535+10 (FA-2) and A535+15 (FA-3) are shown in Figures 4.3(a)-(e) respectively. The phase compositional data for FA, FA-1, Hybrid-1, FA-2 and FA-3 using XRF are given in Table 4.1. The bulk elemental composition of major oxides in FA, FA-1, FA-2 and FA-3 using XRF are given in Table 4.2. The primary phase in FA is a glassy component, which is mostly derived from dehydroxylation of clay minerals in the parent coal. Dehydroxylation is the chemical process that decomposes one or more hydroxyl (OH^-) groups in the clay minerals thereby reducing them. The approximate composition of the glassy phase is $Na_{0.2}K_{0.3}Ca_{0.3}Mg_{0.2}Fe_{0.2}Si_{3.8}Al_{1.7}O_{11}$ obtained by TOPAS^{TM}, a Rietveld refinement software. Other phases present in FA are magnetite, hematite, quartz, mullite and minor quantities of anhydrite.

The phase composition of Hybrid-1 showed an increase in SiC to fly ash ratio from 50:50 to 60:40. This is an indication that the SiC phase remained passive during treatment while the fly ash reacted with the A535 alloy and the Aqua Regia. FA-2 and FA-3 contained the same phases as that of FA. However, a spinel phase ($MgAl_2O_4$) was also identified in them. The amount of spinel ($MgAl_2O_4$) was detected to increase with

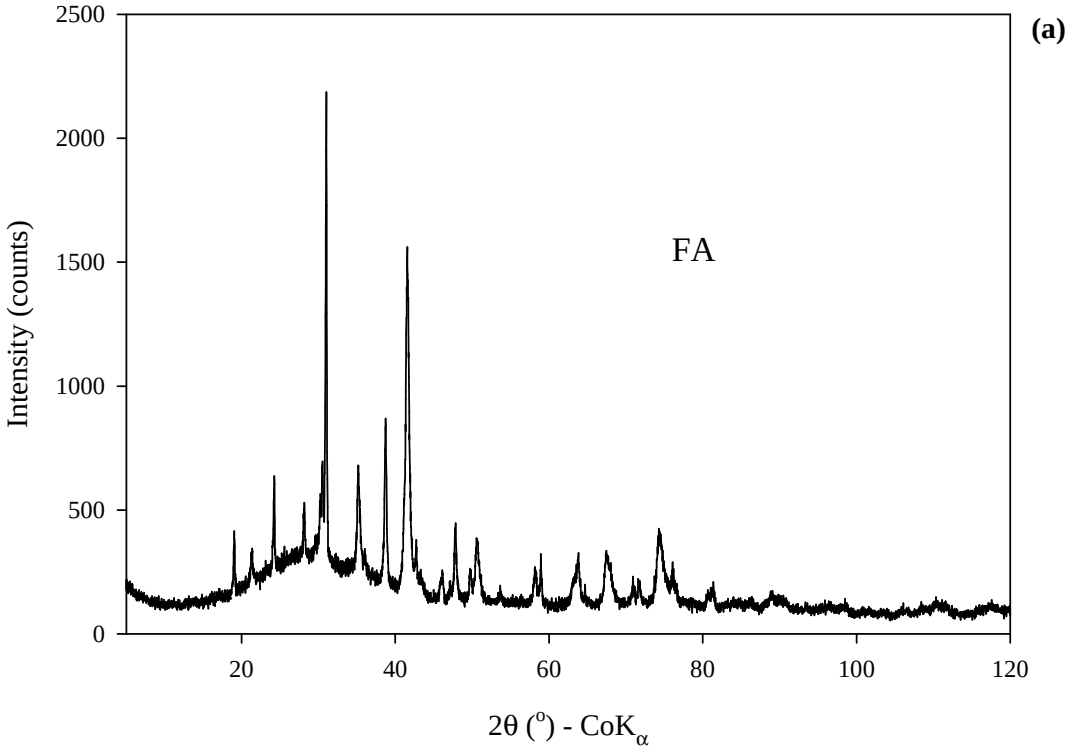
(a)
FA
Intensity (counts)
2θ (°) - CoKα
0
500
1000
1500
2000
2500
20
40
60
80
100
120

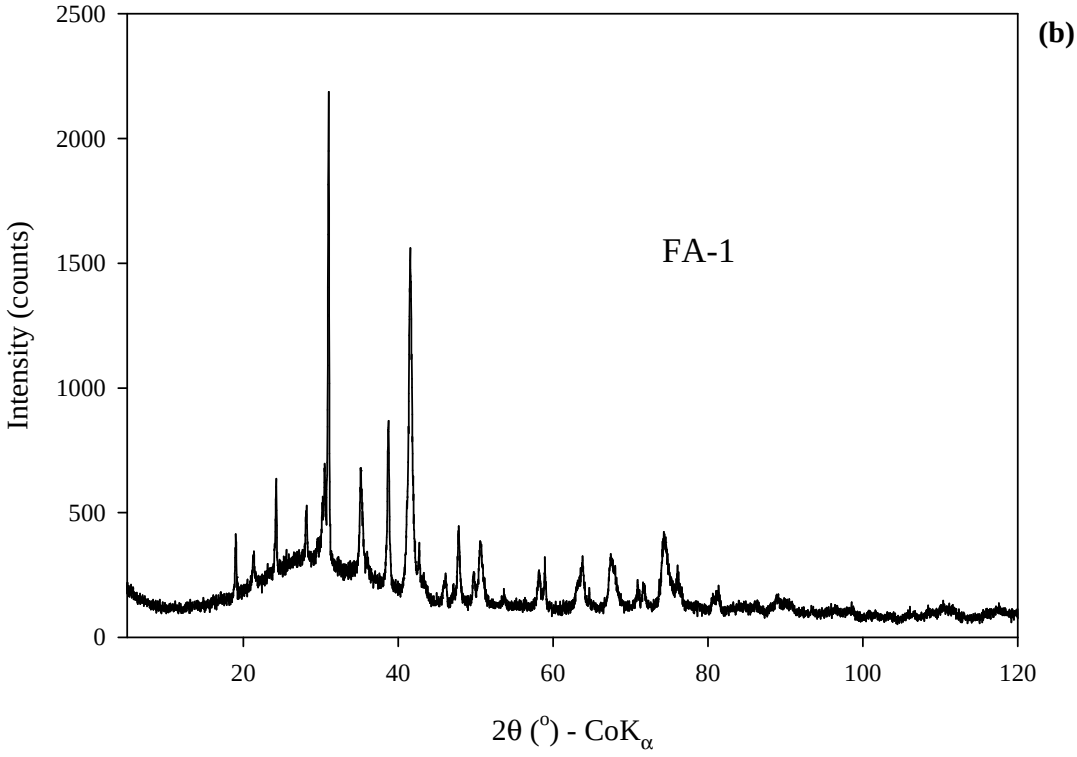
(b)
FA-1
Intensity (counts)
2θ (°) - CoKα
0
500
1000
1500
2000
2500
20
40
60
80
100
120

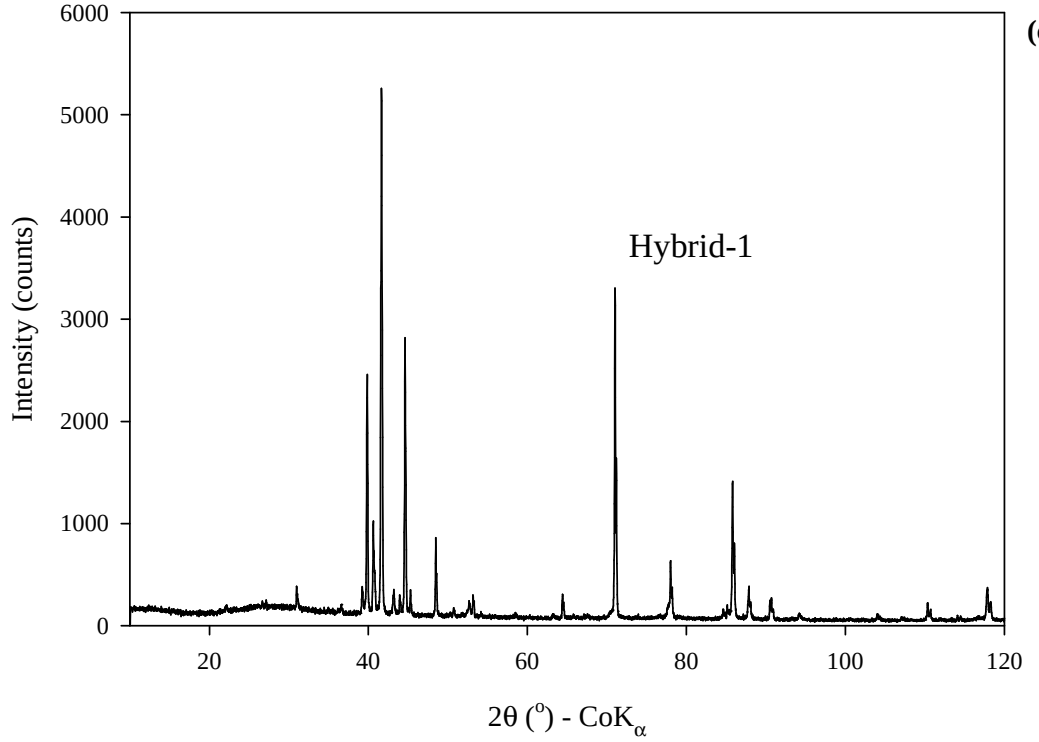
(c)
Hybrid-1
Intensity (counts)
6000
5000
4000
3000
2000
1000
0
20
40
60
80
100
120
2θ (°) - CoKα

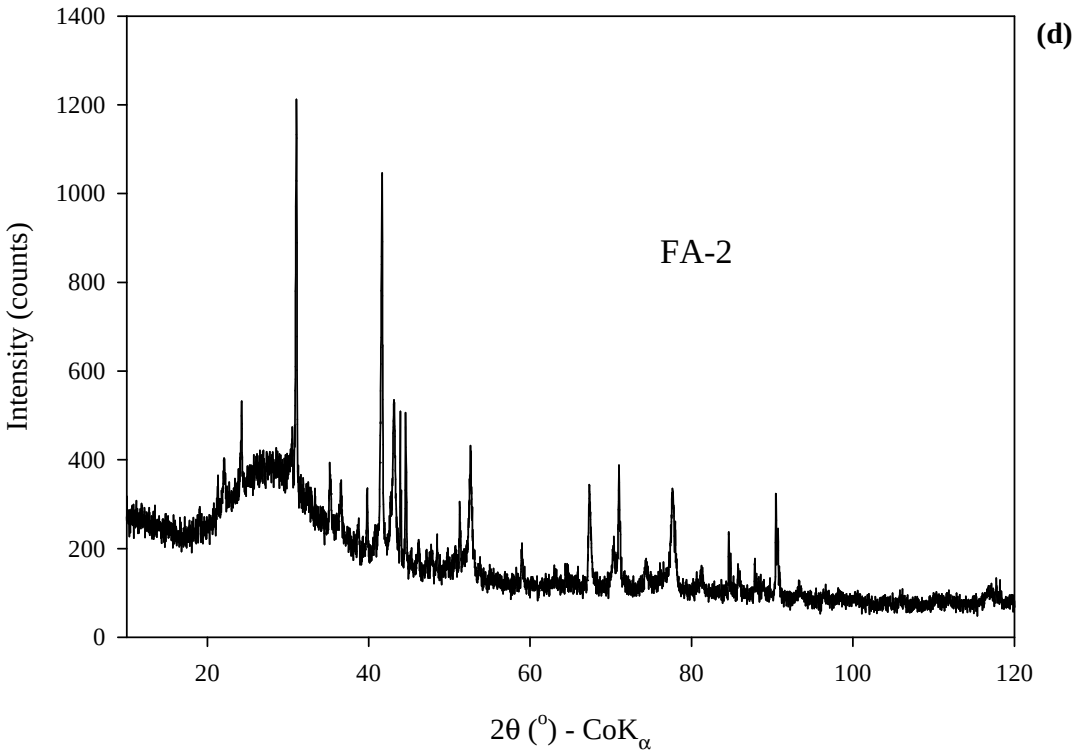
(d)
FA-2
Intensity (counts)
1400
1200
1000
800
600
400
200
0
20
40
60
80
100
120
2θ (°) - CoKα

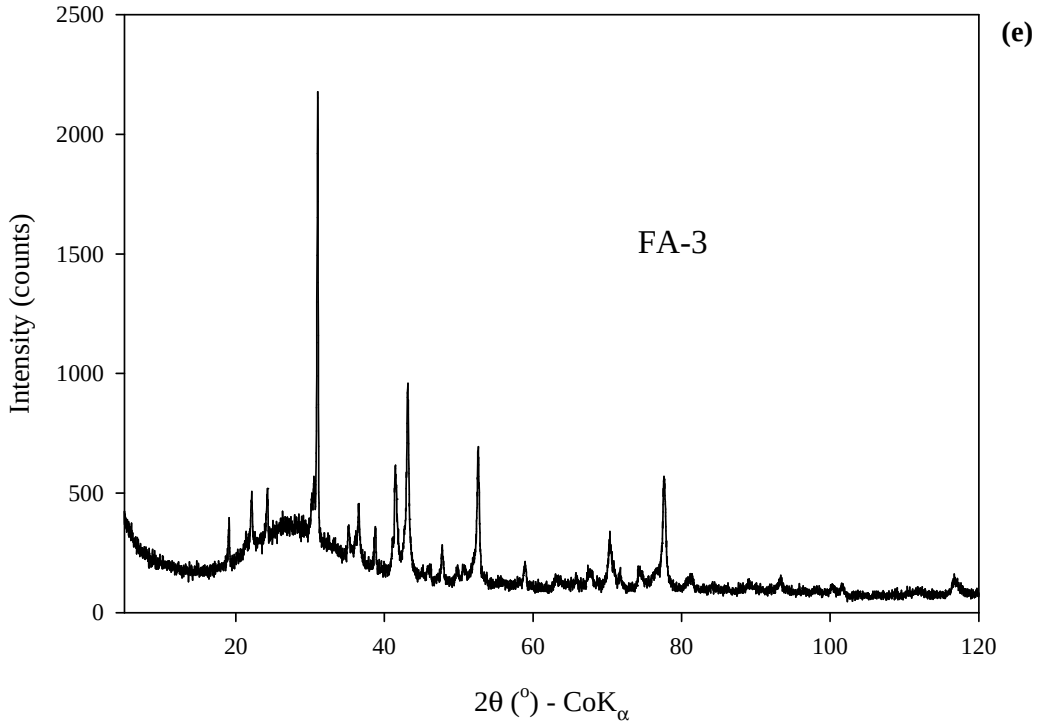

Figure 4.3. X-ray patterns of (a) FA, (b) FA-1, (c) Hybrid-1, (d) FA-2 and (e) FA-3.

Table 4.1. Phase composition (in wt.%) of significant oxides using XRF.

Compound	FA	FA-1	Hybrid-1	FA-2	FA-3
Aluminosilicate glass	59.5	61.6	33.1	66.1	58.3
Spinel ($MgAl_2O_4$)	-	-	6.1	13.4	22.5
Quartz (SiO_2)	6.6	7.3	0.9	4.9	5.1
Mullite ($Al_6Si_2O_{13}$)	12.5	14.3	-	4.4	8.1
Magnetite (Fe_3O_4)	14.7	11.2	-	3.8	4.8
Hematite (Fe_2O_3)	6.5	5.7	-	-	1.1
Anhydrite ($CaSO_4$)	0.2	-	-	-	-
SiC	-	-	59.9	7.5	-

Table 4.2. Chemical composition (in wt.%) of significant oxides using XRF.

Compound	FA	FA-1	FA-2	FA-3
SiO_2	44.8	49.1	58.0	61.3
Al_2O_3	22.2	23.5	20.9	22.7
Fe_2O_3	24.0	21.1	6.0	4.4
TiO_2	0.8	0.9	0.7	0.5
CaO	1.8	0.8	0.3	0.4
MgO	0.9	0.8	4.1	6.7
Na_2O	0.9	0.7	-	0.2
SO_3	1.4	0.1	0.1	0.1
K_2O	2.4	2.5	0.7	1.4

increasing fly ash content. The quartz and mullite phases present in FA-2 and FA-3 were not significantly affected by the reaction with A535 alloy. The iron oxides were however substantially reduced in the fly ash phase. There is also considerable leaching of Na, Mg, Ca, Al and Fe from the glass phase. The resulting glass phase has an approximate composition of $K_{0.1}Ca_{0.04}Mg_{0.05}Fe_{0.04}Si_{4.8}Al_{0.9}O_{11}$ in FA-2 and $Na_{0.04}K_{0.2}Ca_{0.05}Mg_{0.04}Fe_{0.04}Si_{5.3}Al_{0.1}O_{11}$ in FA-3.

The crystalline phases are widely regarded as forming by direct solid-state reaction from the mineral phases present in the coal [134]. The type of crystalline phases, their amount present and distribution therefore directly reflect the mineral content of the original coal and the combustion technology. The principal crystalline phases present in the fly ash are mullite, magnetite, haematite and quartz. This is consistent with those of Joshi *et al*. [82] on the chemical and mineralogical composition of some Canadian fly ashes.

The phase composition of FA-1 is similar to that of the raw fly ash. However, the Aqua Regia solution appears to have dissolved anhydrite and some of the iron oxides, thereby increasing the glass phase relative to the crystalline minerals. The resulting glass phase in FA-1 has an approximate composition of $Na_{0.1}K_{0.3}Ca_{0.1}Mg_{0.1}Fe_{0.3}Si_{3.9}Al_{1.6}O_{11}$. Aqua Regia dissolution of the crystalline phases and chemical reactions of fly ash and the matrices of the composites are responsible for the low levels of mullite, magnetite, hematite and anhydrite detected in Hybrid-1, FA-2 and FA-3. Based on the low level of CaO obtained in the fly ash used for this study (<1.8), this type of fly ash falls under Class F stated by ASTM C618 [91].

4.3.2 ICP/OES Results

The results obtained, for the major oxides, from inductively coupled plasma/optical emission spectroscopy (ICP/OES) for raw silicon carbide used in fabricating the composite (SiC), FA, Hybrid-1, FA-2 and FA-3 are shown in Table 4.3. The carbon content of the materials were not able to be detected using this procedure. This result compares favourable with that obtained using XRF. Iron oxides are therefore substantially consumed in all the composites. Table 4.4 also shows the trace element composition of these samples. From Table 4.4, it can be seen that fly ash contains some heavy metals (e.g. As, Cd, Cr, Hg, Pb and Zn). The maximum allowable concentration of some heavy metals set by Health Canada for drinking water is shown in Table 4.5 [135]. With the exception of Cd and Hg, whose concentrations were below the detectable limits, the concentrations of the other heavy metals were found to be higher than the allowable concentrations set out by Health Canada for drinking water. Fly ash therefore poses an environmental risk in its usage.

Table 4.3. Chemical composition (in wt.%) of major oxides using ICP/OES.

Compound	SiC	FA	Hybrid-1	FA-2	FA-3
SiO_2	99.9	43.6	87.4	74.3	54.2
Al_2O_3	0.02	20.3	10.2	14.8	26.4
Fe_2O_3	0.02	28.7	0.1	4.9	8.72
TiO_2	0.01	0.87	0.21	0.85	0.75
CaO	-	1.86	0.04	0.21	0.41
MgO	-	1.05	1.96	4.20	7.42
MnO	-	0.06	0.01	0.02	0.02
Na_2O	-	0.90	0.02	0.17	0.48
P_2O_5	-	0.18	0.01	0.04	0.06
K_2O	-	2.48	0.02	0.51	1.52

Table 4.4. Chemical composition (in ppm) of minor elements using ICP/OES.

Element	SiC	FA	Hybrid-1	FA-2	FA-3
Ag	< 0.2	< 0.2	< 0.2	< 0.2	< 0.2
As	< 1	518	1	18	10
Ba	1	821	38	155	354
Be	< 0.1	9.1	17.6	23.2	55.1
Bi	< 1	< 1	< 1	< 1	< 1
Cd	< 0.2	< 0.2	< 0.2	< 0.2	< 0.2
Ce	< 0.1	95	2	16	47
Co	< 0.1	26	< 0.1	5	9
Cr	2	108	1	31	49
Cu	< 0.1	121	57	58	22
Dy	< 0.2	10.2	< 0.2	1.1	4.1
Er	< 0.2	6.9	< 0.2	0.2	3.2
Eu	< 0.2	2.3	< 0.2	0.6	1.4
Ga	< 1	41	15	37	24
Gd	< 0.5	3.5	< 0.5	0.6	2.5
Ge	< 1	1	< 1	< 1	< 1
Hf	< 0.5	4.7	< 0.5	4.7	3
Hg	< 1	< 1	< 1	< 1	< 1
Ho	< 0.4	1	< 0.4	0.5	1.4
La	< 1	54	< 1	9	26
Li	< 1	190	< 1	66	138
Mo	< 1	48	2	37	12
Nb	< 1	11	< 1	6	12
Ni	28	103	4	24	41
Pb	< 1	310	5	30	89
Pr	< 1	10	< 1	1	4
Sb	< 1	1	< 1	< 1	< 1
Sc	< 1	19	< 1	2	9
Se	< 1	1	< 1	< 1	< 1
Sm	< 0.5	8.6	< 0.5	1.3	3.5
Sn	< 1	< 1	13	87	3
Sr	< 1	398	8	78	199
Ta	< 1	< 1	1	< 1	< 1
Tb	< 0.3	< 0.3	< 0.3	< 0.3	< 0.3
Te	< 1	1	< 1	< 1	< 1
Th	< 1	18	< 1	2	8
U	< 2	13	< 2	< 2	3
V	63	245	125	273	152
W	< 1	< 1	< 1	< 1	< 1
Y	< 1	40	< 1	8	18
Yb	0.2	3.8	0.4	0.7	2.6
Zn	3	541	3	64	172
Zr	7	163	25	182	121

Table 4.5. Allowable concentration (in ppm) of hazardous elements in drinking water by Health Canada [135].

Element	Maximum acceptable concentration (ppm)
As	0.0125
Ba	1.0
Cd	< 0.005
Cr	0.05
Hg	0.001
Pb	0.010
Sb	0.006
Se	0.01
U	0.02
Zn	≤ 5.0

4.3.3 ICP/MS Results

The inductively coupled plasma/mass spectroscopy (ICP/MS) was used to determine the total elemental composition of the major elements in the test materials. The results are shown in Table 4.6. As can be seen, the iron content increases with fly ash addition and this can be attributed to the high iron content in the fly ash. The magnesium content in the unreinforced A535 alloy was higher and decreased with fly ash addition. However, the magnesium content in A535+15 was found to be higher than A535+10. This can be attributed to the high contribution of magnesium from the fly ash particles. The chemical composition of minor elements using ICP/MS is shown in Appendix B.

4.4 Physical and Mechanical Properties

4.4.1 Microhardness

Figure 4.4 shows the microhardness of the as-cast and as-quenched solution heat-treated samples of the unreinforced A535 and its composites. It can be observed that the

hardness of A535 decreased with increasing fly ash content. This is contrary to the results published by Rohatgi *et al.* [15,19], Sahin [33], and Amigo *et al*. [34]. For A356.2 aluminium alloy reinforced with precipitator fly ash, Rohatgi and co-workers observed a slight increase in hardness with increasing fly ash content. Sahin [33] reported that the hardness of AA2014 reinforced with SiC particles increased more or less linearly with the volume fraction of particulates. Amigo *et al*. [34] also found that the hardness of AA6061/Si_3N_{4p} composites increased significantly with increasing Si_3N_4 volume fraction.

A535 hybrid and A535+10 composites have the same amount of reinforcement particles (i.e. 10 wt%), but the hardness of the former is substantially greater than that of the latter. This indicates that fly ash is more effective in retarding solid solution strengthening process in A535 than SiC by depleting more Mg (the principal alloying element in A535) from the matrix alloy. It is also noted from Figure 4.4 that the hardness of the as-cast materials is lower than that of solution heat-treated samples, thus showing the effectiveness of heat treatment in improving the hardness of A535 and its composites.

Table 4.6. Chemical composition (in wt.%) of major elements using ICP/MS.

Test Material	Mg	Cu	Mn	Fe	Ti
A535	7.95	0.01	0.12	0.14	0.14
A535 hybrid	6.41	0.00	0.14	0.23	0.16
A535+10	6.15	0.00	0.14	1.53	0.17
A535+15	6.50	0.00	0.13	3.25	0.20

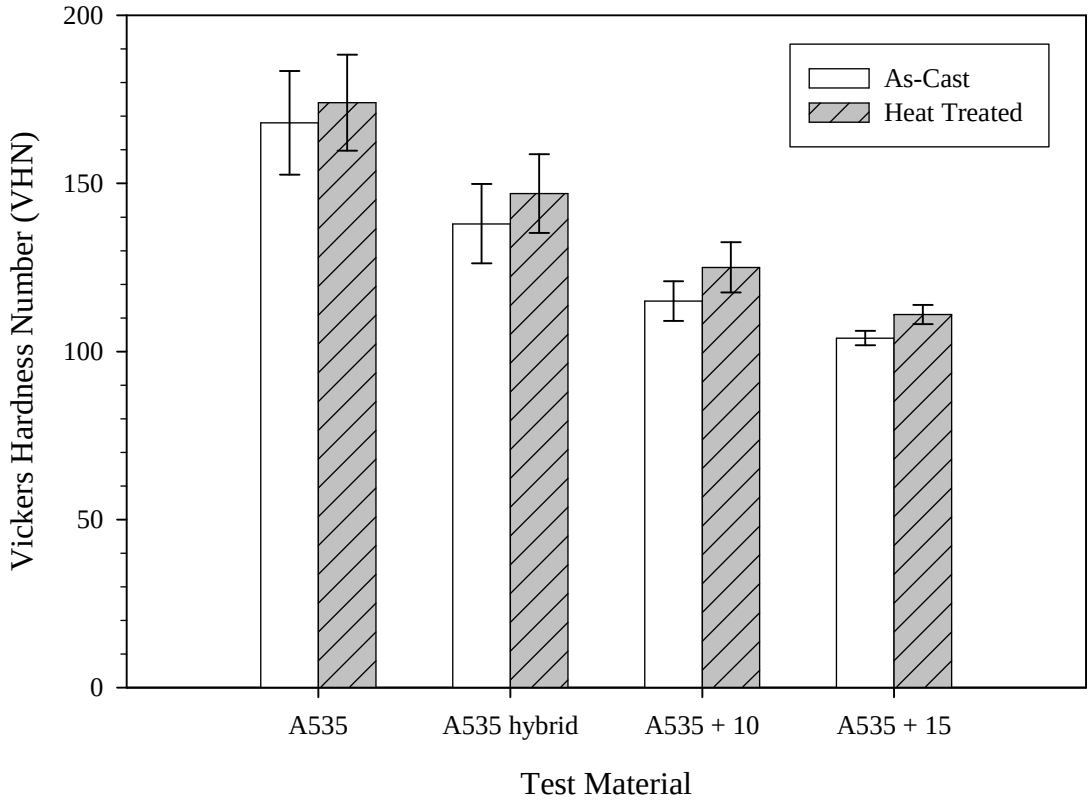

Figure 4.4. Microhardness of as-cast and solution heat-treated samples of A535 alloy, A535 hybrid, A535+10 and A535+15 composites.

To investigate the effect fly ash addition may have on the natural aging behaviour of A535, some solution heat-treated samples were left to age at room temperature for 21 days. The variation of microhardness with aging time for these samples is shown in Figure 4.5. As can be seen from this figure, although reinforcing A535 alloy with fly ash decreased the overall hardness of the composites, it does not alter its natural aging behaviour. Based on this result, it is possible to conclude that the addition of raw fly ash is detrimental to the hardness and, by extension, the strength of A535 alloy.

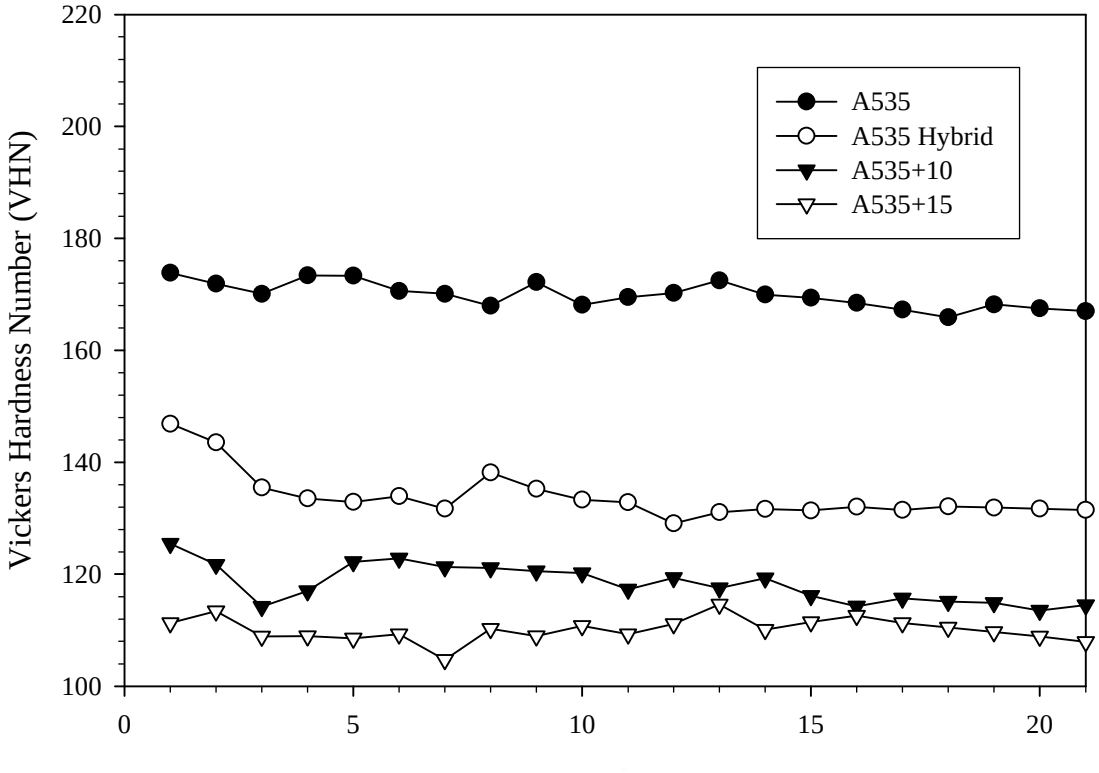

Figure 4.5. Variation of microhardness with aging time at room temperature for A535 alloy, A535 hybrid, A535+10, and A535+15 composites.

4.4.2 Density and Porosity

The bulk density of the SiC and fly ash particles were found to be 3.20 g/cm^3 and 2.61 g/cm^3 respectively. The density of fly ash particles is higher than 2.31 g/cm^3 and 2.46 g/cm^3 stated by Joshi *et al.* [82] for some bituminous fly ashes obtained from Ontario. Kolukisa *et al.* [4] also fabricated fly ash-reinforced aluminium MMCs using fly ashes with densities ranging between 1.8 g/cm^3 and 1.9 g/cm^3. The higher density of the fly ash used in this study suggests the presence of higher amount of iron oxides. Figure 4.6 shows the measured and calculated densities of the as-cast test materials. The measured values decrease with increasing fly ash content while that of the calculated densities

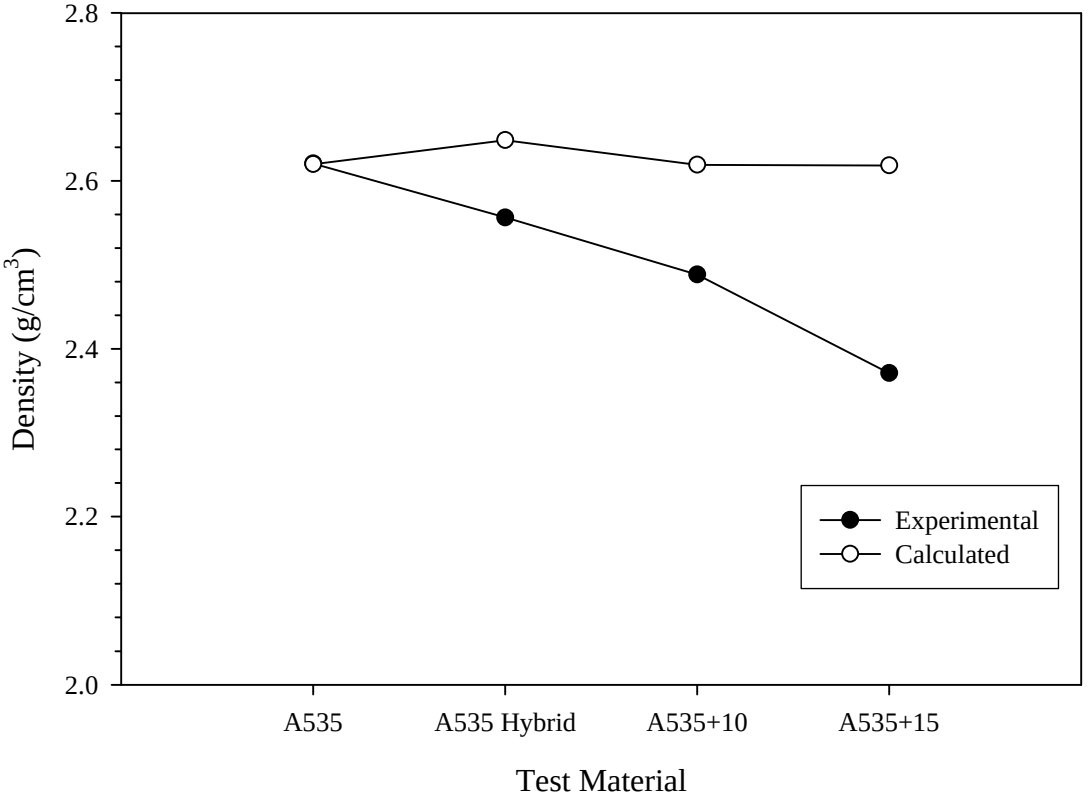

Figure 4.6. Variation of density with fly ash content for as-cast samples.

remain the same except A535 hybrid where a higher value was obtained as a result of the high density of SiC. The measured densities, however, were lower than that obtained from theoretical calculations. The extent of deviation increases with increasing fly ash content. This can be attributed to the increase in porosity with fly ash content. A535 alloy was the heaviest with A535+15 being the lightest. This is in conformity with the results published by Rohatgi *et al.* [13,15] and Kolukisa *et al.* [4]. Rohatgi and co-workers [13,15] reported a decline in the density of the resulting A356.2 composites with increasing fly ash content. Kolukisa *et al.* [4] also reported similar trends for A360 and 443 aluminium alloy composites.

The densities of A535 hybrid and A535+10 composites were however different although both had 10 wt.% reinforcements. A535 hybrid was denser than A535+10. Fly ash is therefore more pronounced in reducing the densities of these composites. The average density measured for the as-cast A535 alloy was 2.62 g/cm^3 which is the same as 2.62 g/cm^3 published in the literature for this alloy [55]. Theoretical calculations resulted in the same value of 2.62 g/cm^3 for the densities of A535, A535+10 and A535+15. This was as a result of the similar values obtained for fly ash and A535 alloy (i.e. 2.61 g/cm^3 for fly ash and 2.62 g/cm^3 for A535 alloy). That of A535 hybrid gave 2.65 g/cm^3.

Figure 4.7 shows the variation in porosity with fly ash content. Tekmen *et al.* [30] reported a porosity of 4.61% for an Al-Si alloy reinforced with 10 vol.% SiC. This is higher than the 3.20% obtained for A535 hybrid but lower than 5.04% obtained for A535+10. The lower porosity in A535 hybrid compared to A535+10 can be attributed to a better wettability of SiC particles to that of fly ash by Al-Mg alloys. A higher porosity of 9.52% was however obtained for A535+15. Porosity therefore increases with increasing fly ash content as can be seen in Figure 4.7. The introduction of porosity into composites has been found to have a negative effect on their mechanical and fatigue properties [30,33,35,136-138]. The fabrication process should therefore be improved in order to reduce the extent of porosity development in the composites.

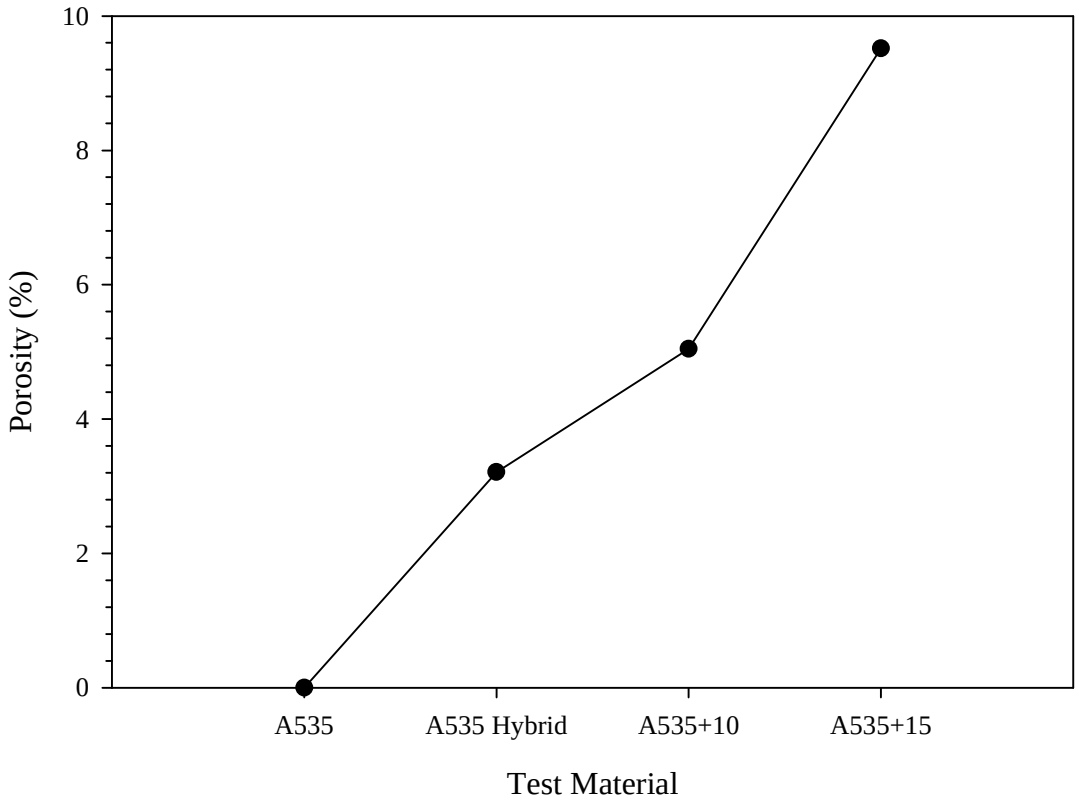

Figure 4.7. Variation of porosity with fly ash content for as-cast samples.

4.4.3 Charpy Impact Test

4.4.3.1 General Description

The Charpy impact test was used to evaluate the relative toughness of the test materials. Figure 4.8 shows the variation of Charpy impact energy with increasing weight percent of fly ash. It can be observed that the energy absorbed in fracturing the specimens decreased with increasing fly ash content. Also, a significant difference in impact strength exists between the unreinforced alloy and the MMCs (A535 hybrid and A535+10). The decrease in the impact resistance of the composites is attributed to the observed porosity. Again, when A535 hybrid and A535+10 composites are compared, it

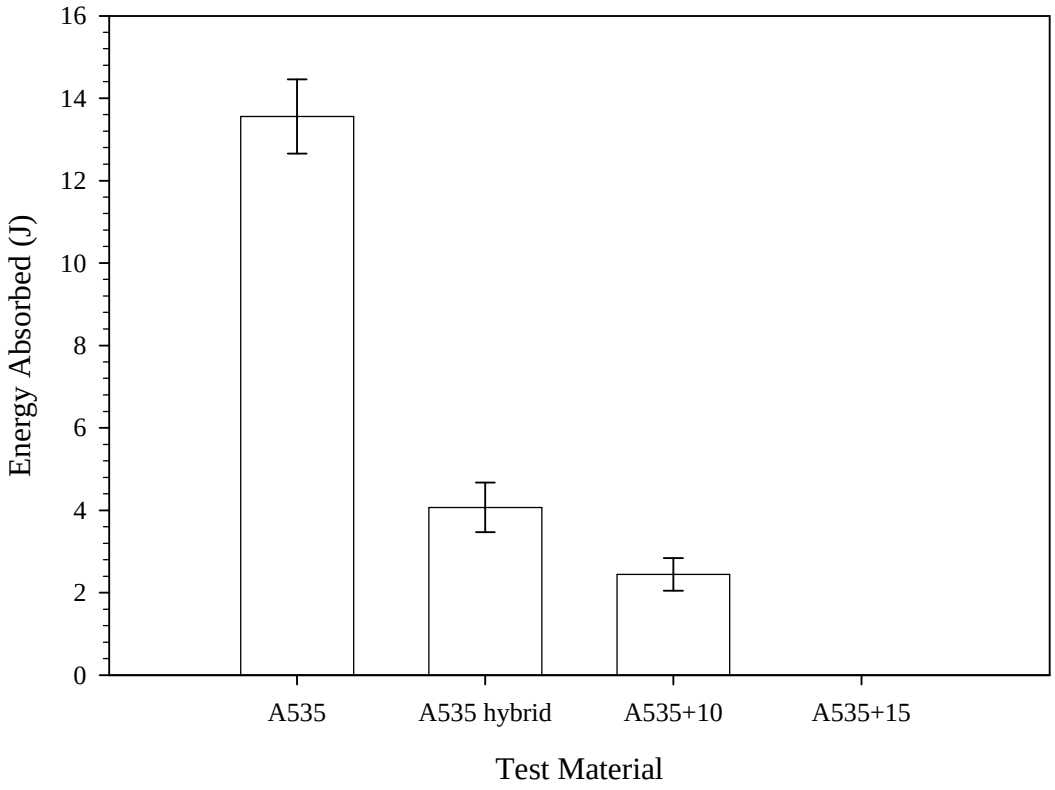

Figure 4.8. Variation of Charpy Impact energy with fly ash content for the samples tested.

can be seen that fly ash is more effective than SiC in reducing the mechanical properties of A535. The impact energy of A535+15 could not be measured as no energy could be detected on fracturing it.

4.4.3.2 Fractography

Typical optical micrographs of fractured samples of unreinforced A535 alloy and its MMCs are shown in Figures 4.9(a) – (d). The amount of lateral expansion on the compression side of the specimens can be seen to decrease with increasing fly ash content. No lateral expansion is observed in A535+10 and A535+15 specimens.

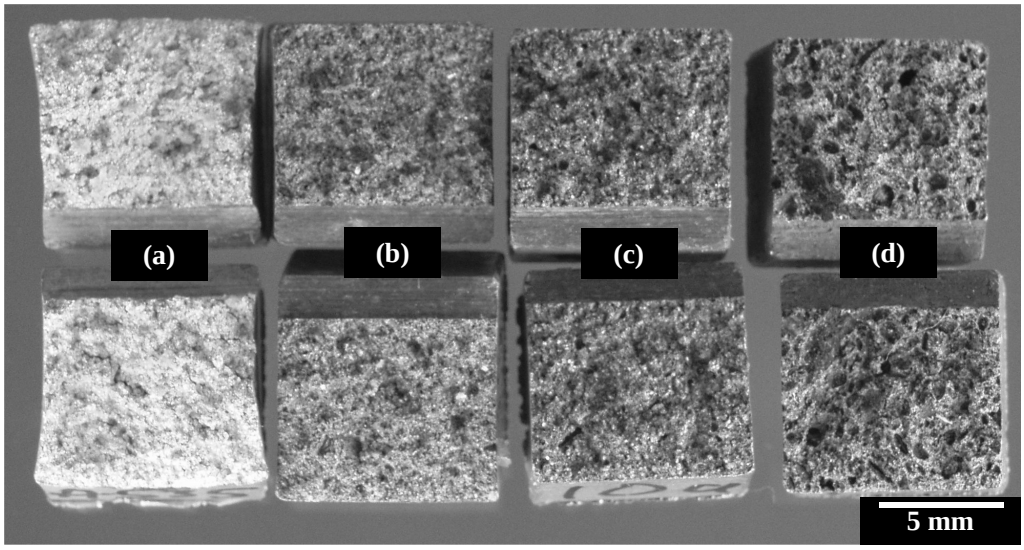

Figure 4.9. Optical micrographs showing the fracture surface appearance for: (a) A535, (b) A535 hybrid, (c) A535+10 hybrid and (d) A535+15 after impact testing.

The SEM micrographs of fractured surfaces of the unreinforced A535 alloy, A535 hybrid, A535+10 and A535+15 composites obtained from Charpy testing are shown in Figures 4.10(a) – (d) respectively. These fractographs reveal some important variations in the appearance of the fractured surfaces with respect to the level of reinforcement. The fracture surface of A535 is characterized by the presence of colonies of small ductile dimples, large cleavage facets and matrix cracks, which underscores the brittle nature of this alloy. Increasing the fly ash content resulted in more flat, faceted appearance, coupled with poorly defined dimples.

Particle pullout was observed in the MMCs as indicated by the white arrow labelled X in Figure 4.10(b). These pullouts tend to occur near particles where the matrix stresses are large, or near particle clusters where the local plastic strains are likely to be highest [139]. Particle fracture, driven by the development of large particle stresses was also observed in the MMCs as indicated by arrows Y in Figures 4.10(b) – (d).

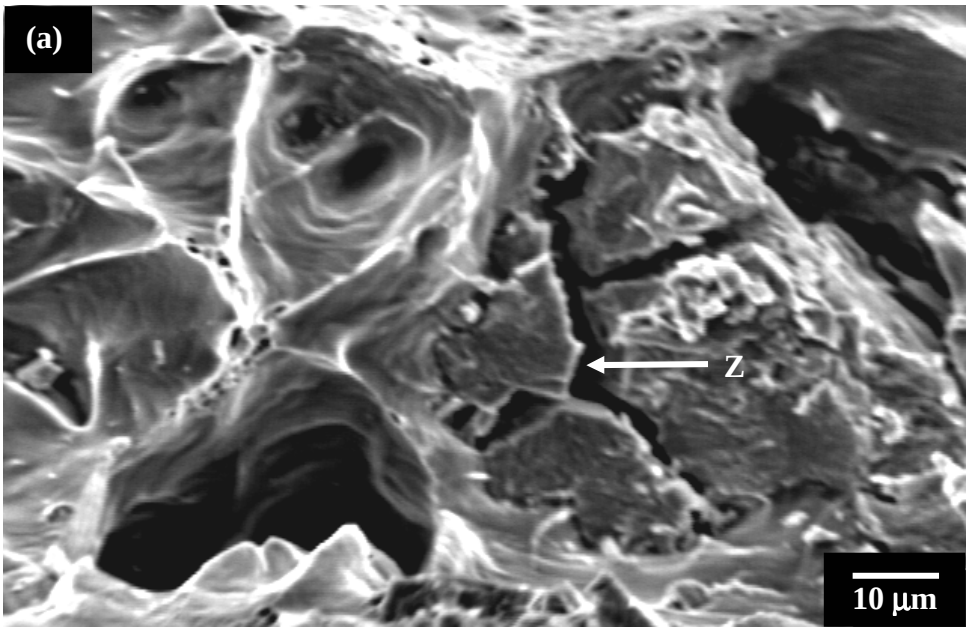
(a)
Z
10 µm

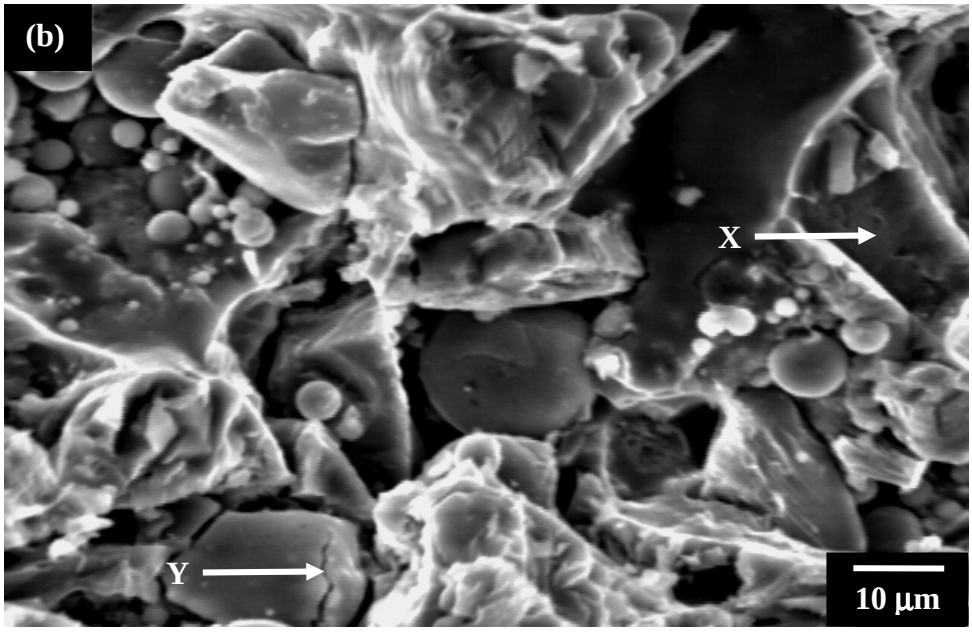
(b)
X
Y
10 µm

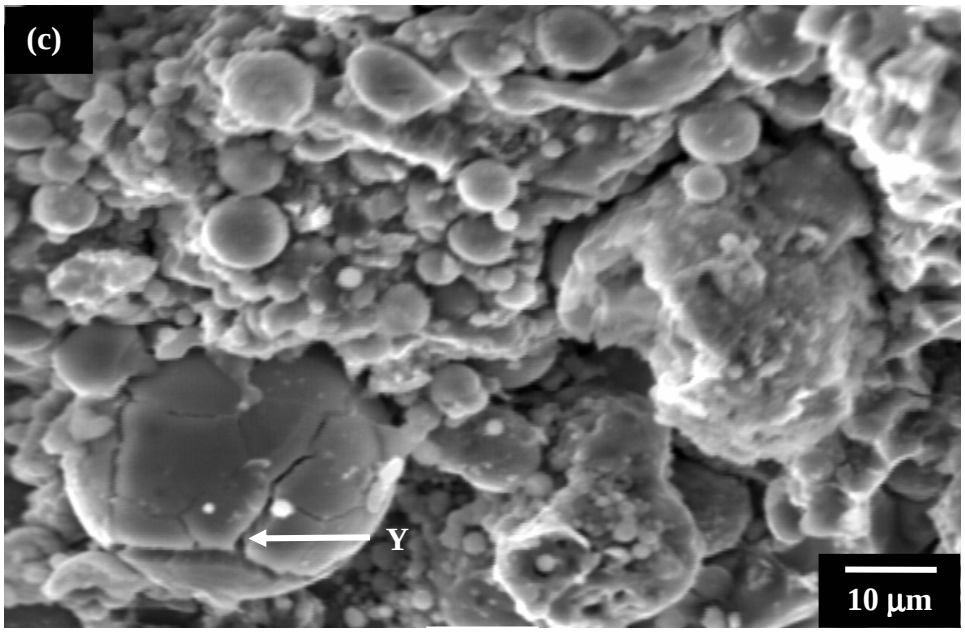

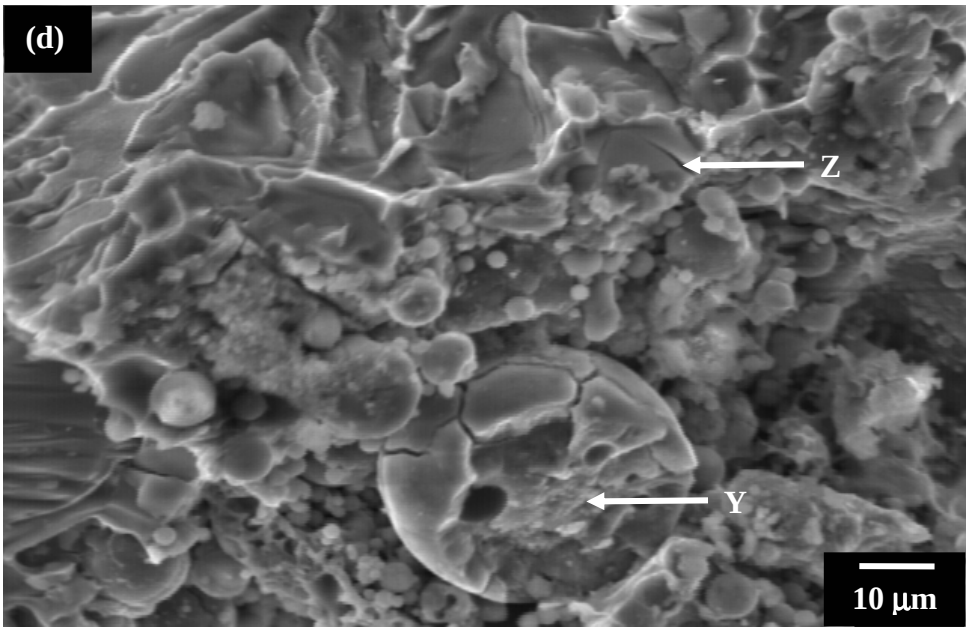

Figure 4.10. SEM fractographs of Charpy samples of (a) A535alloy, (b) A535 hybrid, (c) A535+10 and (d) A535+ 15.

Generally, the larger particles are more susceptible to breakage than the smaller ones. This may be attributed to the fact that there is a higher probability of finding a flaw of

critical size in larger particles than in their smaller counterparts. Larger particles are also more likely to be cracked during the fabrication processes [140,141].

Stress relieving cracks were also observed in the unreinforced A535 alloy and MMCs as indicated by arrows Z in Figures 4.18(a) and (d). A mismatch in the coefficients of thermal expansion (CTE) of the reinforcement particles and the matrix results in a mismatch in strain, which induces thermal stresses in the constituents during fabrication. The CTE of the particles is usually much less than that of the matrix. During the cooling process, both constituents shrink but the full contraction of the matrix is constrained as a consequence of being bonded to the particle. The particle is therefore compressed by the constrained shrinkage of the matrix. As a result, residual axial compressive stresses are induced in the particle. At the same time, the matrix is constrained by the particle from fully shrinking, and as a result, is stressed in tension. Stress transfer from particle to matrix then takes place leading to the development of cracks in the matrix [142].

4.4.4 Tensile Test

4.4.4.1 Room Temperature

Figure 4.11 shows the typical room temperature stress versus strain curves obtained for the solution heated treated test materials from which the tensile strength and 0.2% offset yield strength were calculated. The typical room temperature stress versus strain curves for as-cast test materials is shown in Appendix C. The variation in the tensile strength of the unreinforced A535 and the three MMCs with fly ash content is shown in Figure 4.12

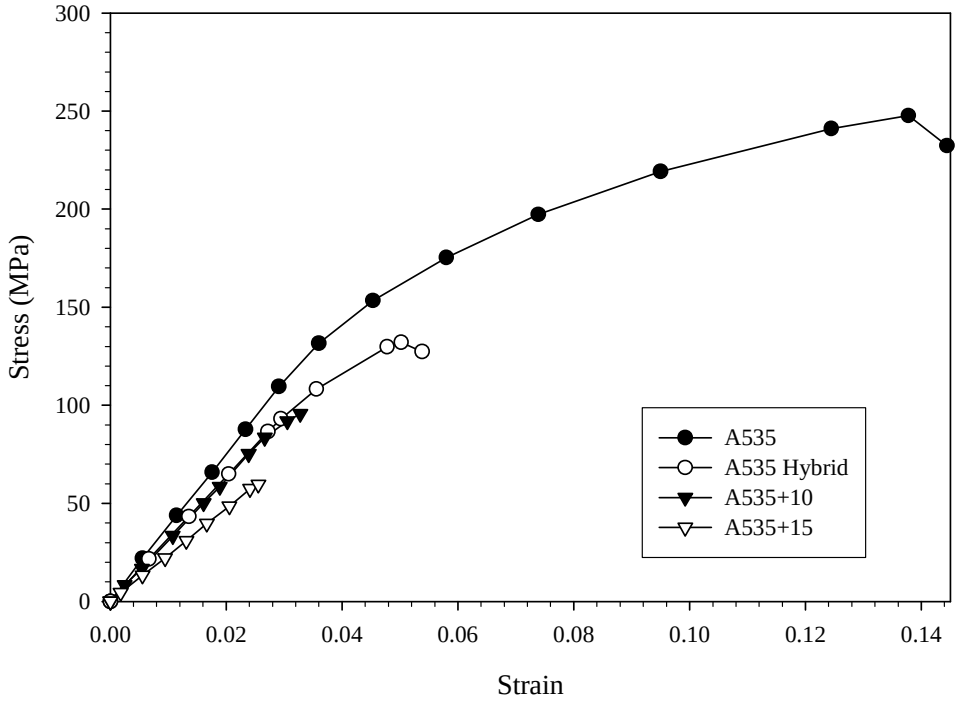

Figure 4.11. Typical stress versus strain curves obtained for solution heat treated samples at room temperature.

for the as-cast and solution heat treated conditions. Both curves show similar pattern. As observed in the previous results, increasing the weight percent of fly ash in A535 decreased the tensile properties of the resulting MMCs. The tensile result is contrary to the results published by Kolukisa *et al.* [4]. They observed an increase in tensile strength with increasing fly ash content (up to 15 vol.%) for A360 and 443 aluminium alloys.

The tensile strength of A535 hybrid was again higher than that of A535+10. Since both composites contain porosity, though to different levels, the better performance of the hybrid composite is attributed mainly to a higher wettability of SiC particles by molten Mg in the matrix melt. Higher wettability of the SiC particles was as a result of their planar shape and coarser sizes compared to that of fly ash [128,143,144].

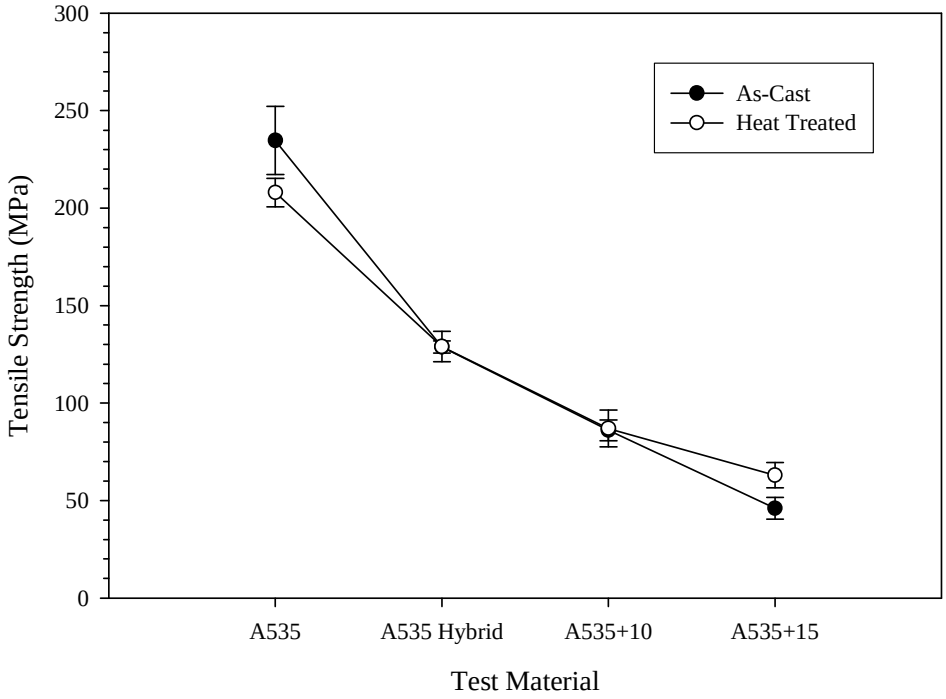

Figure 4.12. Variation of tensile strength with fly ash content for test materials at room temperature.

It seems the presence of superficially oxidized particles in fly ash inhibit the formation of adhesive bonding between the molten matrix and the fly ash constituents. The average tensile strength obtained for the as-cast A535 was 235 MPa and that for the solution heat-treated samples was 228 MPa. These compare fairly well with 241 MPa published in the literature for this alloy [55,56].

Figure 4.13 shows the variation of the yield strength of the alloy and composites with fly ash content for the as-cast and solution heat-treated samples. The yield strength of A535+15 composite could not be determined because the sample failed without any measurable plastic deformation. The average yield strengths of the as-cast (137 MPa) and heat-treated (133 MPa) are slightly higher than 124 MPa in Reference [55, 56] for A535 alloy.

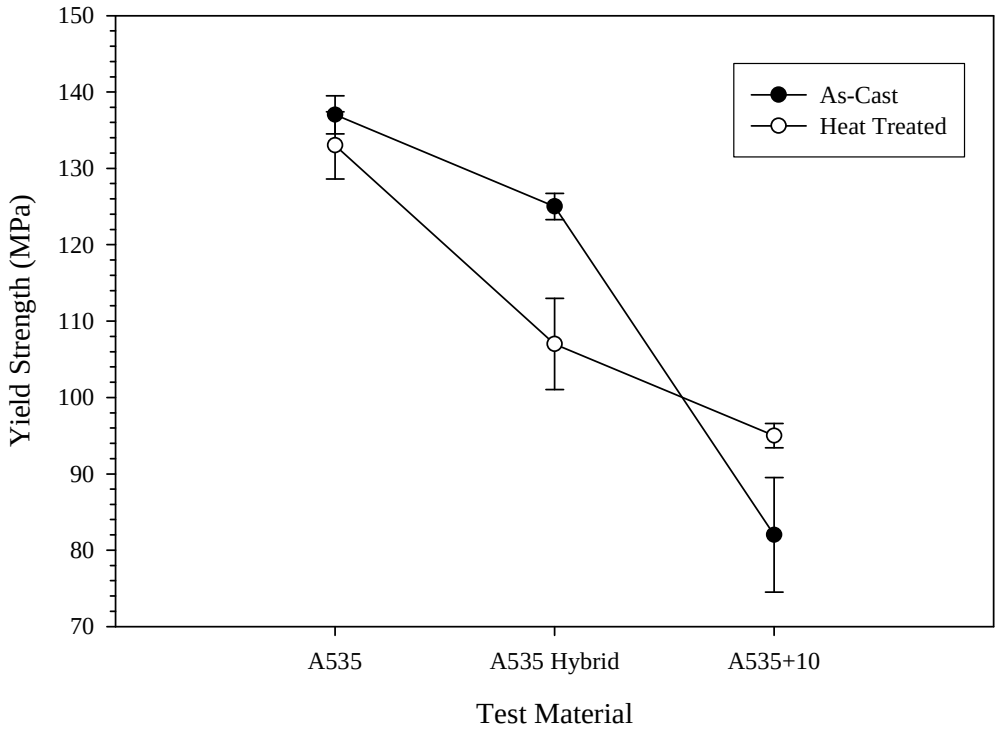

Figure 4.13. Variation of yield strength with fly ash content for test materials at room temperature.

Figure 4.14 shows the variation of percent elongation with fly ash content for the samples. The percent elongation of the as-cast and solution heat treated specimens showed similar pattern to that obtained for the tensile strength. Increased reinforcement content led to a decline in percent elongation. The percent elongation conforms to the results published by Kolukisa *et al.* [4]. They observed a decrease in percent elongation with increasing fly ash content for A360 and 443 aluminium alloys. The percent elongation of A535 hybrid is again higher than that of A535+10 thus reinforcing the point that the mechanical properties of A535 are more adversely affected by the presence of fly ash than SiC due to the size and shape of the particles.

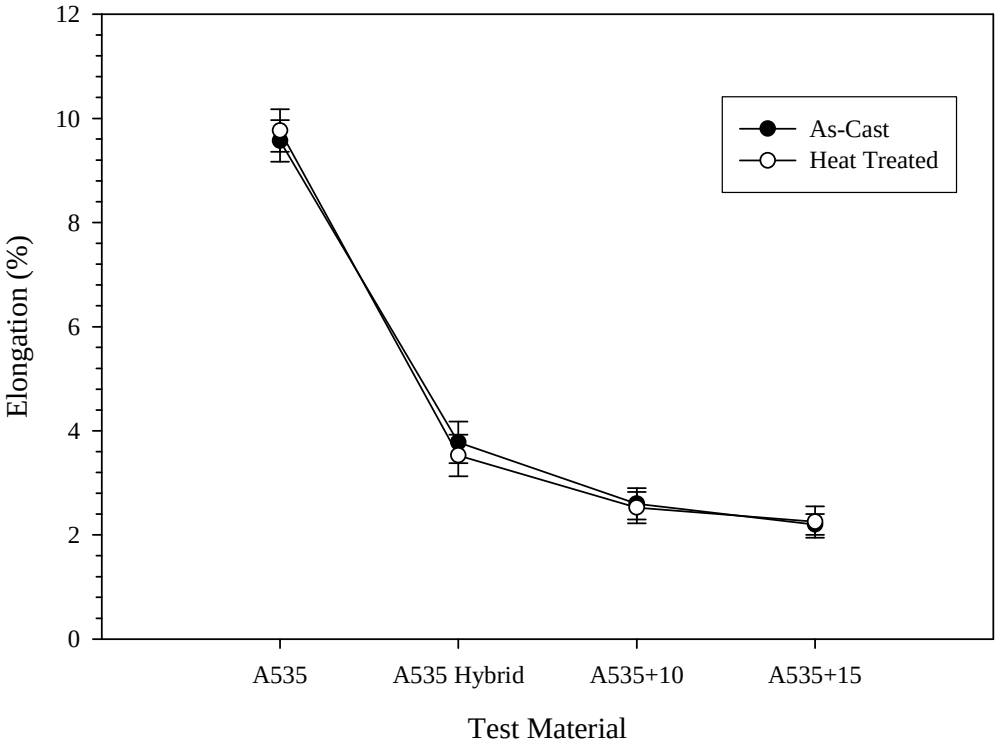

Figure 4.14. Variation of percent elongation with fly ash content for test materials at room temperature.

The decrease in the mechanical properties of the composites is attributed to porosity and particle clustering, which increased with increasing fly ash content. The high level of porosity in the composites increases crack initiation sites. Several researchers have studied the effect of porosity on the mechanical properties of metallic alloys and MMCs [30,33,35,136-138].

The general conclusions from the tensile studies are that:

(i) pores located at the matrix-reinforcement interface cause debonding of the particles from the matrix under low stress thereby reducing the ability of the matrix to transfer load to the particles,

(ii) pores (especially those located in the matrix away from the particles) reduce the effective cross-sectional area supporting the applied load, and

(iii) pores act as stress concentrators - for isolated pores of different geometries, an applied tensile stress is amplified by several factors.

4.4.4.2 High Temperature Mechanical Properties

In order for these composites to be applied in automobiles engines, their high temperature tensile behaviour were determined. Temperature of 150 °C, 200 °C, 250 °C and 300 °C were chosen because the maximum temperature of an automobile engine ranges between 240 °C and 250 °C. Figure 4.15 shows the typical stress versus strain curves obtained at 150 °C for the test materials. The tensile strength and 0.2% offset yield strength at 150 °C were calculated from this stress versus strain curves. The typical room temperature stress versus strain curves for the test materials at temperatures of 150 °C, 250 °C and 300 °C are shown in Appendix C.

The variation in the tensile strength of A535 alloy and the three MMCs with fly ash content is shown in Figure 4.16 for the high temperature tests. Similar to earlier tests, all the curves followed the same pattern. The tensile strength decreased with increasing temperatures. They also decreased with increasing weight percent fly ash in A535 alloy. This is in agreement to the results obtained by Chan *et al.* [145]. They also observed a decrease in tensile strength with increasing temperatures for A356 alloy between the temperatures of 150 °C and 300 °C.

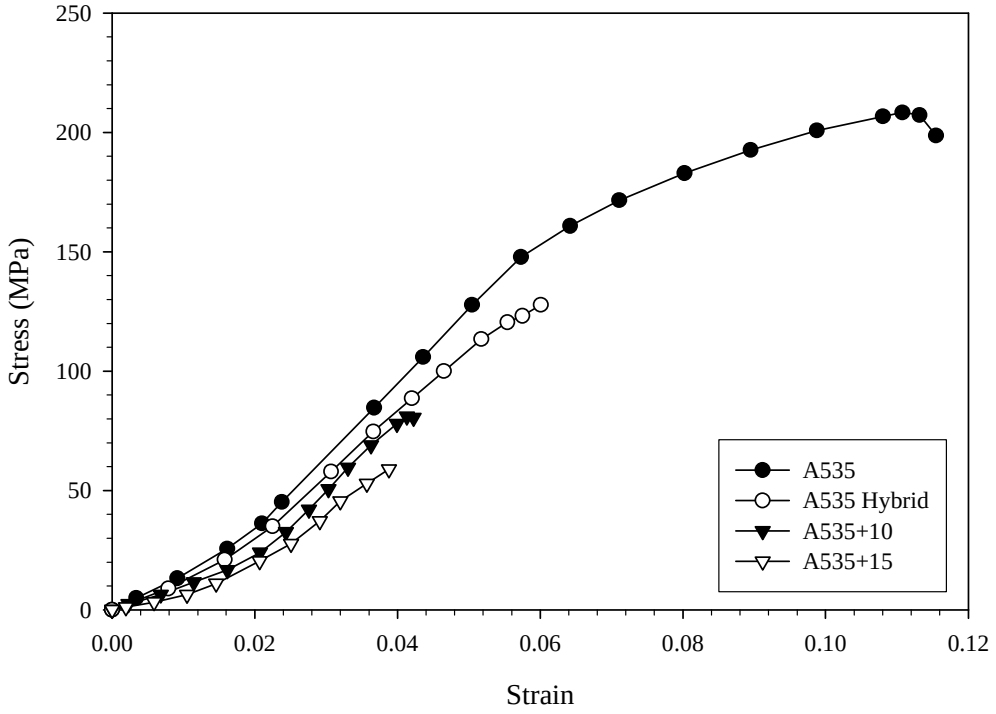

Figure 4.15. Typical stress versus strain curves obtained for test materials at 150 °C.

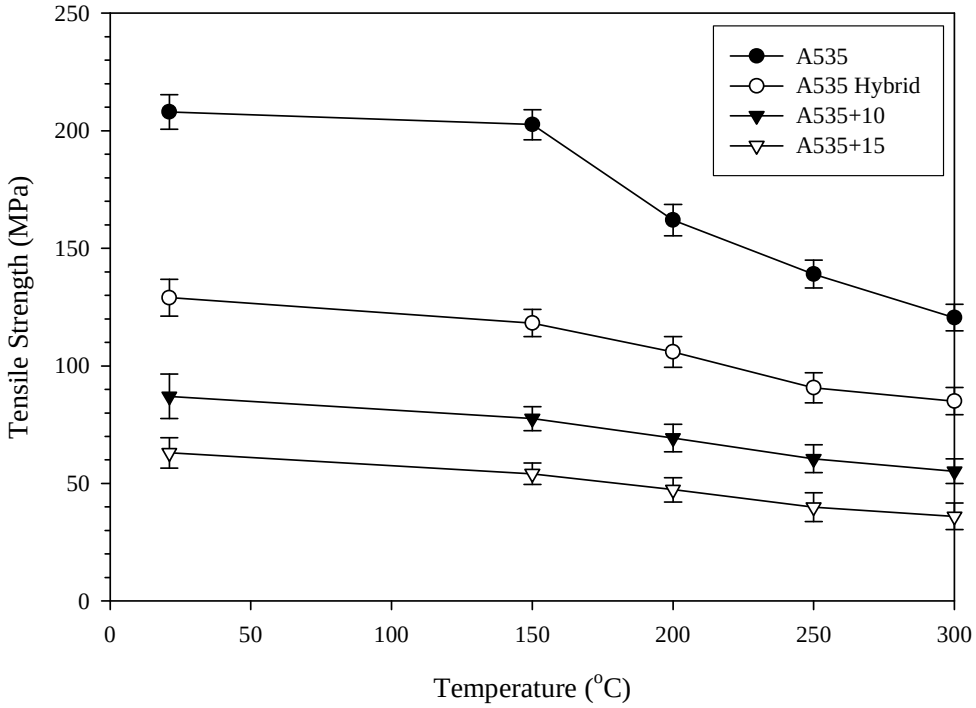

Figure 4.16. Variation of tensile strength with fly ash content for test materials at elevated temperatures.

The yield strengths of the composites could not be determined at the elevated temperatures. They failed without any observable plastic deformation. The variation of yield strength of A535 alloy with temperature is shown in Figure 4.17. The yield strength decreases with increasing temperature. Chan *et al.* [145] however observed an increase in the yield strength of A356 alloy with temperature up to 250 °C. They then noticed a drastic decline in the yield strength with temperature above 250 °C. Figure 4.18 shows the variation of percent elongation with fly ash content for the test materials at elevated temperatures. The percent elongation was found to increase with temperature up to 150 °C for all the test materials. It then decreased with increasing temperature. Increasing fly ash content was also seen to affect the percent elongation. Chan *et al.* [145] also observed similar findings with A356 alloy. They reported that the percent elongation of A356 alloy was independent of temperature below 150 °C. The percent elongation then begins to fall with increasing temperature up to 300 °C.

Dorward [146] reported the heterogeneous precipitation of Mg_2Si at temperatures above the GP zone solvus temperature, about 146 °C, for Al-Si-Mg alloys containing 0.6% to 0.9% Mg_2Si. Hence, precipitation takes places during the tension tests at these elevated temperatures. This resulted in the depletion of solid solution strengthening magnesium in the matrix which further led to the observed decline in mechanical properties with increasing temperature. The lower mechanical properties of A535+10 compared with A535 hybrid further reinforces the fact that fly ash is more pronounced in affecting the overall mechanical behaviour of A535 than SiC.

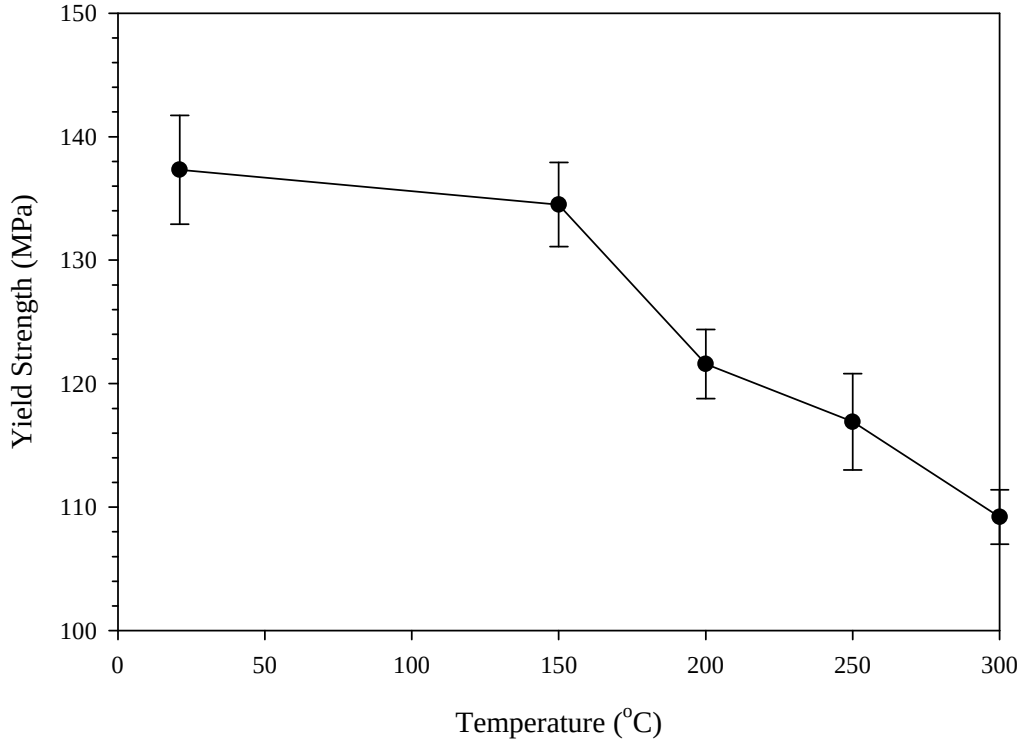

Figure 4.17. Variation of yield strength with temperature for A535 alloy.

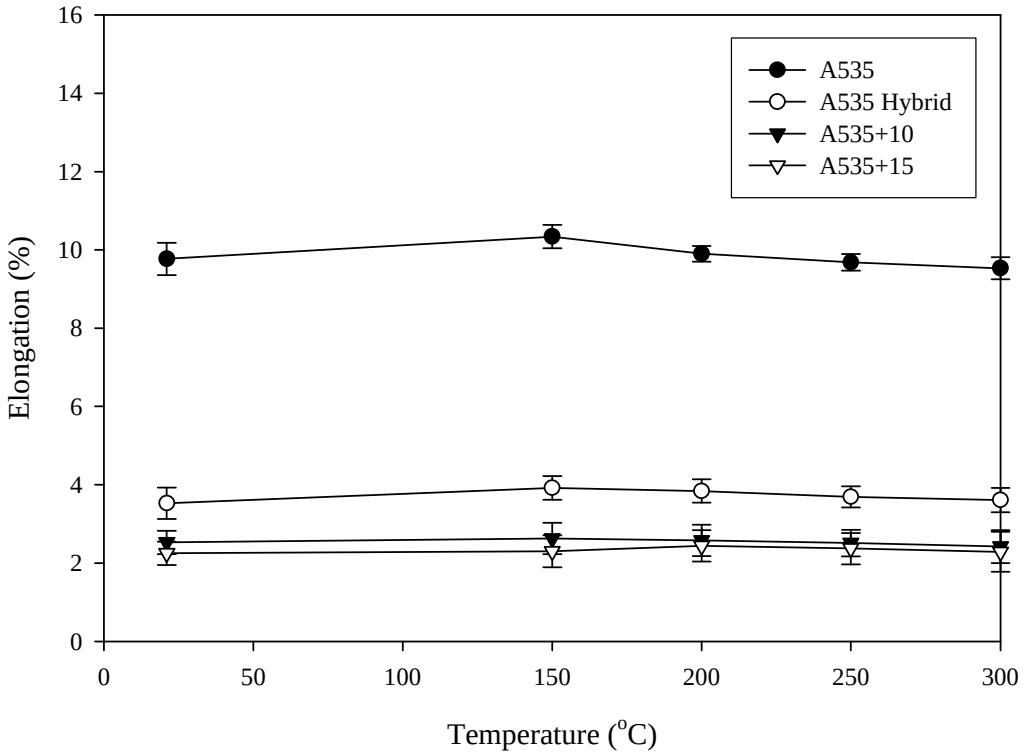

Figure 4.18. Variation of percent elongation with fly ash content for test materials at elevated temperatures.

4.4.4.3 Fractography

Figures 4.19(a) – (d) show the respective SEM micrographs of fractured surfaces of the unreinforced A535 alloy, A535 hybrid, A535+10 and A535+15 composites obtained from tensile testing at room temperature. The results of these fractographs are similar to those obtained from the Charpy test. Colonies of small ductile dimples and large cleavage facets were the main features observed on the fractured surface of A535 alloy. The addition of reinforcement particles led to a more flat, faceted appearance, coupled with poorly defined dimples. Particle pullout and cracks were also seen in the MMCs.

Particle pullout in the MMCs is labelled by arrows X in Figures 4.19(b) – (d). Particle fracture is indicated by arrow Y in Figure 4.19(c) while arrow Z in Figure 4.19(d) is used to label the stress relieving cracks. The presence of stress relieving cracks reaffirms the brittle nature of A535 alloy. Also, increasing reinforcement content leads to a more brittle material. Particle debonding, matrix cracking and particle fracture are therefore the main damage mechanisms observed in these MMCs under any mechanical loading.

4.5 Microstructural Studies

4.5.1 Nature of Fly Ash Particles

The distribution of reinforcement particles was examined using a JEOL Model 5600 Scanning Electron Microscope equipped with an EDAX Genesis 7000 Energy Dispersive X-ray Spectrometer. Figures 4.20(a) – (h) are the X-ray maps showing the

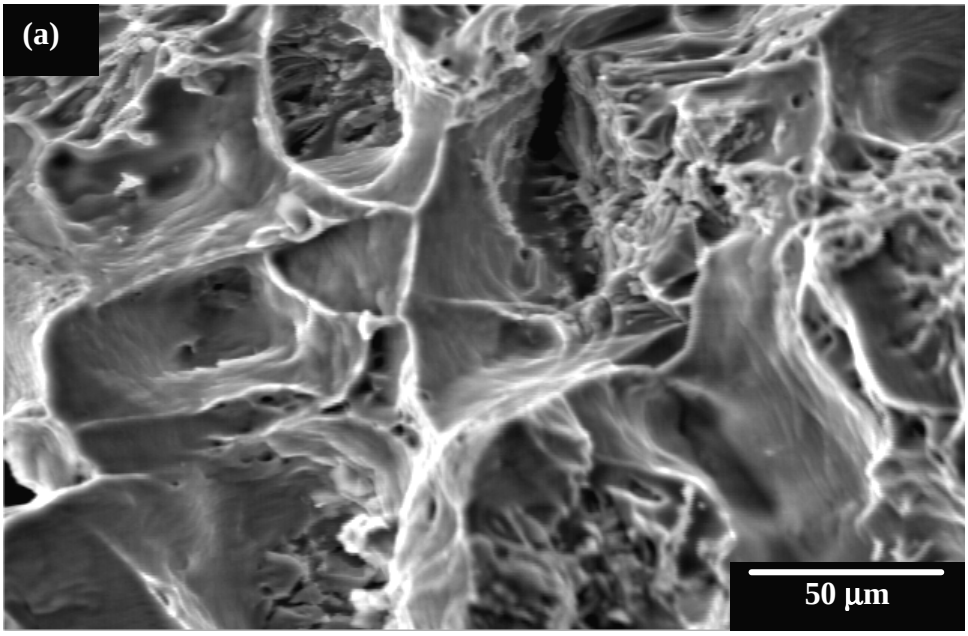
(a)
50 µm

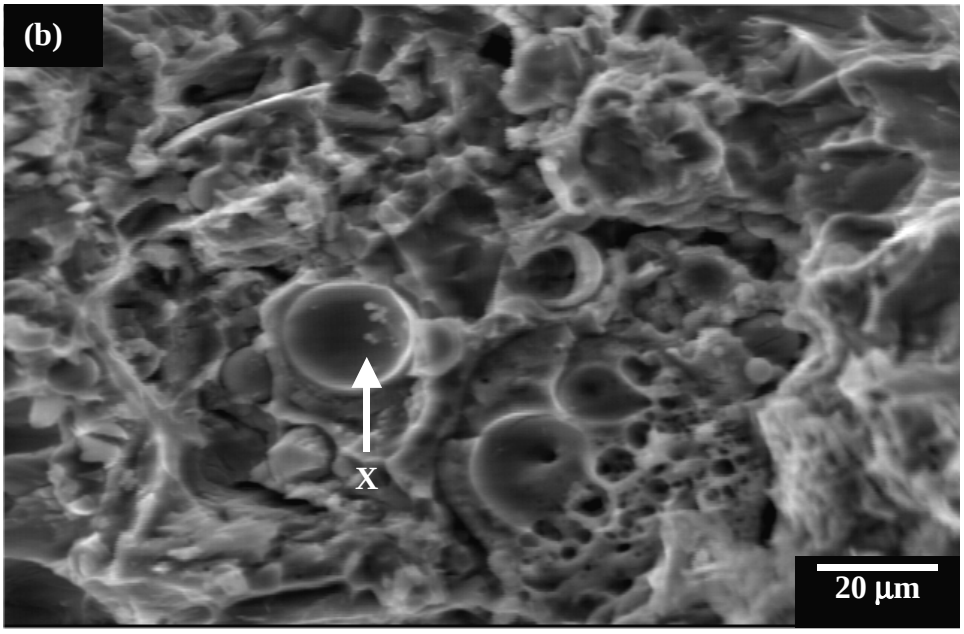
(b)
X
20 µm

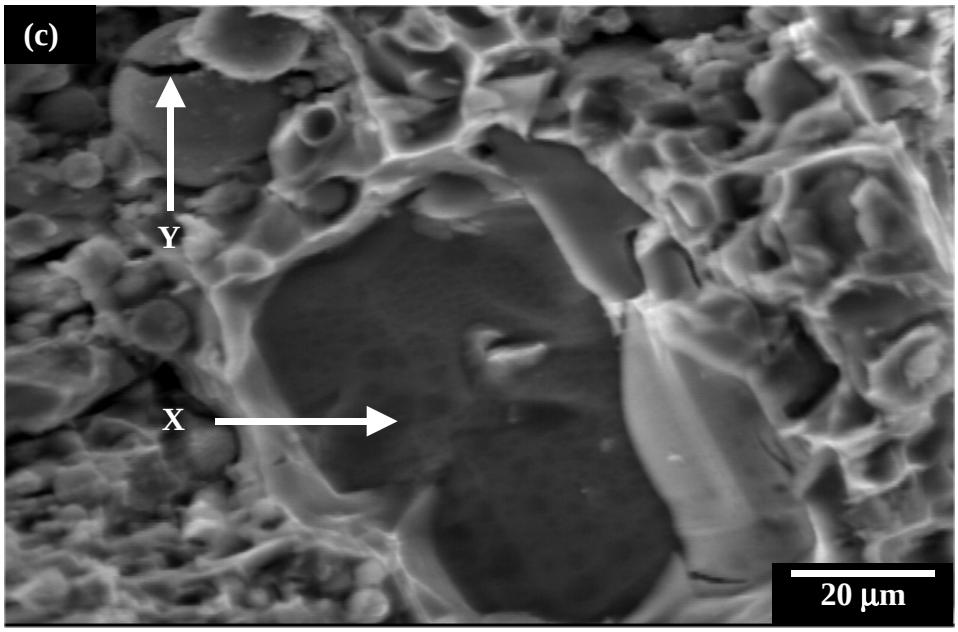

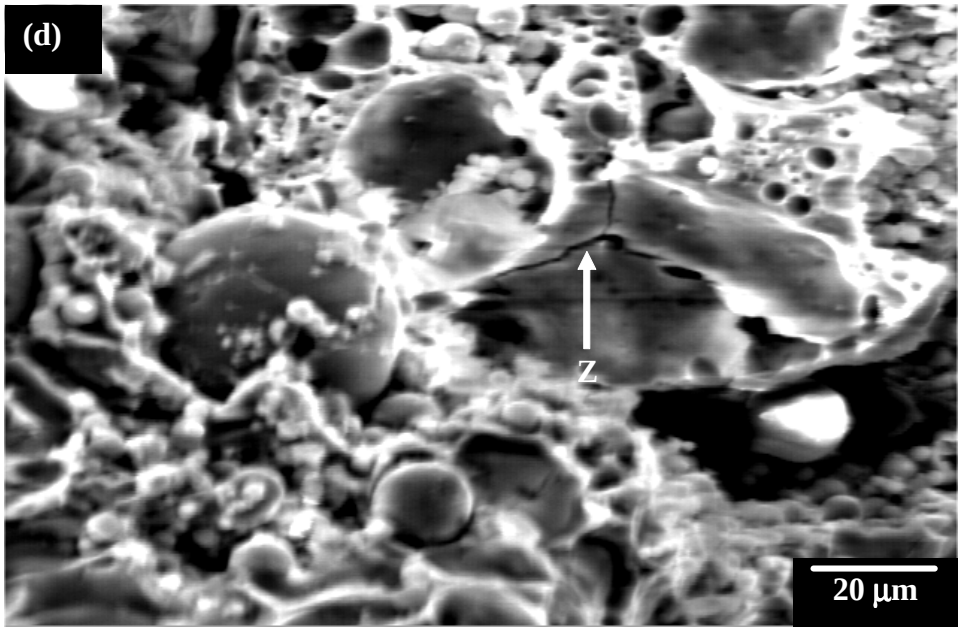

Figure 4.19. SEM fractographs of tensile samples of (a) A535alloy, (b) A535 hybrid, (c) A535+10 and (d) A535+ 15.

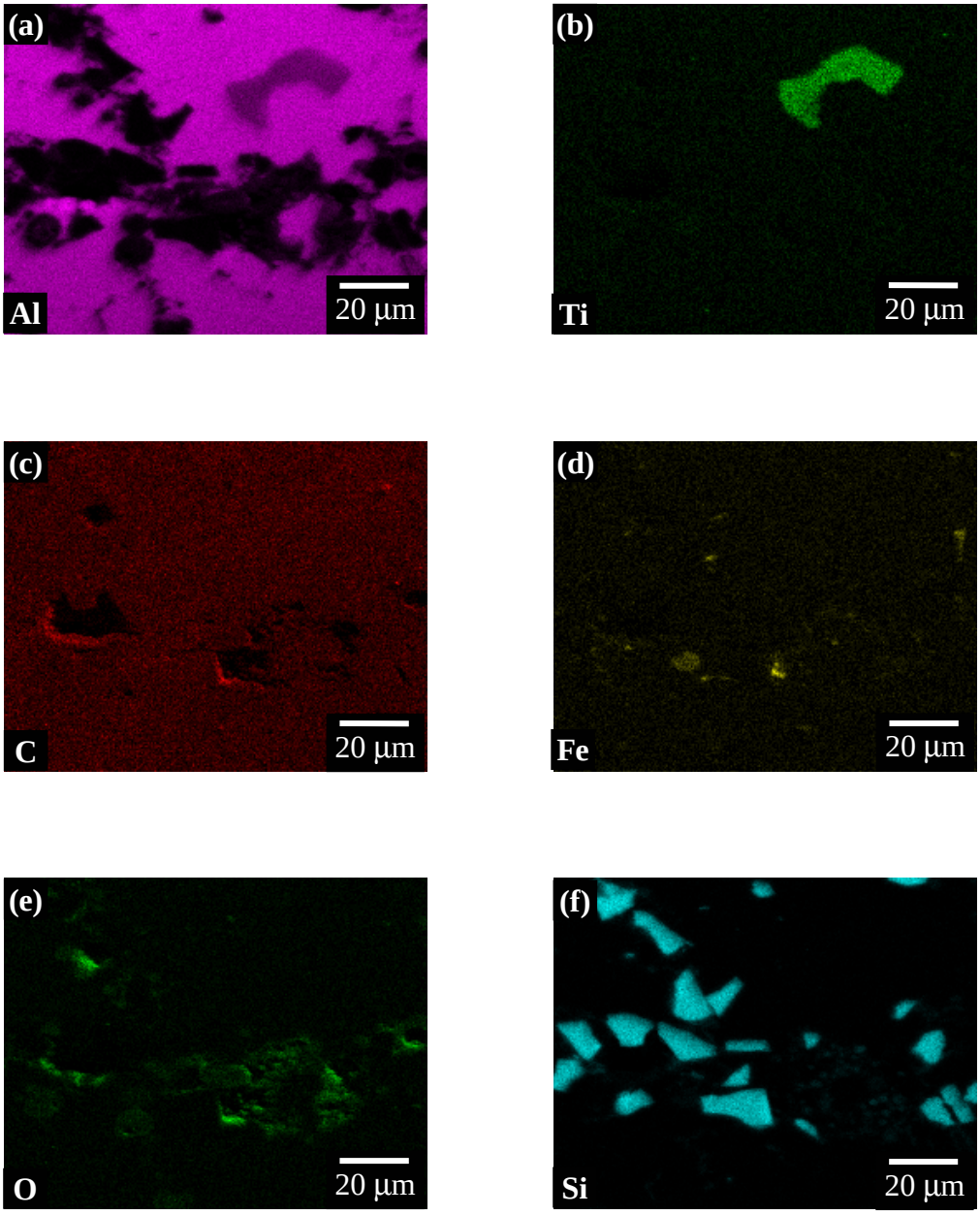
(a)
Al
20 µm
(b)
Ti
20 µm
(c)
C
20 µm
(d)
Fe
20 µm
(e)
O
20 µm
(f)
Si
20 µm

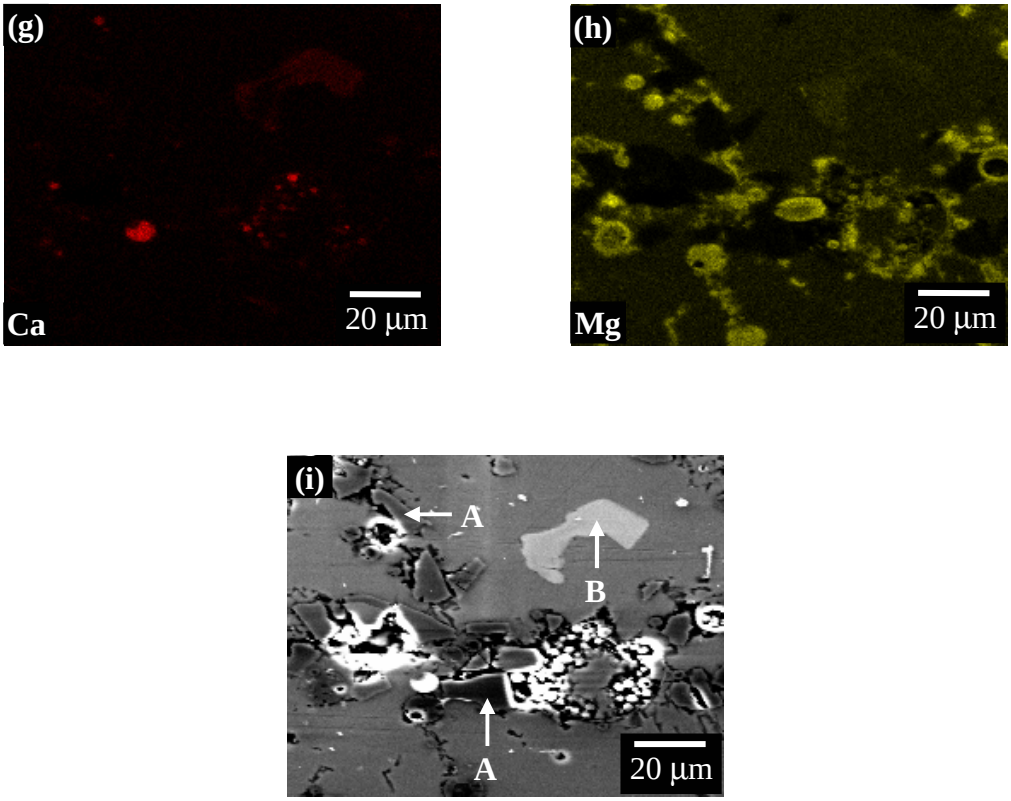

Figure 4.20. X-ray maps showing (a) aluminium, (b) titanium, (c) carbon, (d) iron, (e) oxygen, (f) silicon, (g) calcium, and (h) magnesium, in (i) heat treated A535 hybrid.

distribution of aluminium, titanium, carbon, iron, oxygen, silicon, calcium and magnesium respectively in an heat treated A535 hybrid (see Figure 4.20(i)). Figures 4.21 (a) and (b) show the energy dispersive spectrometry (EDS) of a typical SiC particle and a Ti rich intermetallic particle respectively. Figures 4.22(a)-(h) are the X-ray maps showing the distribution of aluminium, oxygen, titanium, iron, manganese, silicon, calcium, and magnesium respectively in a heat-treated A535+10 composite (see Figure 4.22(i)). Figures 4.23(a) – (c) show the EDS of typical high Fe and Mn rich; high Si, Fe, and O rich; and high Mg and O rich particles respectively.

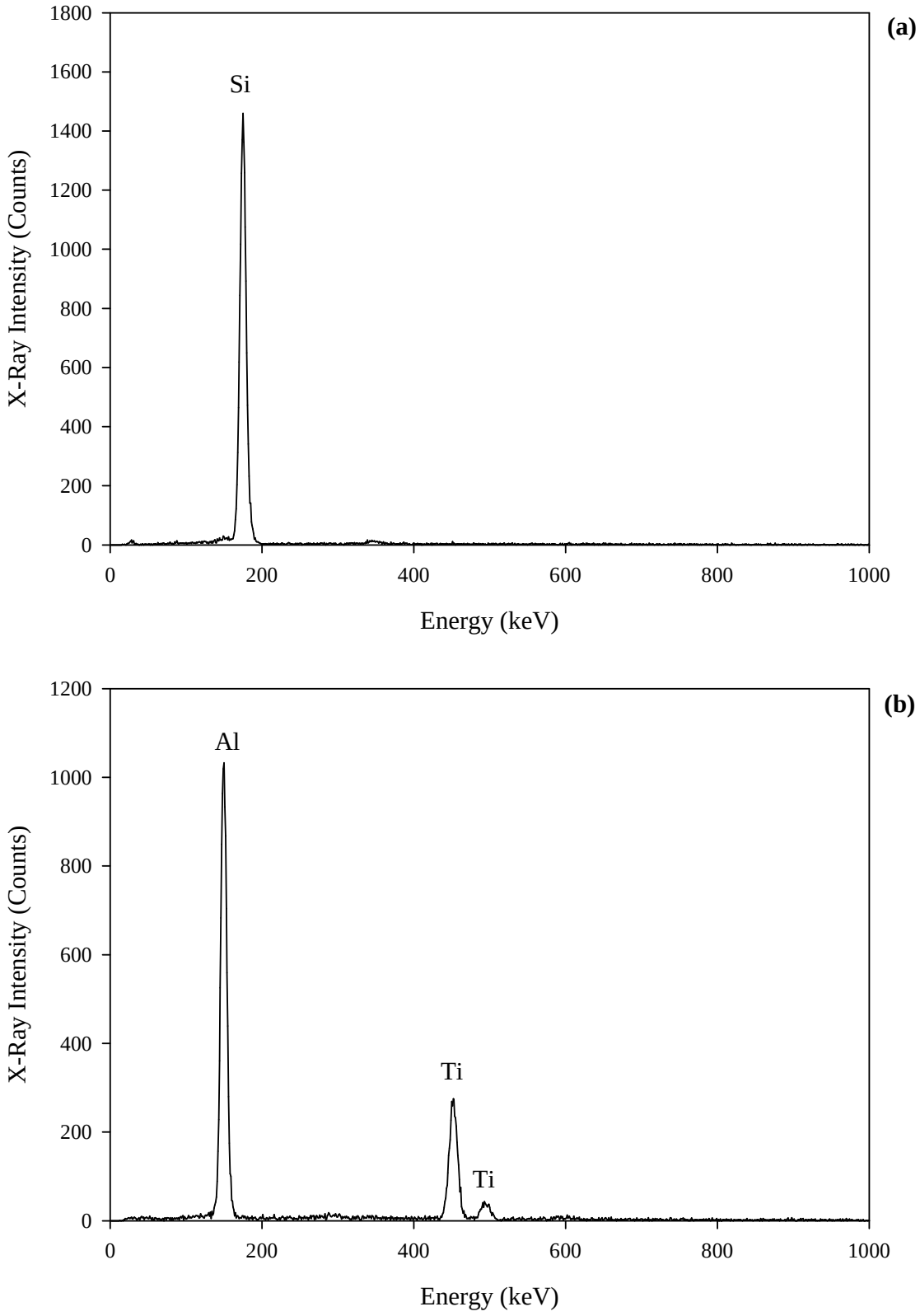

Figure 4.21. EDS spectra from (a) a SiC particle and (b) a Ti rich intermetallic particle labelled A and B respectively in Figure 4.14(i).

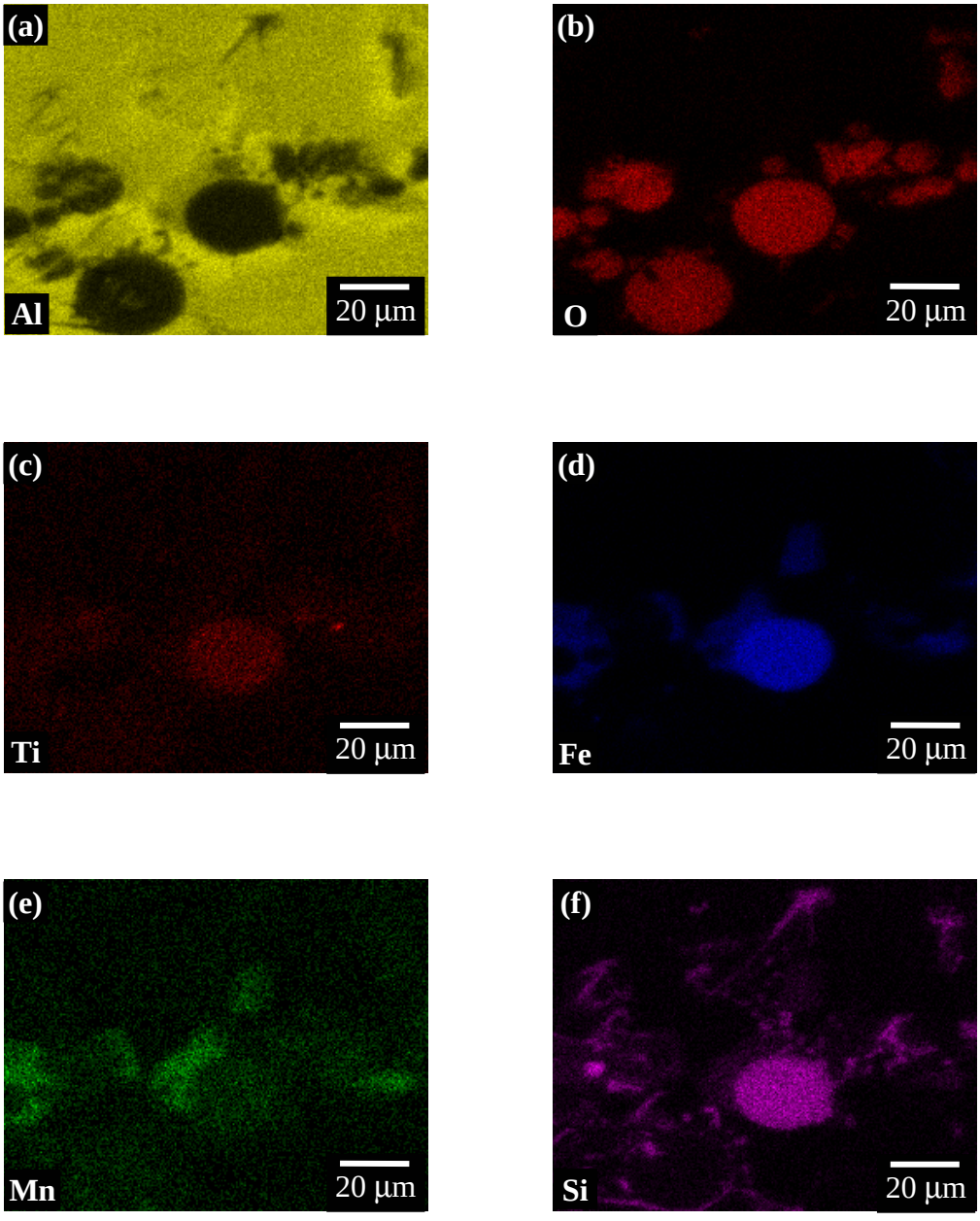
(a)
Al
20 µm
(b)
O
20 µm
(c)
Ti
20 µm
(d)
Fe
20 µm
(e)
Mn
20 µm
(f)
Si
20 µm

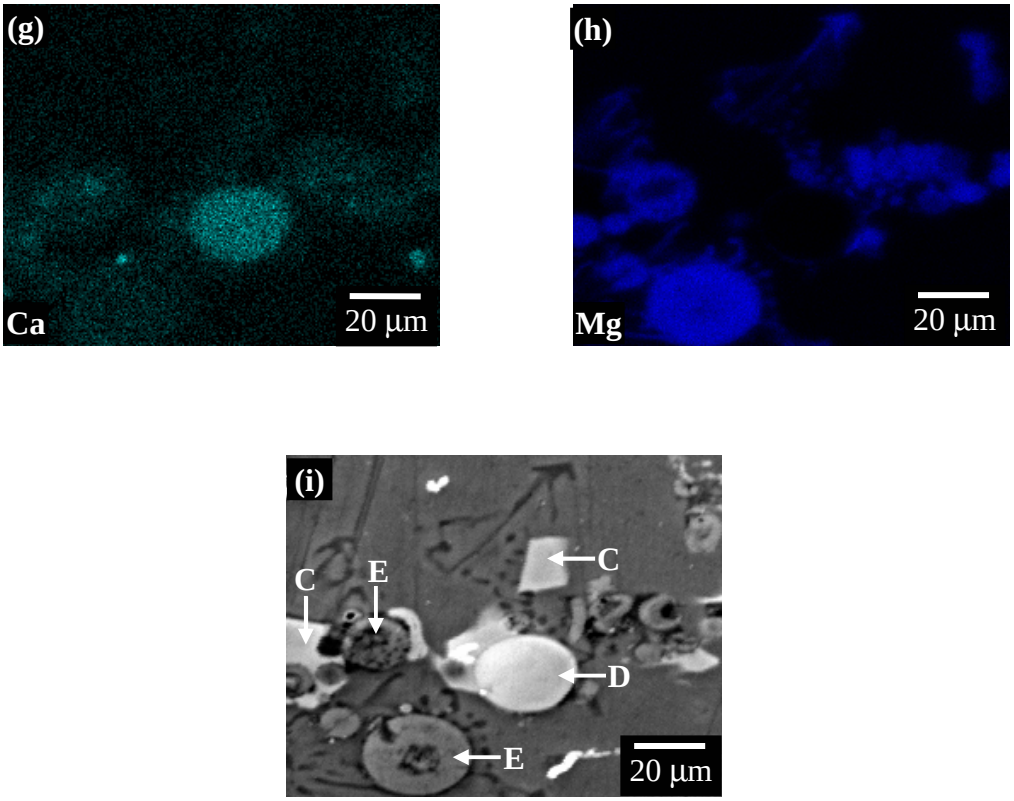

Figure 4.22. X-ray maps showing (a) aluminium, (b) oxygen, (c) titanium, (d) iron, (e) manganese, (f) silicon, (g) calcium, and (h) magnesium, in (i) heat treated A535+10.

The EDAX Genesis 7000 Energy Dispersive X-ray Spectrometer could not generate peaks at low energy levels. Hence carbon could not be quantified for this study. SiC particles were identified in Figure 4.20(i) to be mostly angular, irregular shaped, and of different sizes. The bulk chemical composition of ashes is basically characterized by high amounts of SiO_2, Al_2O_3, and Fe_2O_3. The phase composition of these ashes is very complex. However, X-ray maps and EDS made it easier to identify the elements present in the various particles in the composites.

The Fe content was observed to be responsible for the white coloration in the fly ash particles. It was observed that the higher the Fe content, the whiter the particle. Particles containing Fe greater than 60 wt.% were found to be spherical in shape. Particles containing about 30 wt.% Fe with high Al content and minor amounts of Mn and Si were identified due to their unique shapes. These particles are labelled C in Figure 4.22(i). Particles of this shape were absent from the morphology of the fly ash particles studied using the SEM (see Figure 3.1). The EDS spectra of this high Fe and Mn rich; high Si, Fe, and O rich; and high Mg and O rich particles are shown in Figures 4.23 (a) – (c). These particles are believed to form during fabrication of the composites and as such, are responsible for the depletion of the Fe content observed from the chemical analysis of the extracted fly ash particles from the composites. Mg and O rich particles containing Al and Si (labelled E in Figure 4.22(i)) were also identified. They were found to be spherical in shape but darker in colour.

4.5.2 Other Intermetallic Phases

Two intermetallic particles were identified in the heat-treated A535 alloy. They are labelled B (Al-Ti rich) and C (Al-Fe-Mn rich) in the SEM micrograph as shown in Figures 4.24(a) and 4.25(a) respectively. A quantitative EDS of five respective particles of Al-Ti rich particle is shown in Table 4.7 with a typical EDS spectrum shown in Figures 4.24(b). Table 4.8 also shows the quantitative EDS of five respective particles of Al-Fe-Mn rich intermetallic particle with their typical EDS spectrum shown in Figure 4.25(b).

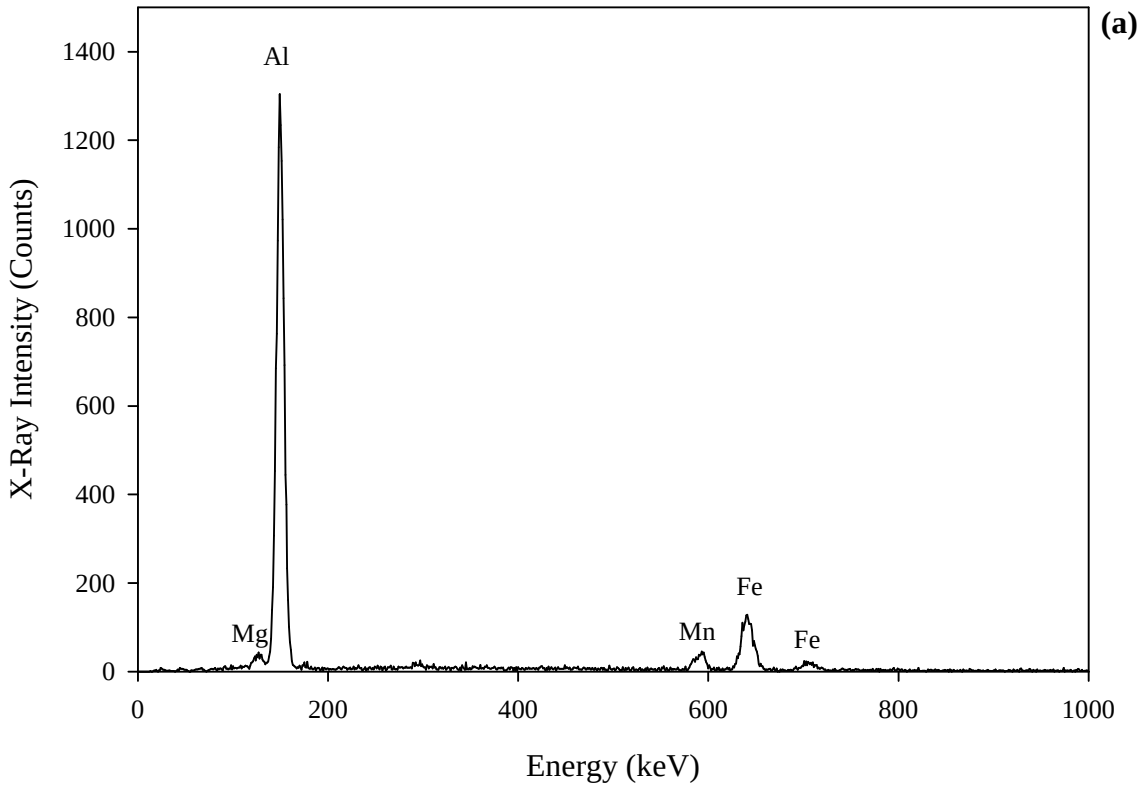
(a)
X-Ray Intensity (Counts)
Energy (keV)
Al
Mg
Mn
Fe
Fe
0
200
400
600
800
1000
1200
1400

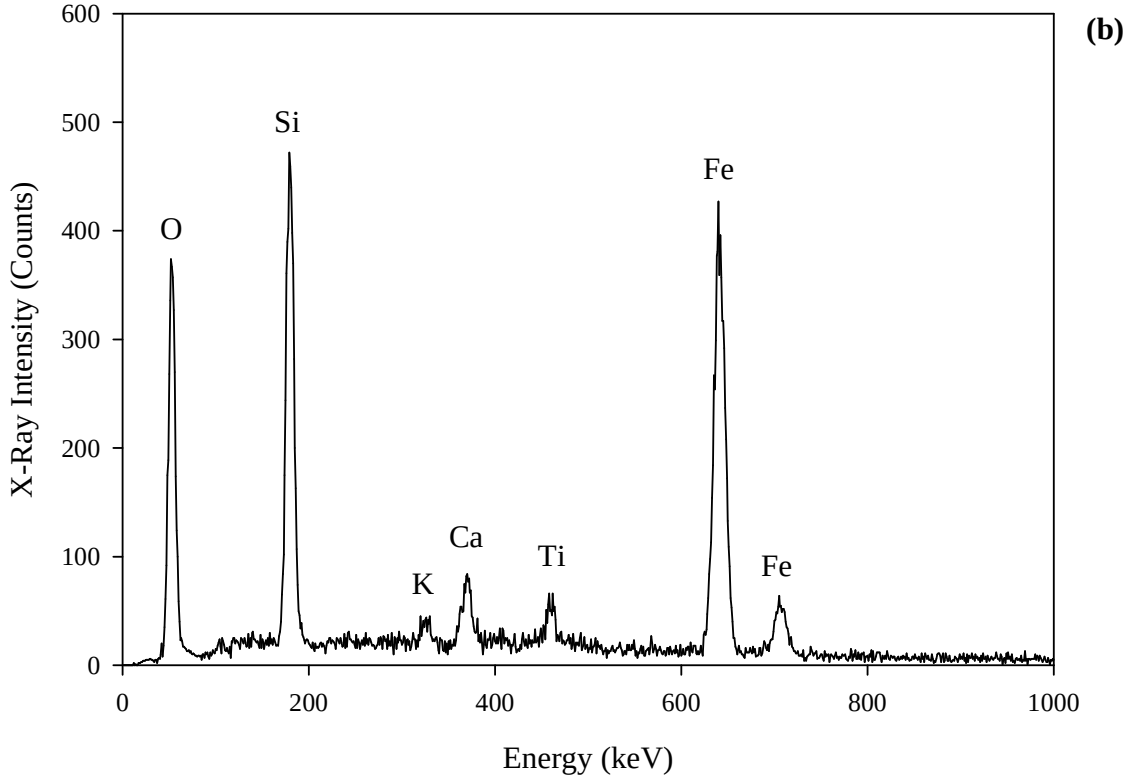
(b)
X-Ray Intensity (Counts)
Energy (keV)
O
Si
K
Ca
Ti
Fe
Fe
0
100
200
300
400
500
600

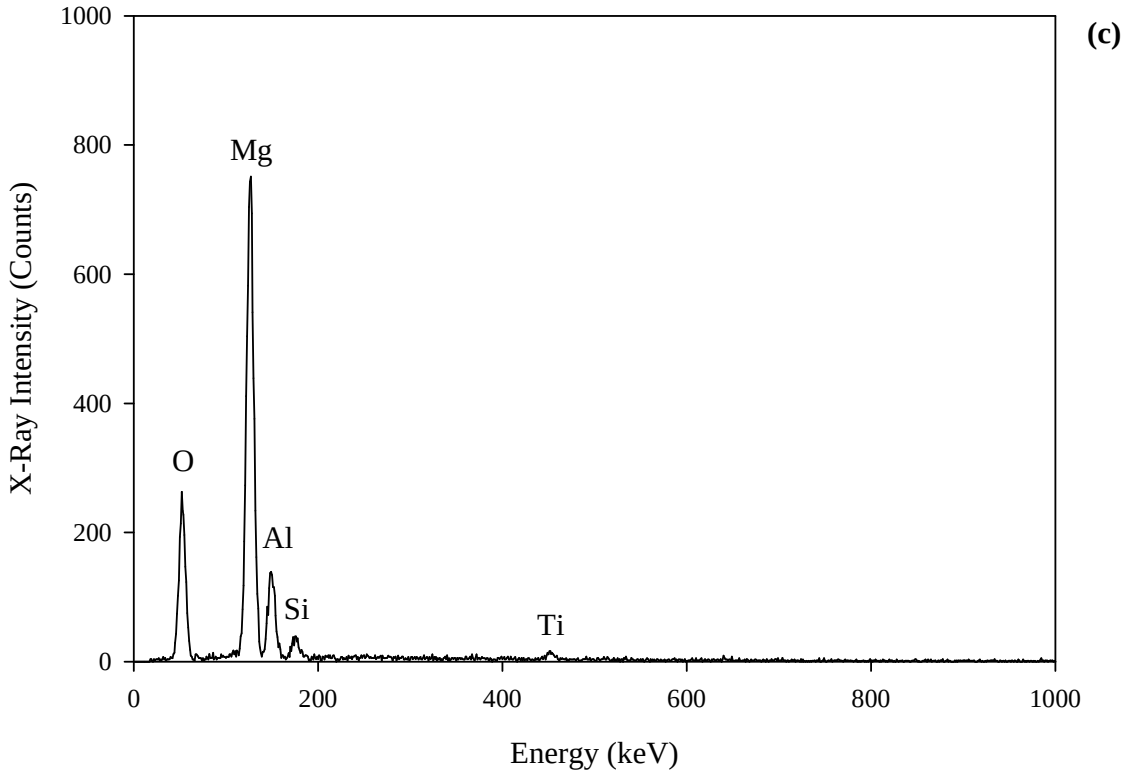

Figure 4.23. EDS spectra from a (a) high Fe, Mn rich, (b) high Si, Fe, and O rich, and (c) high Mg and O rich particles labelled C, D and E respectively in Figure 4.16(i).

The Al-Ti phase diagram (shown in Figure 4.26) compiled by Murray [147] gives an indication of the Al-Ti compounds that can be formed. The chemical formula from EDS analysis of these Al-Ti rich intermetallic particles in the test materials yielded Al_5Ti (See Table 4.7). However, the Al-Ti phase diagram only predicts the maximum number of Al atoms to be 3 resulting in the formation of Al_3Ti. Knight *et al.* [148] and Perepezko [149] have reported the existence of these Al_3Ti intermetallics with 75 at.% Al in aluminium alloys. They also reported these intermetallic particles to have face centred cubic structures. Fabrication and post-fabrication processes for the test materials used in this study may have been the reason for the low level of Ti atoms observed in the Al-Ti rich intermetallic particles.

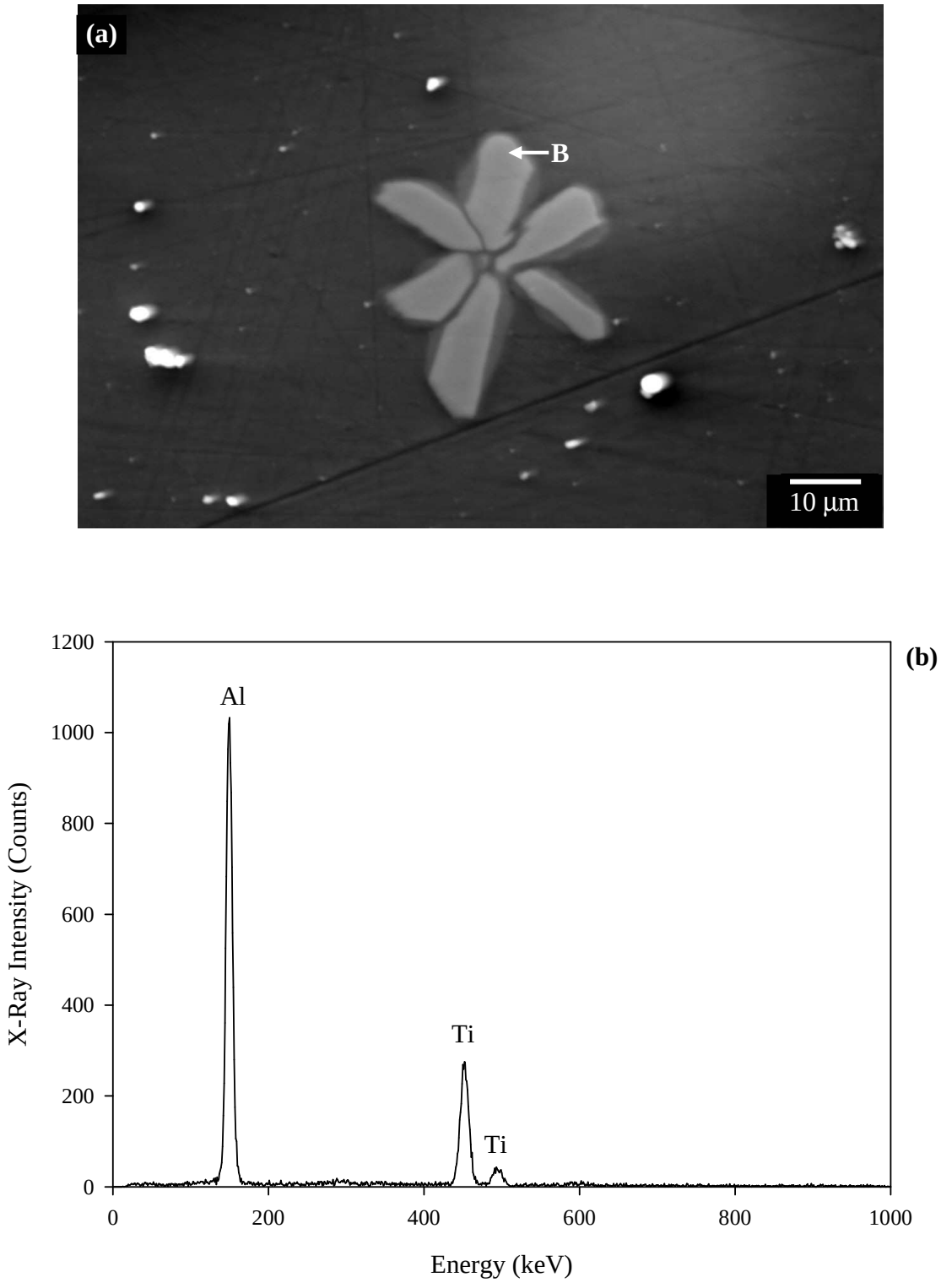

Figure 4.24. (a) Microstructure of typical Ti-rich intermetallic particle in A535 alloy (b) its EDS spectra labelled B.

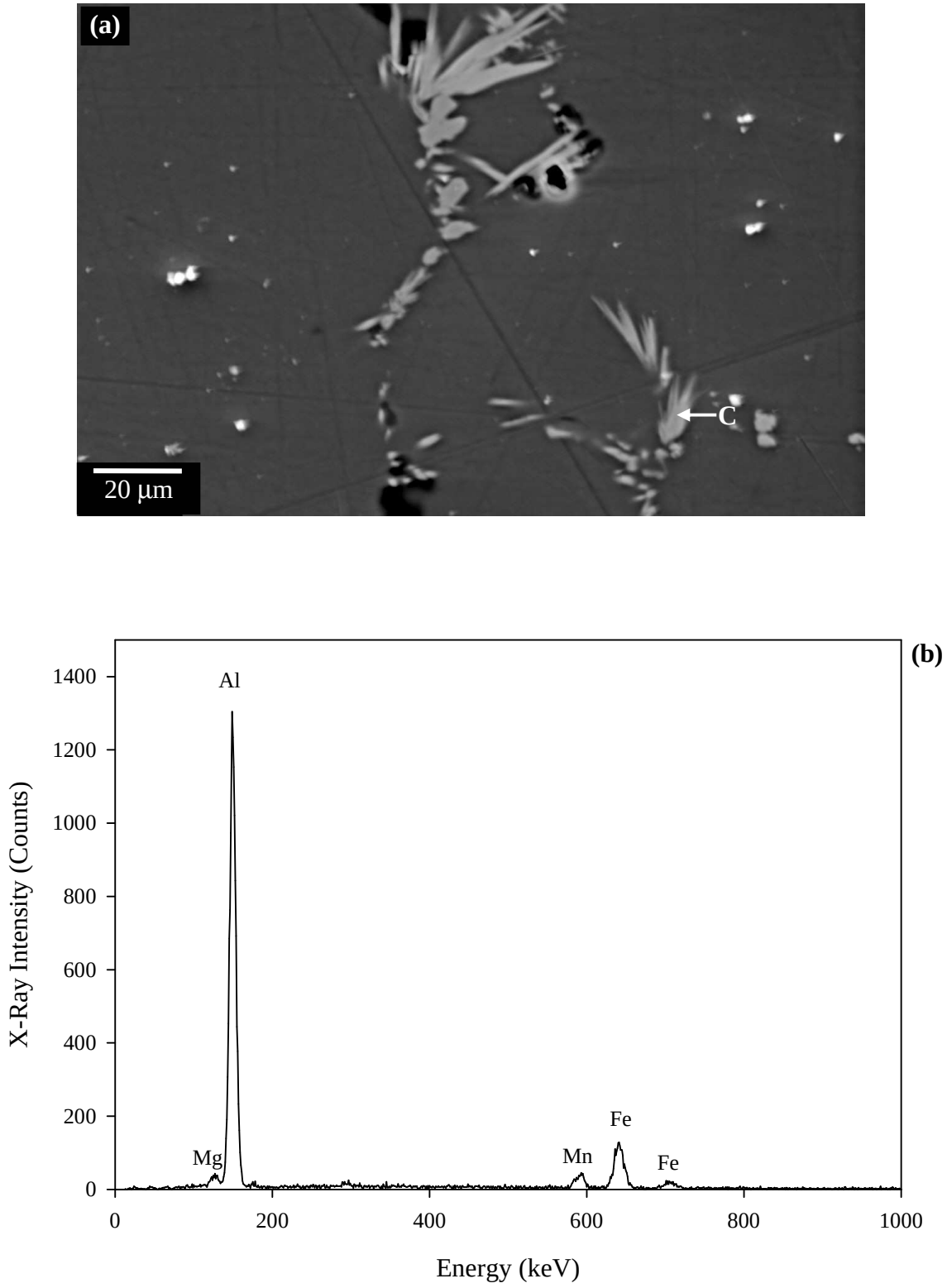

Figure 4.25. (a) Microstructure of typical Fe-rich intermetallic particle in A535 alloy (b) its EDS spectra labelled C.

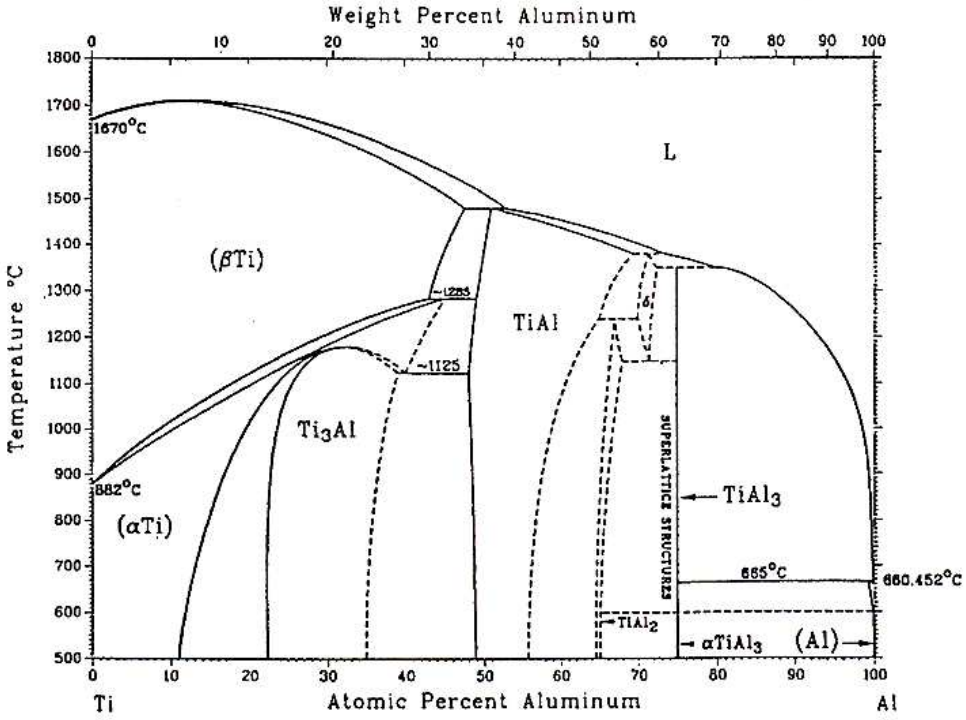

Figure 4.26. Al-Ti Phase Diagram.

Table 4.7. EDS point analysis from Al-Ti intermetallic particle.

Particle #	Element (wt.%)							Likely Phase
	Al	Mg	Si	Ti	Mn	Fe	Cu	
1	60.23	0.85	0.73	35.49	1.48	0.64	0.58	$TiAl_5$
2	59.24	1.08	0.59	35.75	1.56	0.94	0.85	$TiAl_5$
3	60.31	1.12	0.63	34.50	1.98	0.75	0.72	$TiAl_5$
4	60.82	1.22	1.08	35.95	0.93	0.00	0.00	$TiAl_5$
5	59.69	0.74	0.29	36.27	1.79	0.82	0.39	$TiAl_5$

Table 4.8. EDS point analysis from Al-Fe-Mn rich intermetallic particle.

Particle #	Element (wt.%)							Likely Phase
	Al	Mg	Si	Ti	Mn	Fe	Cu	
1	62.82	1.14	1.40	0.47	6.97	26.06	1.15	$Al_{37}Fe_4Mn$
2	59.53	1.97	0.45	0.45	6.22	30.53	1.05	$Al_{40}Fe_5Mn$
3	64.87	1.90	1.07	0.32	7.25	23.45	1.15	$Al_{37}Fe_3Mn$
4	65.39	1.57	1.18	0.68	6.15	24.44	0.60	$Al_{44}Fe_4Mn$
5	65.23	1.57	1.43	0.52	6.69	23.48	1.08	$Al_{40}Fe_3Mn$

Knight *et al*. [148] also reported the formation of the intermetallic species Al_3Ti being favoured at temperatures greater than 350°C. High temperature fabrication of the test materials is, therefore, responsible for the formation of the Al-Ti intermetallic particles in A535 alloy. These intermetallic particles exhibit excellent high temperature properties including strength, stiffness and environmental resistance [148,150]. Their long range superlattice structure is capable of reducing dislocation mobility and diffusion processes under these conditions. Aluminium alloys containing Al_3Ti intermetallic species are therefore well suited to demanding applications such as the fabrication of aerospace and high performance automotive engine components.

A metastable Al_xFe_y intermetallics have been reported to be formed during fabrication and post-fabrication processes of Al alloys containing Fe and Mn. These intermetallics are stabilized by Mn replacing part of the Fe, which results in an $Al_m(Fe,Mn)$ intermetallics. The presence of these $Al_m(Fe,Mn)$ intermetallics has been reported in Al-Fe-Mn alloys [151-153]. The literature mainly reports the presence of $Al_{12}FeMn$ [151-153] which is different from the structural formulae obtained from this study. The strong influence of the Al matrix was believed to be the main reason for this difference.

4.5.3 Depletion of Magnesium in the Composite Matrix

Table 4.9 shows the chemical composition of A535 alloy and its composites obtained using quantitative EDS. Special emphasis was placed on the change in the amounts of the solid solution strengthening element, Mg, with the addition of fly ash. Figure 4.27 shows the variation of Mg content with increasing weight fraction of reinforcements. It

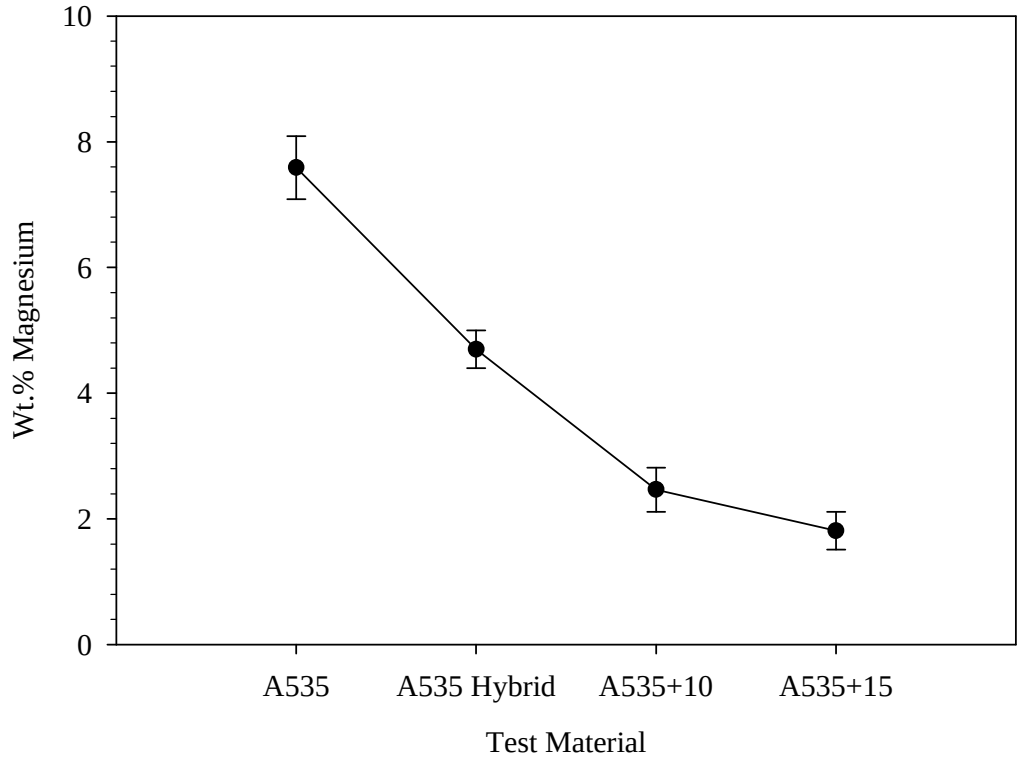

Figure 4.27. Effect of reinforcement addition on the Mg content (wt.%) of test materials.

Table 4.9. Chemical composition of A535 alloy and the matrices of its MMCs using EDS.

Material	Element (wt.%)*					
	Mg	Cu	Mn	Si	Fe	Ti
A535	7.59	0.76	0.69	0.57	0.53	1.08
A535 hybrid	4.70	0.47	0.53	0.45	0.57	0.32
A535+10	2.46	0.43	0.51	0.26	0.59	0.37
A535+15	1.81	0.38	0.50	0.56	0.57	0.52

* Balance = aluminium.

can be seen that the Mg content of A535 alloy decreased with increasing weight fraction of fly ash thus indicating that Mg is depleted from the matrix with the addition of fly ash. The addition of fly ash to A535 alloy led to the release of Si which combined with the Mg in the matrix to form Mg_2Si. This is consistent with previous studies on the

precipitation of the Mg_2Si phase in the microstructure of particle-reinforced aluminium alloy MMCs [36,37,125,128].

Figures 4.28(a) – (d) show the distribution of the Mg_2Si phase in A535 alloy and its composites while Figure 4.28(e) shows typical EDS spectra obtained for Mg_2Si. The amount of the Mg_2Si phase in the materials tested in this study was found to increase with increasing fly ash content. The Chinese-script-like morphology of the Mg_2Si phase is consistent with the results of Liu *et al*. [129]. It can also be seen that as fly ash content increases, the complexity of Mg_2Si network decorating the matrix increases. The Mg_2Si phase is known to enhance precipitation hardening in age-hardenable 6000 series aluminium alloys where it precipitates as fine particles [154,155]. In the present case, it is too large to act as a barrier to dislocation motion. As such, the Mg atoms that usually participate in solid solution strengthening are tied up in this complex network of Mg_2Si that offers no appreciable strengthening to the material.

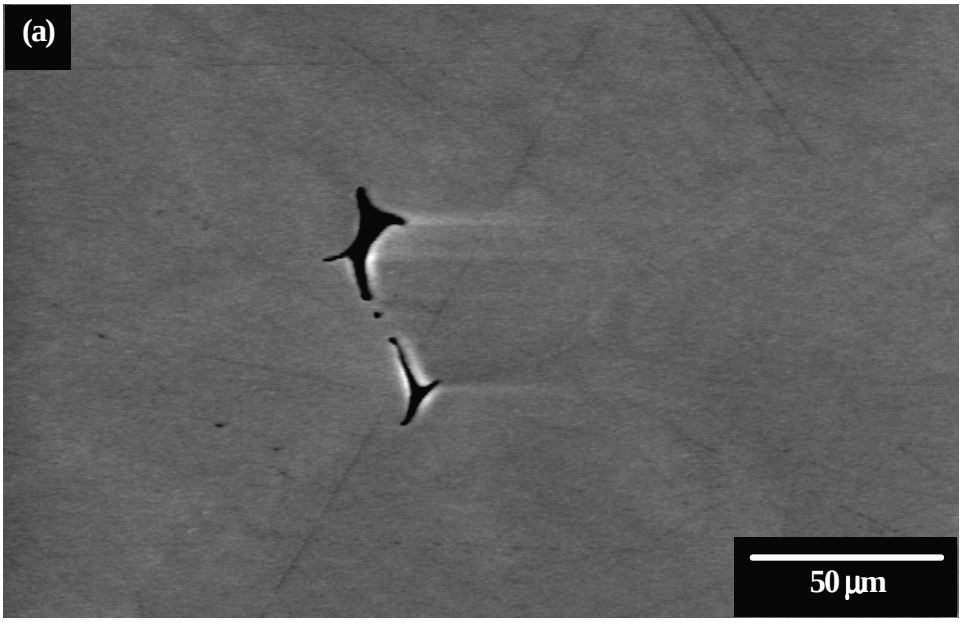
(a)
50 µm

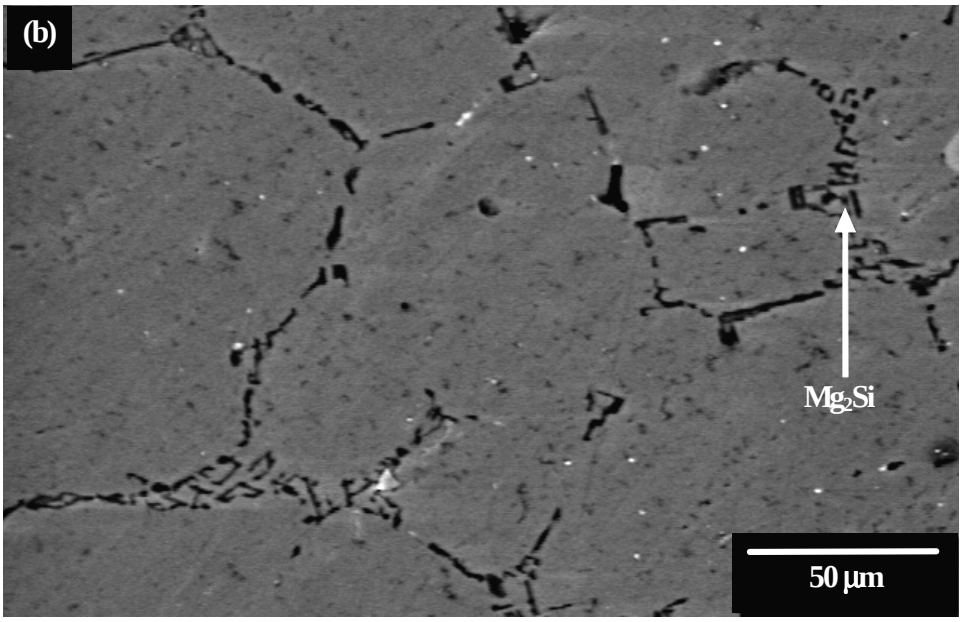
(b)
Mg2Si
50 µm

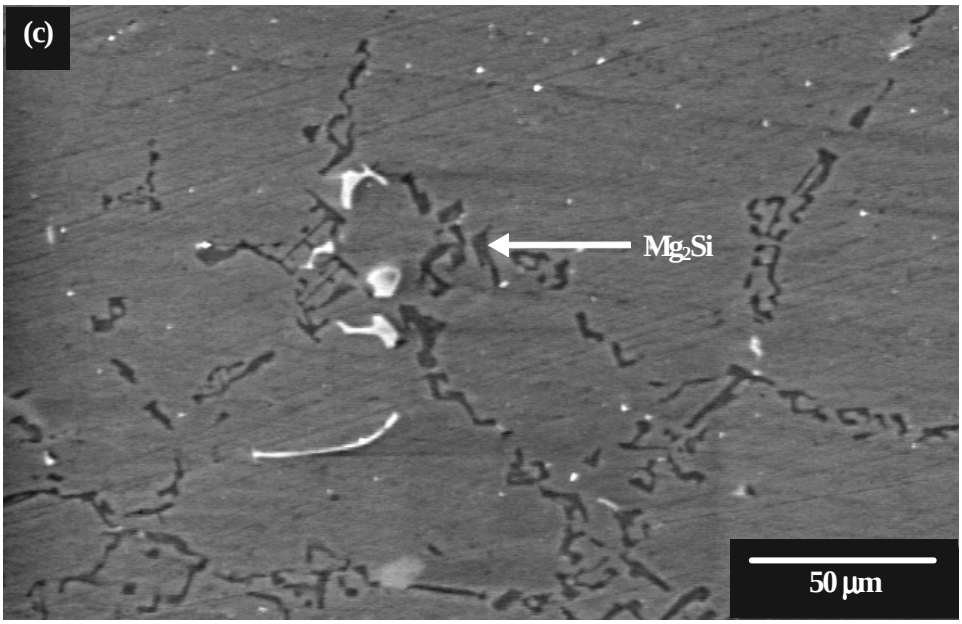
(c)
Mg2Si
50 µm

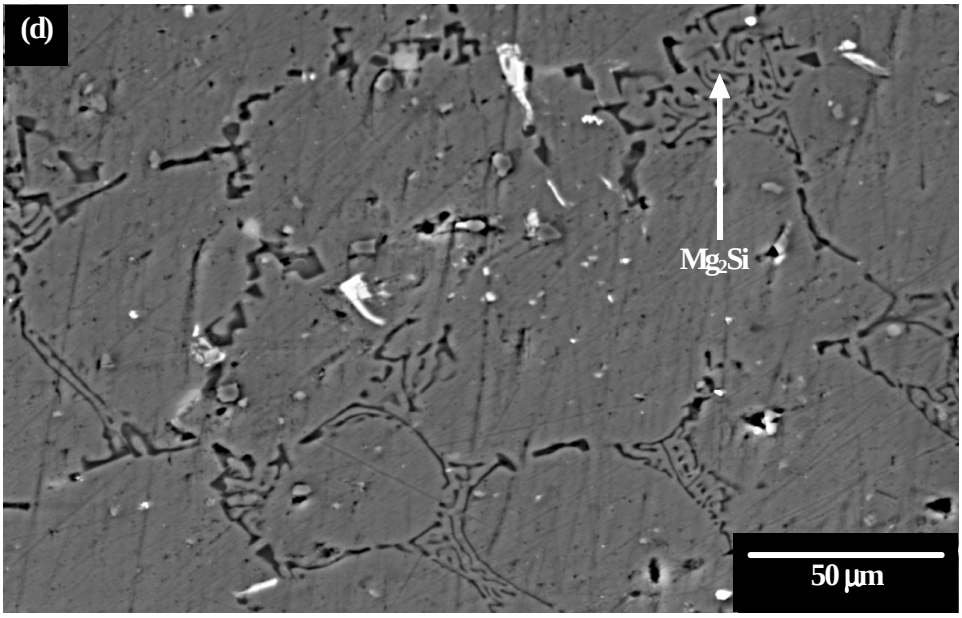
(d)
Mg2Si
50 µm

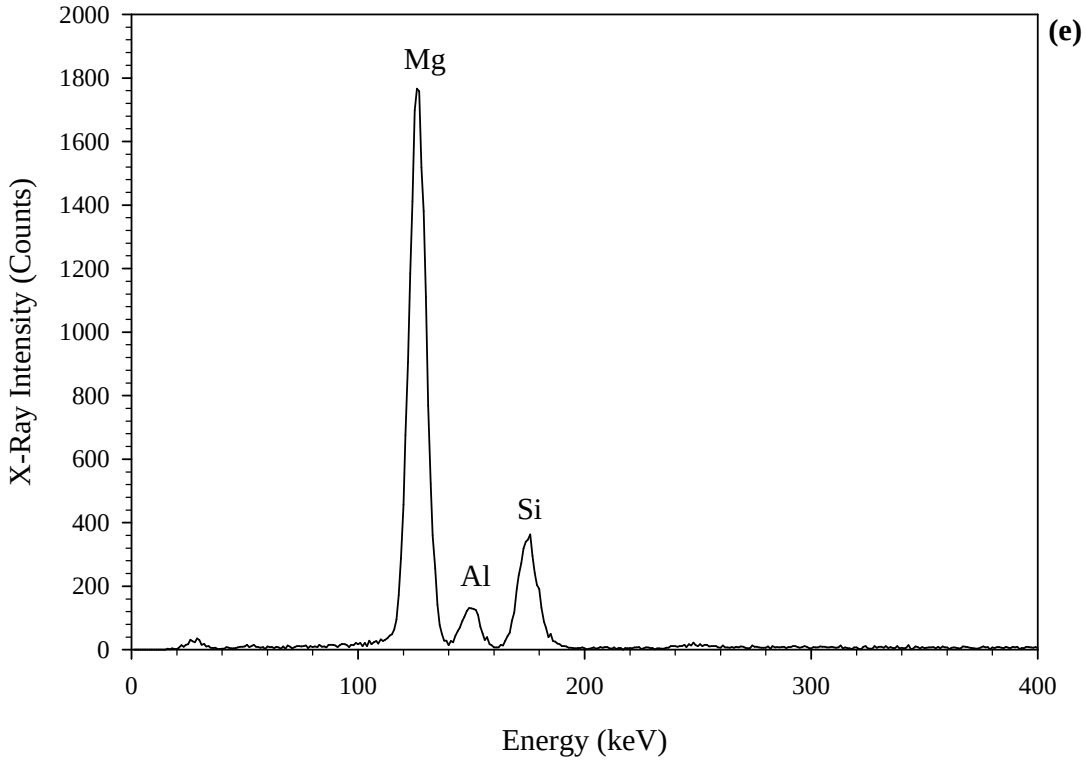

Figure 4.28. (a)-(d) SEM micrographs showing the distribution of Mg_2Si in A535 alloy, A535 hybrid, A535+10 and A535+15 composites, respectively. (e) Typical EDS spectra of Mg_2Si.

5. CONCLUSIONS AND RECOMMENDATIONS

5.1 Conclusions

In this study, different experimental techniques were used to characterize some physical and mechanical properties as well as the microstructural behaviour of aluminium casting alloy A535 and its composites containing different weight fractions of SiC and fly ash particles. The results were investigated by means of density measurements, microhardness measurements, tensile testing, Charpy impact testing, optical microscopy, inductively coupled plasma/mass spectrometry (ICP/MS), inductively coupled plasma/optical emission spectrometry (ICP/MS), scanning electron microscopy (SEM), energy dispersive X-ray spectrometry (EDS), X-ray diffractometry (XRD) and X-ray fluorescence spectroscopy (XRF). The following conclusions can be drawn from the study.

5.1.1 Chemical and Physical Properties

1. Glassy and crystalline phases were observed in the fly ash used in this study. The SiO_2, Al_2O_3 and Fe_2O_3 content accounted for about 90% of the total oxides. The fly ash particles can be classified as Class F based on ASTM C618 due to its low CaO content. The Aqua Regia, used in extracting the reinforcement particles, leached out some of the iron and calcium oxides in the fly ash

2. The density of the composites decreased with increasing reinforcement content. The density of A535+10 was lower than that of A535 hybrid indicating the pronounced effect of fly ash on the overall density of the composite.

Fly ash-reinforced A535 composites can therefore be used as a filler material in applications where weight reductions are desirable.

5.1.2 Mechanical Properties

1. Reinforcing A535 alloy with fly ash decreased the overall hardness of the resulting composites without altering its natural aging behaviour. Solution heat-treatment was however, effective in improving the hardness of A535 alloy and its composites.

2. The Charpy impact energy decreased with increasing fly ash content. The impact energy of A535+15 was so low it could not be detected. Porosity was observed to be responsibly for the decline in Charpy impact energy with fly ash addition.

3. Tensile strength, yield strength and percent elongation were determined for the test materials. Increasing fly ash resulted in a decline in the tensile properties of the resulting composites. The decrease in the mechanical properties of the composites is attributed to the decrease in solid solution strengthening magnesium as well as an increase in porosity and particle clustering with increasing fly ash content.

5.1.3 Microstructure

1. The intermetallic species Al_5Ti was observed in the matrix of A535 alloy. This was believed to be formed during fabrication of the test materials. These intermetallic particles are responsible for the extra strength, stiffness and environmental resistance in the matrix with the capability of reducing dislocation mobility and diffusion processes in these materials.

2. Fly ash particles are not uniformly distributed in the composites, as they seem to segregate along the α-aluminium dendrite boundaries. Clustering of these particles at the dendrite boundaries leads to the development of adverse porosity in the composites.

3. Mg_2Si was observed in the matrix of A535 alloy. The complexity of Mg_2Si network decorating the matrix increases with increasing fly ash content. They are suggested as the main causes of magnesium depletion in the composite matrix and subsequently to a decrease in solid solution strengthening.

It can be concluded from this study that the addition of raw fly ash is detrimental to the strength of A535 alloy. Fly ash-reinforced A535 composites can therefore be used for applications where strength is not a priority.

5.2 Recommendations

Based on the results of the present study, the following recommendations are deemed to be significant in further understanding the properties of fly ash-reinforced A535 composites.

1. The Aqua Regia used in extracting the reinforcement particles for analyses leached out some of the major constituents of the fly ash (i.e. anhydrite and some of the iron oxides). Other reagents such as phosphoric acid, which tend to have less effect on these particles, should be used. This will eliminate the possibility of some major constituents being consumed during the extraction process.

2. This study showed that the level of difficulty in cutting the as-cast samples increased with increasing fly ash content. Wear rate is therefore expected to increase with increasing fly ash content. This property can be exploited in applications requiring high wear resistance. Wear tests should therefore be carried out to ascertain this fact.

3. Reactivity of fly ash particles depends on their sizes. Sieve analysis should be used to characterize the fly particles. Less reactive but coarser size fractions can then be used in fabricating the composites.

4. This study has shown that the addition of raw fly ash is detrimental to the strength of A535 alloy due to the development of porosity within the resulting

composites. In addition, the depletion of magnesium in the composite matrix also leads to a decrease in solid solution strengthening. Beneficiation of fly ash should, therefore, be carried out before its utilization in composites. Density separation can be used in obtaining hollow glass spheres with densities <1 g/cm^3. The sphericity, controlled particle size and low density of these fly ash particles are likely to reduce the reactivity of the fly ash particles as well as decrease the densities and apparent porosity of the resulting composites.

REFERENCES

1. M. Ebisawa, T. Hara, T. Hayashi and H. Ushio, "Production Processes of Metal Matrix Composite (MMC) Engine Block", *SAE Transaction.*, Vol. 100, (1991), 826-838.

2. M. J. Tan and X. J. Li, "Processing Metal-Matrix Composites for Superplastic Properties", *Materials Science Forum*, Vols 437-438, (2003), 165-168.

3. X. F. Zhang, D. J. Wang and G. Xie, "Manufacturing of Aluminium/Fly Ash Composites with Liquid Reactive Sintering Technology", *Acta Metallurgica Sinica*, Vol. 15, (2002), 465-470.

4. S. Kolukisa, A. Topuz and A. Sagin, "The Production and Properties of Fly Ash Containing Aluminium Matrix Composite Materials", Practical Metallography, Vol. 40, (2003), 357-368.

5. J. Bienias, M. Walczak, B. Surowska and J. Sobczak, "Microstructure and Corrosion Behaviour of Aluminum Fly Ash Composites", *Journal of Optoelectronics and Advanced Materials*, Vol. 5, (2003), 493-502.

6. J. Sobczak, Z. Slawinski, N. Sobczak, P. Darlak, R. Asthana and P. K. Rohatgi, "Thermal Fatigue Resistance of Discontinuous Reinforced Cast Aluminium-Matrix Composites", *Journal of Materials Engineering and Performance*, Vol. 11, (2002), 595-602.

7. P. K. Rohatgi, R. Guo, B. N. Keshavaram, and D. M. Golden, "Cast Aluminium, Fly Ash Composites for Engineering Applications", *Transactions of the American Foundrymen's Society*, Vol. 99, (1995), 575-585.

8. R. Q. Guo, P. K. Rohatgi and D. Nath, "Compacting Characteristics of Aluminium-Fly Ash Powder Mixtures", *Journal of Materials Science*, Vol. 31, (1996), 5513-5519.

9. R. Q. Guo, P. K. Rohatgi and D. Nath, "Preparation of Aluminium-Fly Ash Particulate Composite by Powder Metallurgy Technique", *Journal of Materials Science*, Vol. 32, (1997), 3971-3974.

10. T. Matsunaga, J. K. Kim, S. Hardcastle and P. K. Rohatgi, "Crystallinity and Selected Properties of Fly Ash Particles", *Materials Science & Engineering: A*, Vol. A325, (2002), 333-343.

11. R. Q. Guo, P. K. Rohatgi, and S. Ray, "Casting Characteristics of Aluminium Alloy. Fly Ash Composites", *Transactions of the American Foundrymen's Society*, Vol. 104, (1996), 1097-1102.

12. P. K. Rohatgi, J. K. Kim, R. Q. Guo, D. P. Robertson and M. Gajdardziska-Josifovska, "Age Hardening Characteristics of Aluminium Alloy – Hollow Fly Ash Composites", *Metallurgical & Materials Transaction A*, Vol. 33A, (2002), 1541-1547.

13. P. K. Rohatgi and R. Q. Guo, "Low Cost Cast Aluminium – Fly Ash Composites for Ultralight Automotive Application", *TMS Annual Meeting, Automotive Alloys*, (1997), 157-168.

14. D. M. Golden, "Solidification Processing of Metal Matrix Fly Ash Particle Composites", *EPRI Journal*, (1994), 46-49.

15. P. K. Rohatgi, "Low-Cost, Fly Ash Containing Aluminium Matrix Composites", *JOM*, Vol. 29, (1994), 55-59.

16. P. K. Rohatgi, R. Q. Guo, P. Huang, and S. Ray, "Friction and Abrasion Resistance of Cast Aluminium Alloy-Fly Ash Composites", *Metallurgical & Materials Transaction A*, Vol. 28A, (1997), 245-250.

17. P. K. Rohatgi, R. Q. Guo and B. N. Keshavaram, "Cast Aluminium Alloy - Fly Ash Composites", *Key Engineering Materials*, Vols. 104-107, (1995), 283-292.

18. P. K. Rohatgi, R. Q. Guo, H. Iksan, E. J. Borchelt and R. Asthana, "Pressure Infiltration Technique for Synthesis of Aluminium-Fly Ash Particulate Composite", *Metallurgical & Materials Transaction A*, Vol. A244, (1998), 22-30.

19. R. Q. Guo and P. K. Rohatgi, "Chemical Reactions Between Aluminium and Fly Ash During Synthesis and Reheating of Aluminium-Fly Ash Composite", *Metallurgical & Materials Transaction B*, Vol. 29B, (1998), 519-525.

20. R. Q. Guo, D. Venugopalan and P. K. Rohatgi, "Differential Thermal Analysis to Establish the Stability of Aluminium-Fly Ash Composites during Synthesis and Reheating", *Metallurgical & Materials Transaction A*, Vol. A241, (1998), 184-190.

21. I. N. A. Oguocha and S. Yannacopoulos, "Microstructure and Age Hardening Characteristics of 2618 Aluminium Matrix Composites", *Science and Engineering of Composite Materials*, Vol. 7, (1998), 299-314.

22. R. Mogilevsky, S. R. Bryan, W. S. Wolbach, T. W. Krucek, R. D. Maier, G. L. Shoemaker, J. M. Chabala, K. K. Soni and R. Levi-Setti, "Reactions at the Matrix/Reinforcement Interface in Aluminium Alloy Matrix Composites", *Metallurgical & Materials Transaction A*, Vol. A191, (1995), 209-222.

23. S. Zhongliang, J.-M. Yang, J. C. Lee, D. Zhang, H. I. Lee and R. Wu, "The Interfacial Characterization of Oxidized SiC_p/2014 Al Composites", *Metallurgical & Materials Transaction A*, Vol. A303, (2001), 46-53.

24. Y. Le Petitcorps, J. M. Quenisset, G. Le Borgne and M. Barthole, "Segregation of Magnesium in Squeeze-Cast Aluminium Matrix Composites Reinforced with Alumina Fibres", *Materials Science & Engineering A*, Vol. A135, (1991), 37-40.

25. H. Ribes, M. Suery, G. L'esperance and J. G. Legoux, "Microscopic Examination of the Interface Region in 6061-Al/SiC Composites Reinforced with As-Received and Oxidized SiC Particles", *Metallurgical Transactions.*, Vol. 21, (1990), 2489-2496.

26. D. J. Lloyd, H. P. Lagace and A. D. McLeod: in "Controlled Interphases in Composite Materials", H. Ishida, (ed.), Elsevier Science Pub. Co., NY, (1990), 359-376.

27. V. Massardier, P. Kerdelhue, P. Merle and J. Besson, "Experimental Study of the Interaction of Magnesium with the Reinforcement in Al-Mg-Si Alloy/α-Alumina Platelet Composites", *Materials Science & Engineering: A*, Vol. A191, (1995), 267-276.

28. W. M. Zhong, G. L'Esperance and M. Suery, "Effect of Current Mg Concentration on Interfacial Reactions during Remelting of Al-Mg(5083)/Al_2O_{3p} Composites", *Materials Characterization*, Vol. 49, (2003), 113-119.

29. J. C. Lee, G. H. Kim and H. I. Lee, "Characterization of Interfacial Reactions in $(Al_2O_3)_p$/6061 Aluminium Alloy Composite", *Materials Science & Technology*, Vol. 13, (1997), 182-186.

30. C. Tekmen, I. Ozdemir, U. Cocen and K. Onel, "The Mechanical Response of Al-Si-Mg/SiC_p Composite: Influence of Porosity", *Materials Science & Engineering: A*, Vol. A360, (2003), 365-371.

31. P. N. Bindumadhavan, T. K. Chia, M. Chandrasekaran, H. K. Wah, L. N. Lam and O. Prabhakar, "Effect of Particle-Porosity Clusters on Tribological Behaviour of Cast Aluminium Alloy A356-Sic_p Metal Matrix Composites", *Materials Science & Engineering: A*, Vol. A315, (2001), 217-226.

32. A. M. Samuel, A. Gotmare and F. H. Samuel, "Effect of Solidification Rate and Metal Feedability on Porosity and SiC/Al_2O_3 Particle Distribution in an Al-Si-Mg (359) Alloy", *Composites Science & Technology*, Vol. 53, (1995), 301-315.

33. Y. Sahin, "Wear Behaviour of Aluminium Alloy and its Composites Reinforced by SiC Particles using Statistical Analysis", *Materials and Design*, Vol. 24, (2003), 671-679.

34. V. Amigo, J. L. Ortiz and M. D. Salvador, "Microstructure and Mechanical Behaviour of 6061Al Reinforced with Silicon Nitride Particles, Processed by Powder Metallurgy", *Scripta Materialia*, Vol. 42, (2000), 383-388.

35. S. J. Zhu and T. Iizuka, "Fabrication and Mechanical Behaviour of Al Matrix Composites Reinforced with Porous Ceramic of In-Situ Grown Whisker Framework", *Materials Science & Engineering: A*, Vol. A354, (2003), 306-314.

36. H. Ahlatci, E. Candan and H. Cimenoglu, "Mechanical Properties of Al-60 pct SiC_p Composites Alloyed with Mg", *Metallurgical & Materials Transactions A*, Vol. 35A, (2004), 2127-2141.

37. Z. Shi, J.-M. Yang, J. C. Lee, Di Zhang, H. I. Lee and R. Wu, "The Interfacial Characterization of Oxidized $SiC_{(p)}$/2014 Al Composites", *Materials Science & Engineering: A*, Vol. A303, (2001), 46-53.

38. M. Kobashi and T. Choh, "Wettability and the Reaction for SiC Particle/Al Alloy System", *Journal of Materials Science*, Vol. 28, (1993), 684-690.

39. H. Ahlatci, M. S. Karakas, E. Candan and H. Cimenoglu, "Effect of Magnesium Addition on Wear Behaviour of Al-70 Vol.-% Al_2O_{3p} Composites", *Materials Science & Technology*, Vol. 19, (2003), 949-954.

40. M. P. Thomas and J. E. King, "Comparison of the Ageing Behaviour of PM 2124 Al Alloy and Al-SiC_p Metal-Matrix Composite", *Journal of Materials Science*, Vol. 29, (1994), 5272-5278.

41. K. B. Lee, J. P. Ahn and H. Kwon, "Characteristics of AA6061/BN Composite Fabricated by Pressureless Infiltration Technique", *Metallurgical & Materials Transactions A*, Vol. 32, (2001), 1007-1018.

42. D. L. Zhang and B. Cantor, "TEM Characterization of 2618/SiC_p Composites", in *Proc. 2nd European Conf. on Advanced Materials and Processes*, University of Cambridge, (1991), 197-207.

43. R. C. Joshi and R. P. Lohtia "Fly Ash in Concrete Production, Properties and Uses", Gordon and Breach Science Publishers, Amsterdam, (1997), 1-47.

44. V. M. Malhotra and A. A. Ramezanianpour, "Fly Ash in Concrete", 2nd edn, CANMET, Natural Resource of Canada, Ottawa, (1994), 1-18.

45. R. A. Helmuth, "Fly Ash in Cement and Concrete", Portland Cement Association, Skokie, Illinois, (1987), 1-64.

46. R. S. Iyer and J. A. Scott, "Power Station Fly Ash – A Review of Value-Added Utilization Outside of the Construction Industry", *Resources, Conservation, and Recycling.*, Vol. 31, (2001), 217-228.

47. Canadian Minerals Yearbook: Natural Resources Canada, Ottawa (2002).

48. P. A. Jarvala and P. K. Jarvala, "Multicomponent Compounding of Polypropylene", *Journal of Materials Science,* Vol. 31, (1996), 3853–3860.

49. K. T. Verghese and B. K. Chaturvedi, "Fly Ash as Fine Aggregate in Polyester Based Polymer Concrete", *Cement & Concrete Composites*, Vol. 18, (1996), 105–108.

50. M. S. Yildirim, B. Yasar and Y. Cengiz, "Utilization of Fly Ash and Polypropylene Wastes in the Production of a New Porous Composite Material", *Journal of Porous Materials*, Vol. 3, (1996), 189–191.

51. L. Yadong, D. J. White and R. L. Peyton, "Composite Material from Fly Ash and Post-Consumer PET", *Resources, Conservation, and Recycling*, Vol. 24, (1998), 87–93.

52. S. M. Kulkarni and Kishore, "Effects of Surface Treatments and Size of Fly Ash Particles on the Compressive Properties of Epoxy Based Particulate Composites", *Journal of Materials Science*, Vol. 37, (2002), 4321-4326.

53. W. M. Kriven, J. L. Bell, L. Jonathon and M. Gordon, "Microstructure and Microchemistry of Fully-Reacted Geopolymers and Geopolymer matrix composites", *Ceramic Transactions*, Vol. 153, (2004), 227-250.

54. S. M. Kulkarni, D. Anuradha, C. R. L. Murthy and Kishore, "Analysis of Filler-Fibre Interaction in Fly Ash Filled Short Fibre-Epoxy Composites using Ultrasonic NDE", *Bulletin of Materials Science*, Vol. 25, (2002), 137-140.

55. Rainer Cast Parts, Inc., http://rainiercast.com/535.html, cited on August 17th, 2004.

56. Annual Book of ASTM Standards: B108-02, 77-89.

57. J. Bijen, "Fly Ash Aggregates", in Fly Ash, Silica Fume, Slag & Other Mineral By-Products in Concrete, 2nd Ed., V. M. Malhotra (ed.), American Concrete Institute, Detroit, (1983).

58. ACAA International, http://pubs.usgs.gov/fs/fs076-01/fs076-01.pdf cited on June 3rd, 2004.

59. N. Berkowitz, "An Introduction to Coal Technology", 2nd edn, Academic Press, San Diego, (1994).

60. V. M. Malhotra and P. K. Mehtra, "Pozzolanic and Cementitious Materials", Taylor and Francis Publishers, Bristol, (1996), 136.

61. V. Bednarik, M. Vondruska, M. Slid and E. Vondruska, "Characterization of Products from Fluidized-Bed Combustion of Coal", *Journal of Air & Waste Management Association*, Vol. 50, (2000), 1920-1928.

62. M. Kamon and T. Katsumi, "Utilization of Coal Fly Ash from Fluidized Bed Combustion Systems", *Geotechnical Special Publication*, Vol. 46, (1995), 1765-1779.

63. E. V. Churchill and S. N. Amirkhanian, "Coal Ash Utilization in Asphalt Concrete Mixtures", *Journal of. Materials: Civil Engineering*, Vol. 11, (1999), 295-301.

64. G. S. Brady and H. R. Clauser, "Materials Handbook", 13th Edition, McGraw-Hill, Inc., New York, (1991).

65. Energy Information Administration, http://www.eia.doe.gov/emeu/iea/wep.html cited on April 22nd, 2004.

66. M. S. Yildrim, Y. Bicer and C. Yildiz, "Utilization of Fly Ash and Polypropylene Wastes in the Production of a New Porous Composite Material", *Journal of Porous Materials*, Vol. 3, (1996), 189-191.

67. A. Pekrioglu, "Fly Ash Utilization in Grouting Applications", *Geotechnical Special Publication*, Vol. 120, (2003), 1169-1179.

68. D. Dermatas and X. Meng, "Utilization of Fly Ash for Stabilization/Solidification of Heavy Metal Contaminated Soils", *Engineering Geology*, Vol. 70, (2003), 377-394.

69. Z. Konik, A. Derdacka-Grzymek, A. Stok and J. Iwanciw, "Utilization of Fly Ashes from Various Countries for Alumina Production", *Light Metals: Proceedings of Sessions, TMS Annual Meeting*, (1994), 23-27.

70. G. R. Dewey, M. A. Kayser and L. L. Sutter, "Characterization of Electric Utility Coal Fly Ash for Use in Portland Cement Concrete", *Proceedings of the American Power Conference*, Vol. 56, (1994), 483-486.

71. Annual Book of ASTM Standards, C618-03, 319-321.

72. Z. Nalbantoglu, "Effectiveness of Class C Fly Ash as an Expansive Soil Stabilizer" *Construction and Building Materials*, Vol. 18, (2004), 377-381.

73. R. T. Naik, W. B. Ramme and J. H. Tews, "Use of High Volumes of Class C and Class F Fly Ash in Concrete", *Cement, Concrete and Aggregates*, Vol. 16, (1994), 12-20.

74. V. M. Malhotra, “Durability of Concrete Incorporating High-Volume of Low-Calcium (ASTM Class F) Fly Ash”, *Cement & Concrete Composites*, Vol. 12, (1990), 271-277.

75. S. Ghosal, J. L. Ebert and S. A. Self, “Chemical Composition and Size Distributions for Fly Ashes”, *Fuel Processing Technology*, Vol. 44, (1995), 81-94.

76. R. C. Joshi and M. A. Ward, “Self Cementitious Fly Ashes Structure and Hydration Mechanism”, *Proceedings, the International Congress on the Chemistry of Cement*, Paris, (1980), IV/78-IV/83.

77. M. Y. Mollah, T. R. Hess and D. L. Cocke, “Surface and Bulk Studies of Leached and Unleached Fly Ash Using XPS, SEM, EDS and FTIR techniques”, *Cement and Concrete Research*, Vol. 24, (1994), 109-118.

78. R. C. Joshi and R. P. Lohtia, “Fly Ash Classification System Based on Loss on Ignition (LOI)”, *Proceedings, 11th International Symposium on Use and Management of Coal Combustion By-Products (CCBs)*, Vol. 2, (1995), 61-1 to 61-14.

79. Y. Ahn and J.I. Yang, "Physicochemical Properties of Unburned Carbon from Fly Ash", *Journal of Korean Institute of Resources & Recycling*, Vol. 7, (1998), 14-19.

80. W. S. Seames, “An Initial Study of the Fine Fragmentation Fly Ash Particle Mode Generated during Pulverized Coal Combustion”, *Fuel Processing Technology*, Vol. 81, (2003), 109-125.

81. S. S. Thipse, M. Schoenitz and E. L. Dreizin, “Morphology and Composition of the Fly Ash Particles Produced in Incineration of Municipal Solid Waste”, *Fuel Processing Technology*, Vol. 75, (2002), 173-184.

82. R. C. Joshi and B. K. Marsh, “Some Physical, Chemical and Mineralogical Properties of Some Canadian Fly Ashes”, *Proceedings, Materials Research Society*, Vol. 86, (1987), 113-126.

83. S. Slanicka, “Influence of Fly Ash Fineness on the Strength of Concrete”, *Cement and Concrete Research*, Vol. 21, (1991), 285-296.

84. J. Huang and J. Zhang, “Measuring Gradation of Fly Ash with Combination of Sieve Analysis and Photoelectric Particle Size Meter”, *Scientific Research Institute*, Vol. 15, (1998), 28-29.

85. S. Ghosal, J. L. Ebert and S. A. Self, “Fly Ash Size Distributions: Use of Coulter Multisizer and Fitting to Truncated Lognormal Distributions”, *Particle and Particle Systems Characterization*, Vol. 10, (1993), 11-18.

86. S. Ghosal, J. L. Ebert and S. A. Self, "Chemical Composition and Size Distributions for Fly Ashes" *Fuel Process Technology*, Vol. 44, (1995), 81-91.

87. K. Parylak, "Influence of Particle Structure on Properties of Fly Ash and Sand", *Geotechnical Special Publication*, Vol. 2, (1992), 1031-1041.

88. G. Frigione, F. Ferrari and B. Lanzillotta, "Concretes with High Fractionated Fly Ash Content – Influence of C_3A Content of Portland Cement", in Proceedings, 10th International Ash Use Symposium, American Coal Ash Association, *EPRI Journal*, Vol. 2, (1993), 46-1 to 46-9.

89. R. C. Joshi, "Sources of Pozzolanic activity in Fly Ashes – A Critical Review", *Proceedings, 5th International Fly Ash Utilization Symposium*, Atlanta, Georgia, (1979), 610-623.

90. ACI Committee 226, "The Use of Fly Ash in Concrete", *ACI Materials Journal*, Vol. 84, (1987), 381-409.

91. Annual Book of ASTM Standards, B618-03, 459-467.

92. G. J. McCarthy, D. M. Johansen and S. J. Steinwand, "X-ray Diffraction Analysis" in Advances in X-ray Analysis, Vol. 31, C. S. Barrett, P. K. Predecki, J. V. Gilfrich, J. W. Richardson and R. Jenkins, (eds.), Kluwer Academic Pub., Boston, MA, (1988).

93. K. Kiattikomol, C. Jaturapitakkul, S. Songpiriyakij and S. Chutubtim, "A Study of Ground Course Fly Ashes with Different Finenesses from various Sources as Pozzolanic Materials", *Cement and Concrete Composites*, Vol. 23, (2001), 335-343.

94. L. K. A. Sear, "Properties and Use of Coal Fly Ash: A Valuable Industrial By-Product", Thomas Telford Limited, Westminster, London, (2002), 261.

95. F. King, "Aluminium and Its Alloys", Ellis Horwood, New York, (1987), 313.

96. P. C. Varley, "The Technology of Aluminium and its Alloys", CRC Press, Cleveland, Ohio, (1970), 161.

97. Institute of Chemical Technology, http://www.vscht.cz/met/fix/konferen/aki/2000/Nidi/Roehrig.pdf cited on September 11th, 2003.

98. E. Carrington, "Aluminium Alloy Castings, their Founding and Finishing", Charles Griffin and Company, London, (1946), 326.

99. F. W. Smith, “Structure and Properties of Engineering Alloys”, 2nd Edition, McGraw-Hill Inc, New York, (1993), 512.

100. J. E. Hatch (ed.), “Aluminium: Properties and Physical Metallurgy”, ASM, Metals Park, Ohio, (1984), 371.

101. J. D. Bernardin and I. Mudawar, “Validation of the Quench Factor Technique in Predicting Hardness in Heat Treatable Aluminium Alloys”, *International Journal of Heat and Mass Transfer*, Vol. 38, (1995), 863-873.

102. J. G. Kaufman (ed.), “Properties of Aluminium Alloys: Tensile, Creep, and Fatigue Data at High and Low Temperatures”, ASM, Materials Park, Ohio, (1999), 305.

103. J. Eliasson and R. Sandstrom, “Applications of Aluminium Matrix Composites”, *Key Engineering Materials*, Vols. 104-107, (1995), 3-36.

104. M. D. Huda, M. S. J. Hashmi and M. A. El-Baradie, “Metal Matrix Composites: Materials, Manufacturing and Mechanical Properties”, *Key Engineering Materials*, Vol. 104-107, (1995), 37-64.

105. D. Hull, and T. W. Clyne, “An Introduction to Composite Materials”, Cambridge University Press, Cambridge, (1996), 326.

106. T. W. Clyne, “Metal Matrix Composites”, in Comprehensive Composite Materials, Vol. 3, A. Kelly and C. Zweben (eds.), Elsevier Science Ltd., New York, (2000), 1-13.

107. T. Minoru, and R. J. Arsenault, “Metal Matrix Composites: Thermomechanical Behaviour”, Pergamon Press Plc, Oxford, (1989), 264.

108. C. McCullough, P. Galuska and S. R. Pittman, “Criteria for Matrix Selection in Continuous Fibre Aluminium Matrix Composites”, *TMS Annual Meeting*, (1996), 15-28.

109. T. W. Chou, “Fibre Reinforcements and General Theory of Composites”, in Comprehensive Composite Materials, Vol. 1, A. Kelly and C. Zweben (eds.), Elsevier Science Ltd., New York, (2000).

110. Y. L. Klipfel, M. Y. He, R. M. McMeeking, A. G. Evans and R. Mehrabian, “Processing and Mechanical Behaviour of an Aluminium Matrix Composite Reinforced with Short Fibres”, *Acta Metallurgica*, Vol. 38, (1990), 1063-1074.

111. P. S. Gilman, “Discontinuously Reinforced Aluminium. Ready for the 1990s”, *JOM*, Vol. 43, (1991), 47-53.

112. I. N. A. Oguocha and S. Yannacopoulos, "Behaviour of Alumina Particle-Reinforced 2618 Aluminium", *Proceedings of the International Symposium on Developments and Applications of Ceramics and New Metal Alloys*, (1993), 245-258.

113. N. P. Hung, F. Y. C. Boey, K. A. Khor, C. A. Oh and H. F. Lee, "Machinability of Cast and Powder-Formed Aluminium Alloys Reinforced with SiC Particles", *Journal of Materials Processing Technology*, Vol. 48, (1995), 291-297.

114. C. Troadec, R. Fillit, P. Goeuriot, P. Verdier, Y. Laurent, J. Vicens, G. Boitier, J. L. Chermant and B. L. Mordike, "AlN Dispersion Reinforced Aluminium Matrix Composites", *Materials Science Forum*, Vols. 217-222, (1996), 1877-1882.

115. Annual Report, Alcan Aluminium Limited, Montreal, (1993).

116. MMC-Access Webteam, http://mmc-assess.tuwien.ac.at/index1.htm, cited on September 09, 2004.

117. J. Hashim, L. Looney and M. S. J. Hashmi, "Metal Matrix Composites: Production by the Stir Casting Method", *Journal of Materials Processing Technology*, Vols. 92-93, (1999), 1-7.

118. A. R. Kennedy, D. G. McCartney and J. V. Wood, "Homogeneous Metal Matrix Composites Produced by a Modified Stir-Casting Technique", *TMS Annual Meeting*, (1995), 261-274.

119. WE Energies, http://www.we-energies.com/environment/ccp_handbook_ch8.pdf cited on December, 2003.

120. D. J. Lloyd, "Particle Reinforced Aluminium and Magnesium Matrix Composites", *International Materials Reviews*, Vol. 39, (1994), 1-23.

121. R. Asthana, "Reinforced Cast Metals: Part II Evolution of the Interface", *Journal of Materials Science*, Vol. 33, (1998), 1959-1980.

122. M. Nathan, "Interfacial Reactions in Metal Matrix Composites Studied with a Novel Technique", *Journal of Materials Science Letters*, Vol. 8, (1989), 311-314.

123. J. Bouix, M. P. Berthet, F. Bosselet, R. Favre, M. Peronnet, O. Rapaud, J. C. Viala, C. Vincent and H. Vincent, "Physico-Chemistry of Interfaces in Inorganic-Matrix Composites", *Composites Science and Technology*, Vol. 61, (2001), 355-362.

124. S. P. Hannula, P. Lintula, P. Lintunen and T. Lindroos, "Processing and Properties of Metal Matrix Composites Synthesized by SHS", *Materials Science Forum*, Vols 426-432, (2003), 1971-1978.

125. A. Bochenek and K. N. Braszczynska, "Structural Analysis of the $MgAl_5$ Matrix Cast Composites Containing SiC Particles", *Materials Science & Engineering: A*, Vol. A290, (2000), 122-127.

126. M. W. Chase, C. A. Davies, J. R. Downey, Jr., D. J. Frurip, R. A. McDonald and A. N. Syverud (ed.): "JANAF Thermochemical Tables, 3rd Ed", *Journal of Physical and Chemical Reference Data*, Vol. 14, (1985), Sppl. 1.

127. R. C. Weast: in "CRC Handbook of Chemistry and Physics, 70th edn", CRC Press, (1990) D-33.

128. M. C. Gui, J. M. Han and P. Y. Li, "Microstructure and Mechanical Properties of Mg-Al9Zn/SiC_p Composite Produced by Vacuum Stir Casting Process", *Materials Science & Technology*, Vol. 20, (2004), 765-771.

129. Y. L. Liu, S. B. Kang and H. W. Kim, "Complex Microstructures in As-Cast Al-Mg-Si Alloy", *Materials Letters*, Vol. 41, (1999), 267-272.

130. R. J. Arsenault, "Tensile and Compressive Properties of Metal Matrix Composites" in Metal Matrix Composites: Mechanisms and Properties, R. K Everett and R. J. Arsenault (eds.), Academic Press, Boston, (1991), 416.

131. S. V. Prasad, P. K. Rohatgi and T. H. Kossel, "Mechanisms of Material Removal during Low Stress and High Stress Abrasion of Aluminium Alloy-Zircon Particle Composites", *Materials Science and Engineering*, Vol. 88, (1986), 213-220.

132. M. F. Ashby and D. R. H. Jones, "Engineering Materials: An Introduction to their Properties and Applications", Pergamon Press, New York, (1980).

133. Indiana University, http://www.geology.iupui.edu/research/SoilsLab/procedures/bulk/Index.htm cited on September 19, 2004.

134. E. Raask, "Mineral Impurities in Coal Combustion: Behaviour, Problems and Remedial Measures", Hemisphere Publishing Corp, Springer-Verlag (1985).

135. Health Canada, http://www.hc-sc.gc.ca/hecs-sesc/water/pdf/summary.pdf, cited on September 14, 2004.

136. K. Park and T. S. Lee, "Fabrication and Characteristics of Porous AISI 304L Stainless Steels by Ceramic Powder Additions", *Materials Science & Technology*, Vol. 20, (2004), 711-714.

137. C. H. Caceres and B. I. Selling, Casting Defects and the Tensile Properties of an Al-Si-Mg Alloy, *Materials Science & Engineering: A*, Vol. A220, (1996), 109-116.

138. Y-H. Li, L-J. Rong and Y-Y. Li, "Pore Characteristics of Porous NiTi alloy Fabricated by Combustion Synthesis", *Journal of Alloys Compounds*, Vol. 345, (2002), 271-274.

139. S. M. Roberts, J. Kusiak, P. J. Withers, S. J. Barnes and P. B. Prangnell, "Numerical Prediction of the Development of Particle Stress in the Forging of Aluminium Metal Matrix Composites", *Journal of Materials Processing Technology*, Vol. 60, (1996), 711-718.

140. S. Kumai, J. E. King and J. F. Knott, "Short and Long Fatigue Crack Growth in a SiC Reinforced Aluminium Alloy", *Fatigue & Fracture of Engineering Materials & Structure*, Vol. 13, (1990), 511-524.

141. D. L. Davidson, "Fatigue and Fracture Toughness of Aluminium Alloys Reinforced with SiC and Alumina Particles", *Composites*, Vol. 24, (1993), 248-255.

142. M. Y. Quek, "Analysis of Residual Stresses in a Single Fibre-Matrix Composite", *International Journal of Adhesion and Adhesives*, Vol. 24, (2004), 379-388.

143. A. Ureina, P. Rodrigo, L. Gil, M. D. Escalera and J. L. Baldonedo, "Interfacial Reactions in an Al-Cu-Mg (2009)/SiC_w Composite during Liquid Processing. Part I Casting", *Journal of Materials Science*, Vol. 36, (2001), 419-428.

144. K. N. Braszczynska, L. Litynska, A. Zyska and W. Baliga, "TEM Analysis of the Interfaces between the Components in Magnesium Matrix Composites Reinforced with SiC Particles", *Materials Chemistry and Physics*, Vol. 81, (2003), 326-328.

145. K. S. Chan, T. S. Lui and L. H. Chen, "Temperature Dependence of the Tensile Behaviour of Cast and Extruded Al-7Si-0.3Mg Alloys in 213-673K", *Materials Transactions, JIM*, Vol. 36, (1995), 743-748.

146. R. C. Dorward, "Preaging Effects in Al-Mg-Si Alloys Containing 0.6 to 0.9 PCT Mg_2Si", *Metallurgical Transactions*, Vol. 4, (1973), 507-512.

147. J. L. Murray, "Phase Diagrams of Binary Titanium Alloys", J. L. Murray (ed.), ASM International, Metals Park, Ohio, (1987).

148. S. T. Knight, P. J. Evans and M. Samandi, "Titanium Aluminide Formation in Ti Implanted Aluminium Alloy", *Nuclear Instruments and Methods in Physics Research B*, Vol. 119, (1996), 501-504.

149. J. H. Perepezko, Phase Reactions and Processing in the Ti-Al Based Intermetallics, *ISIJ International*, Vol. 31(10), (1991), 1080-1087.

150. D. Eliezer, F. H. Froes and C. Suryanarayana, “Effects of Hydrogen on Titanium Alumindes”, *JOM*, Vol. 43, (1991), 59-62.

151. Y. Birol and F. Sertcelik, “Intermetallic Particles in a Strip-Cast Al-Fe-Mn-Si alloy”, *Materials Research and Advanced Techniques*, Vol. 90, (1999), 329-334.

152. P, Le Brun, L. Froyen and L. Delaey, “Double Mechanical Alloying of Al-5wt.%Fe-4wt.%Mn”, *Materials Science and Engineering A*, Vol. A157, (1992), 79-88.

153. Y. J. Li and L. Arnberg, “A Eutectoid Phase Transformation for the Primary Intermetallic Particle from Al_m(Fe,Mn) to Al_3(Fe,Mn) in AA5182 alloy”, *Acta Materialia*, Vol. 52, (2004), 2945-2952.

154. A. K. Gupta, P. H. Marios and D. J. Lloyd, “Study of the Precipitation Kinetics in a 6000 Series Automotive Sheet Material”, *Materials Science Forum*, Vols 217-222, (1996), 801-808.

155. Y. Ohmori, L. C. Doan and K. Nakai, “Morphology and Crystallography of β-Mg_2Si Precipitation in Al-Mg-Si Alloys”, *Materials Transactions*, Vol. 42, (2001), 2576-2583.

APPENDIX

A ALUMINIUM ALLOY DESIGNATION

A1 Cast Aluminium Alloy Designation System

A system of four-digit numerical designations is used for this type of alloys. The first digit indicate the principal alloying constituent(s), the second two digits identify the specific alloy designation. The last digit, which is separated from the others by a decimal point, indicates the product form, i.e., .casting (0) or ingot (1, 2). A modification of the original alloy is indicated by a serial letter A, B or C before the numerical designation.

Table A1. Cast aluminium alloy designation system

Designation	Principal Alloying Element
1xx.x	Aluminium (99.00% or and greater)
2xx.x	Copper
3xx.x	Silicon, with added copper and/or magnesium
4xx.x	Silicon
5xx.x	Magnesium
7xx.x	Zinc
8xx.x	Tin
9xx.x	Other elements
6xx.x	Unused series

A2 Wrought Aluminium Alloy Designation System

Wrought aluminium alloys also have a different way of designation. A system of four-digit numerical designations is used to identify them. The first digit indicates the principal alloying constituent(s). The second digit indicates the variations in the original

alloy or impurity limits. The last two digits indicate the individual alloy variations (number has no significance but is unique).

Table A2. Wrought aluminium alloy designation system

Designation	Principal Alloying Element
1xxx	Aluminium (99.00% or and greater)
2xxx	Copper
3xxx	Manganese
4xxx	Silicon
5xxx	Magnesium
6xxx	Magnesium and silicon
7xxx	Zinc
8xxx	Other elements
9xxx	Unused series

B CHEMICAL COMPOSITION OF MINOR ELEMENTS IN TEST MATERIALS

Table B. Chemical composition (in ppm) of minor elements in test materials using ICP/MS.

Element	A535	A535 hybrid	A535+10	A535+15
Ag	0.02	0.03	0.01	0.10
As	24.44	34.71	48.22	81.49
Ba	0.11	109.39	73.39	136.55
Ca	167.62	1548.85	1203.06	1941.51
Cd	0.87	1.54	1.39	0.86
Ce	0.28	4.10	9.86	18.59
Co	1.87	1.51	4.12	5.99
Cs	0.01	0.21	0.80	1.54
Dy	0.02	0.23	0.52	0.94
Er	0.01	0.14	0.28	0.48
Eu	-	0.07	0.20	0.37
Ga	223.66	131.21	136.48	146.33
Gd	-	0.29	0.75	1.49
Ho	-	0.05	0.12	0.19
La	0.30	1.93	4.38	7.38
Li	7.07	2.18	13.78	21.64
Mo	0.47	2.06	7.09	8.97
Nd	0.11	1.67	4.11	7.31
Ni	23.93	38.88	99.63	42.24
P	62.88	109.63	161.60	240.70
Pb	8.38	9.73	34.29	54.03
Pr	0.05	0.44	1.09	2.05
Rb	0.01	2.38	9.77	18.42
Sc	0.38	1.09	2.10	3.08
Sm	0.01	0.25	0.72	1.55
Sn	5.45	43.73	42.58	5.37
Sr	0.12	32.21	32.58	54.92
Ta	-	-	0.18	0.30
Th	0.03	0.71	1.13	1.63
Tl	0.43	0.50	1.03	1.48
Tm	-	0.02	0.06	0.07
U	0.69	0.94	1.12	1.48
V	64.46	178.73	164.84	177.09
W	-	-	0.19	0.82
Y	0.08	1.59	3.16	4.48
Yb	-	0.17	0.30	0.44
Zn	164.71	44.07	82.56	114.51
Zr	3.24	19.55	23.63	24.17

C TENSILE ANALYSES

The tensile versus strain curves for as-cast and solution heat treated test materials obtained from room temperature tensile testing are shown in Figures C.1 and C.2 respectively. Figures C.3 to C.6 also show tensile versus strain curves for the test materials at temperatures of 150 °C, 200 °C, 250 °C and 300 °C respectively. The tensile strength and 0.2% offset yield strength were calculated from these stress versus strain curves.

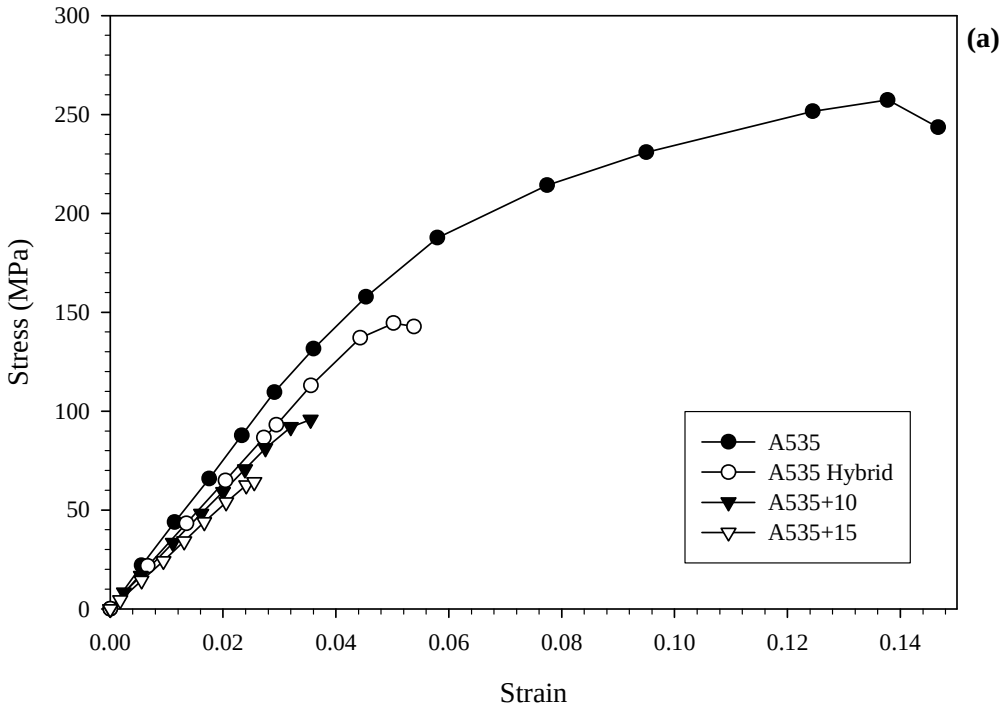

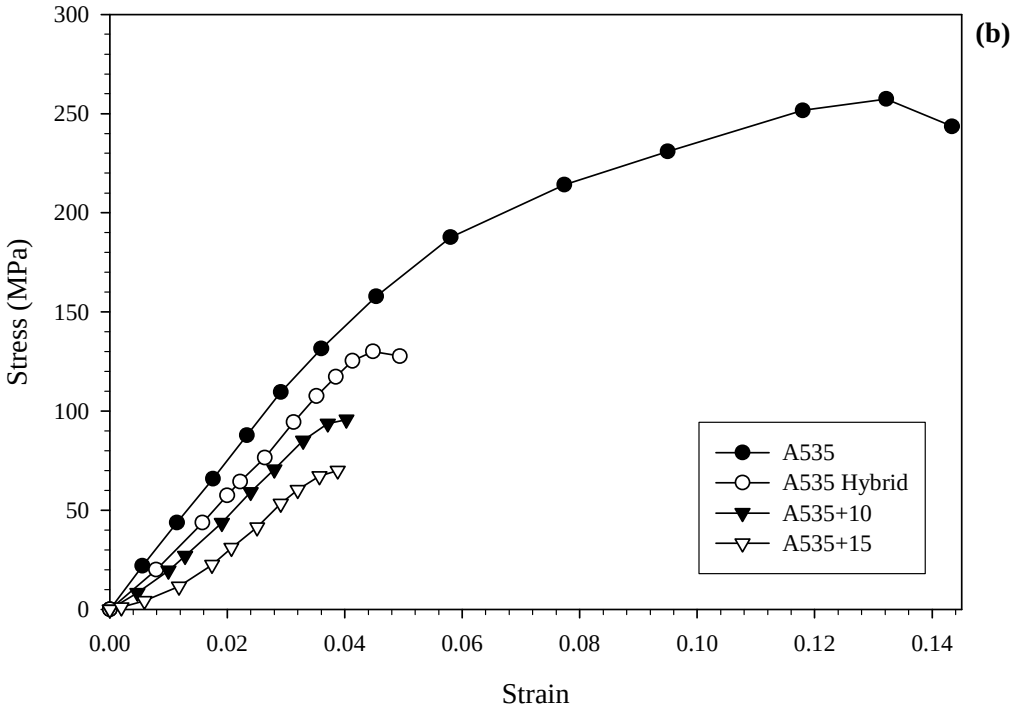

Figure C.1. (a) and (b) Room temperature stress versus strain curves obtained for solution heat treated samples.

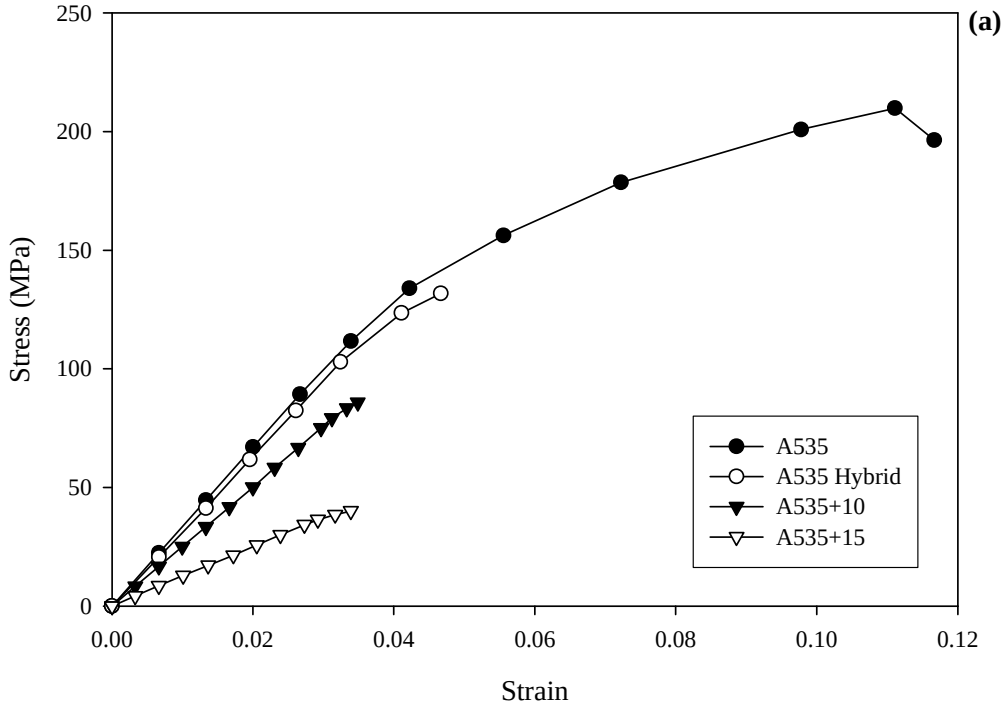

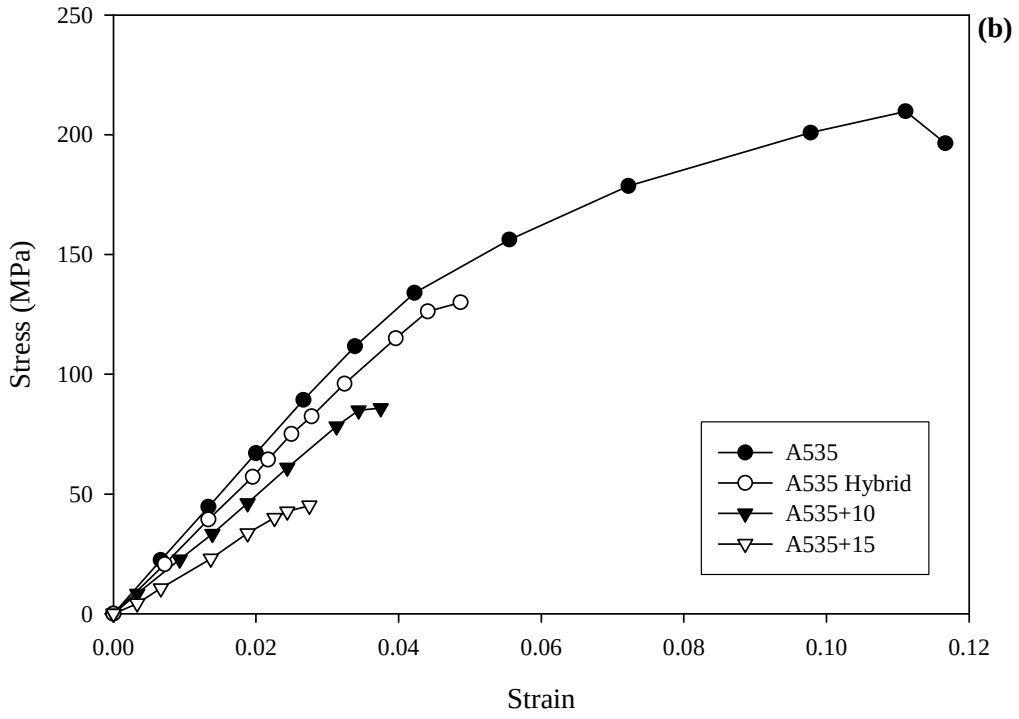

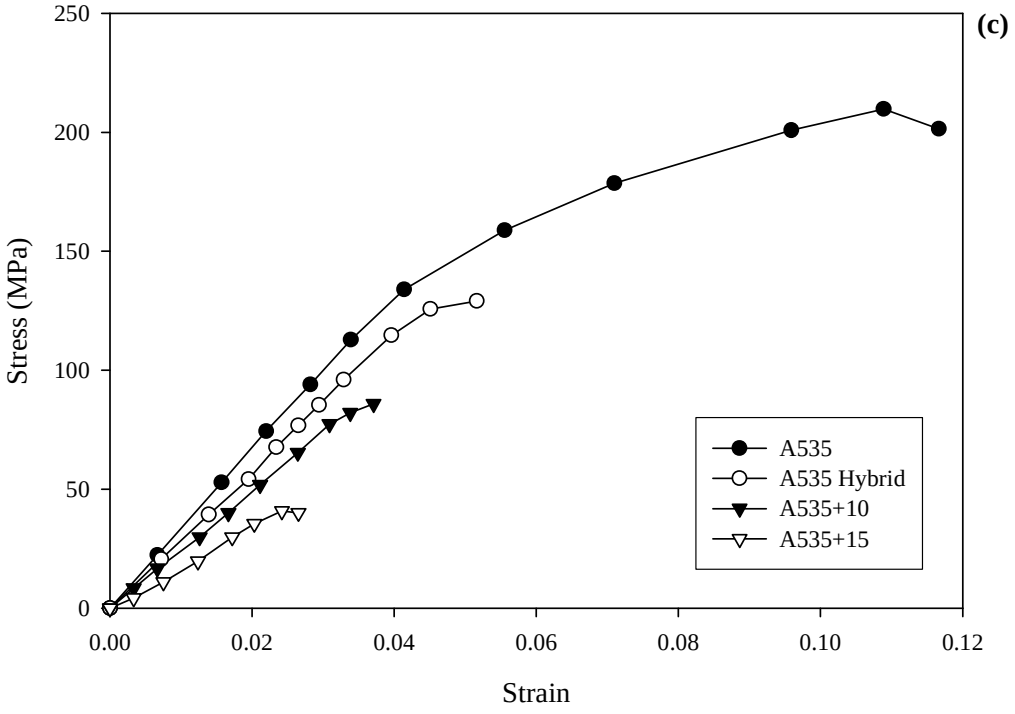

Figure C.2. (a) – (c) Room temperature stress versus strain curves obtained for as-cast samples.

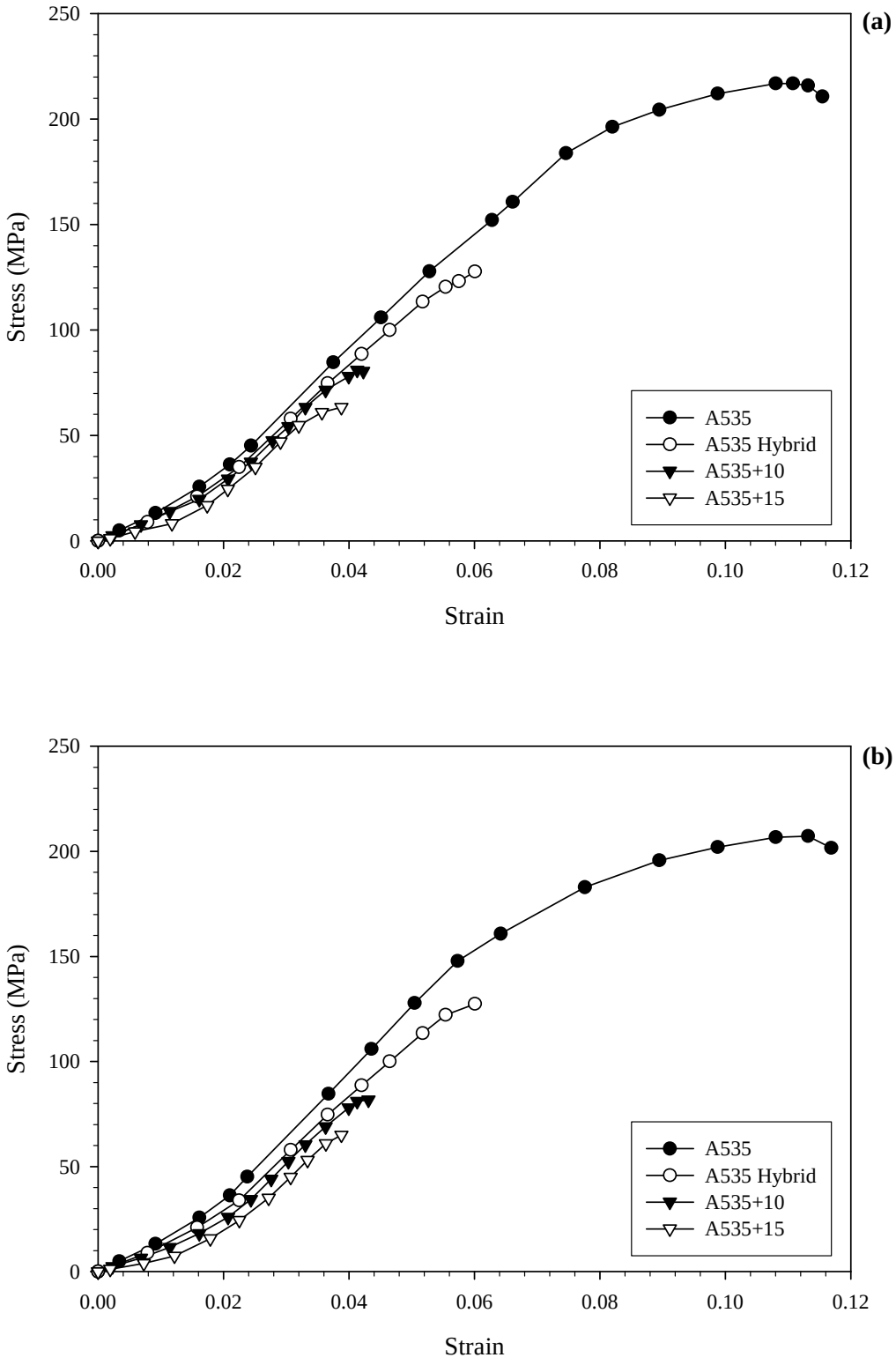

Figure C.3. (a) and (b) Stress versus strain curves obtained for test materials at 150 °C.

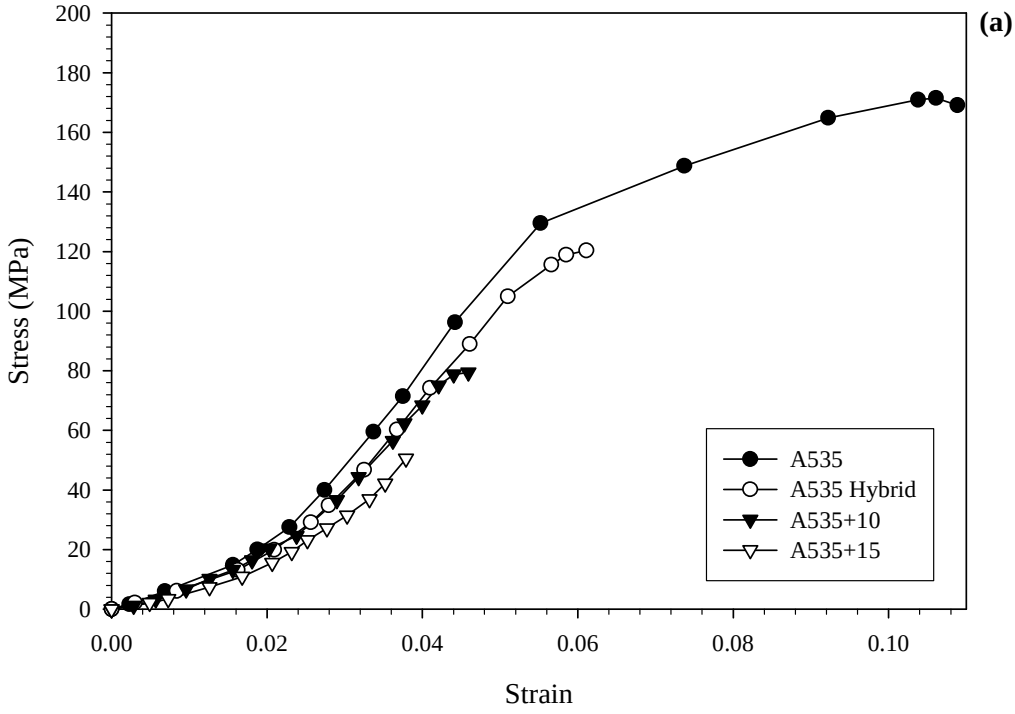
(a)
Stress (MPa)
Strain
A535
A535 Hybrid
A535+10
A535+15

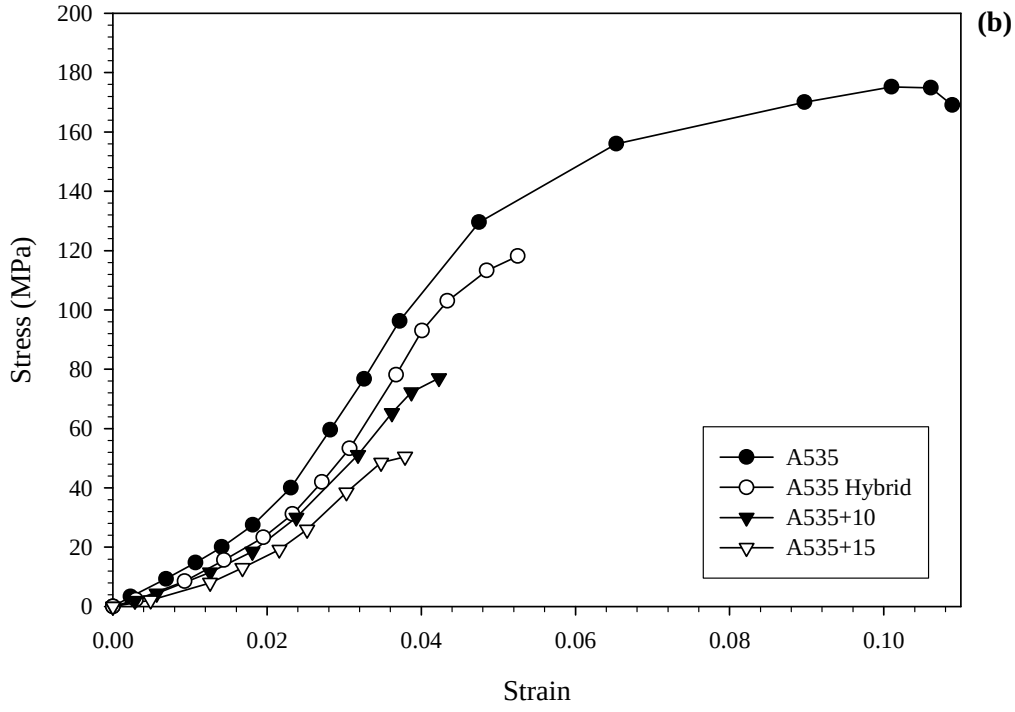
(b)
Stress (MPa)
Strain
A535
A535 Hybrid
A535+10
A535+15

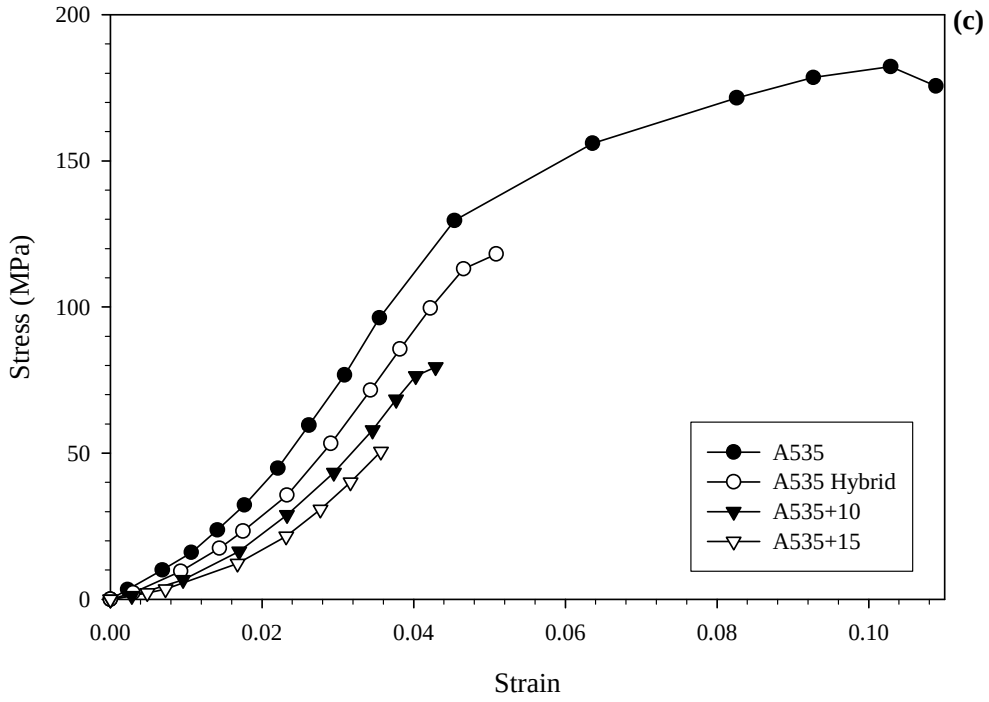

Figure C.4. (a) – (c) Stress versus strain curves obtained for test materials at 200 °C.

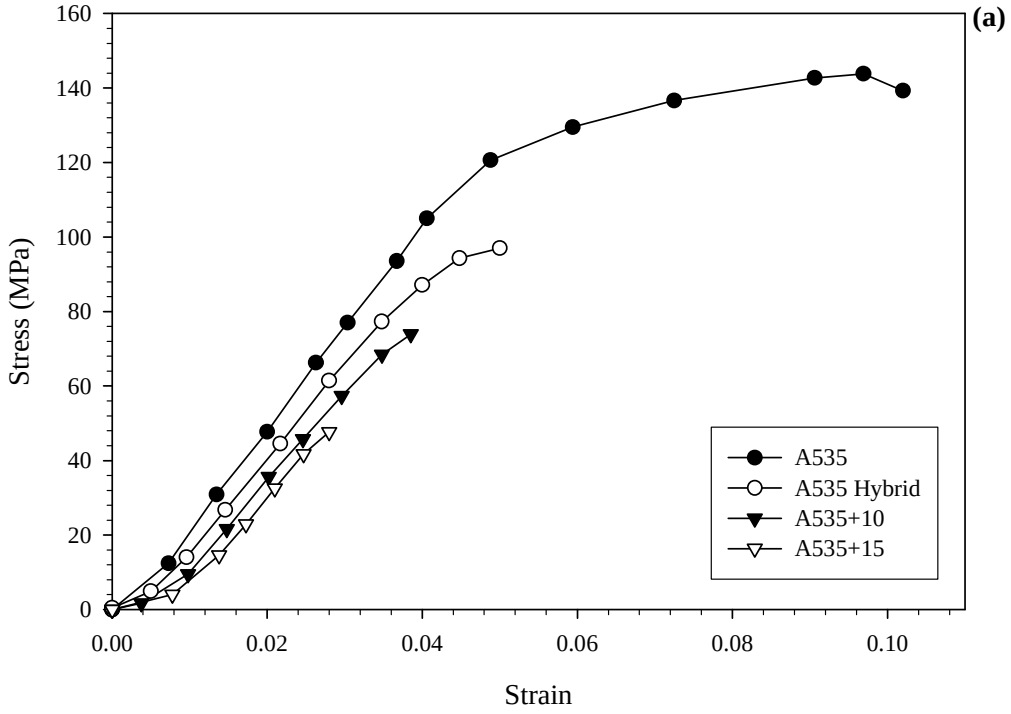

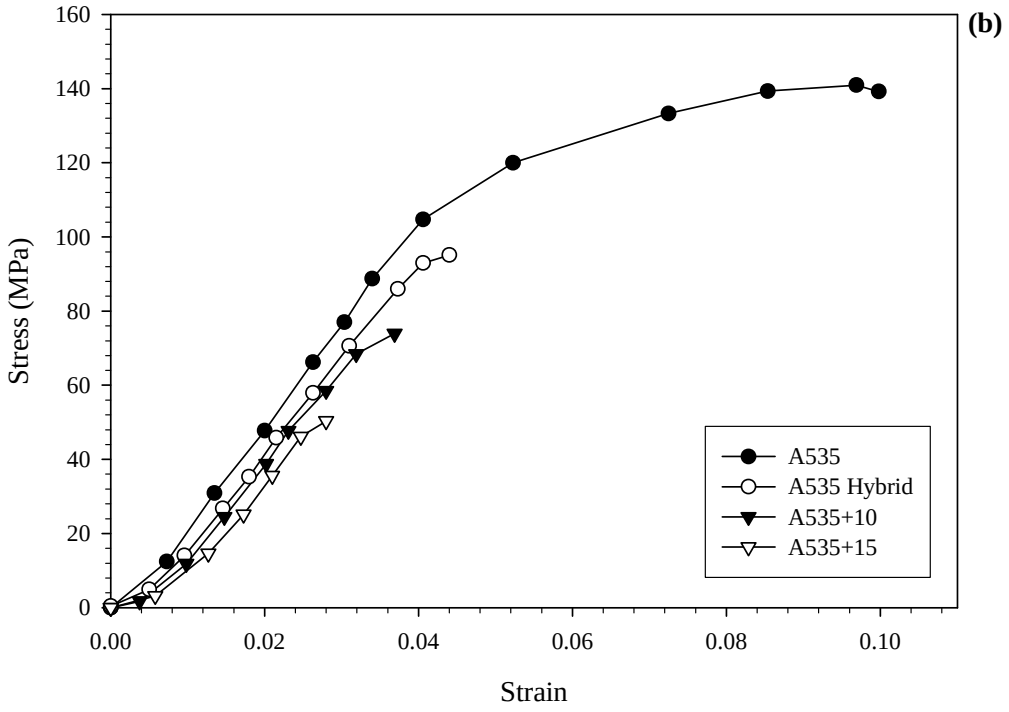

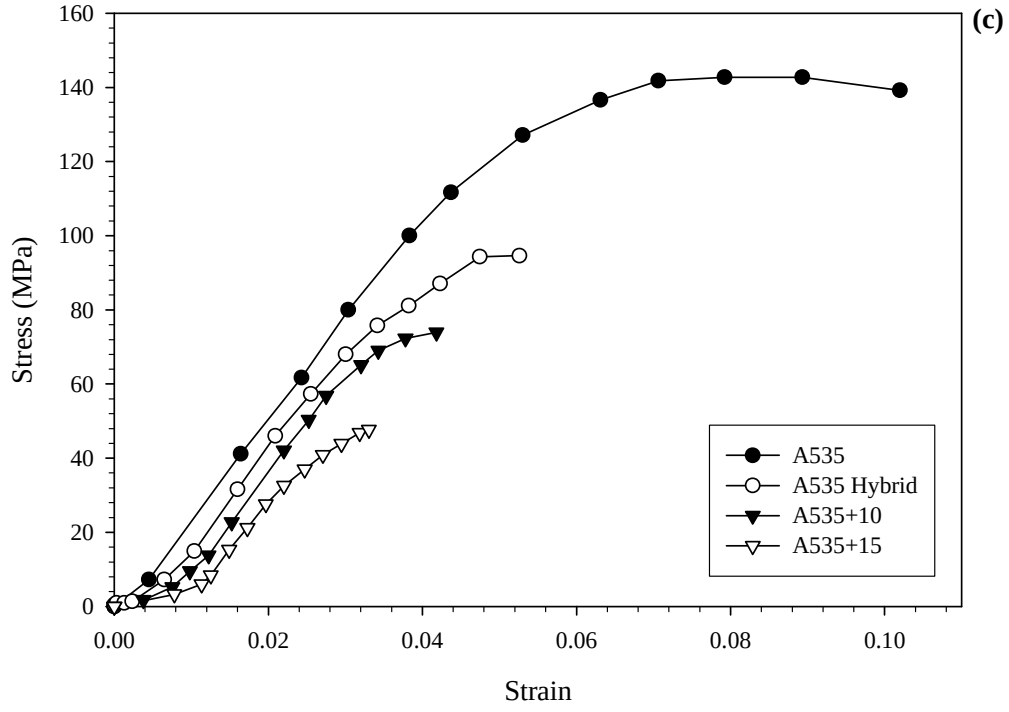

Figure C.5. (a) – (c) Stress versus strain curves obtained for test materials at 250 °C.

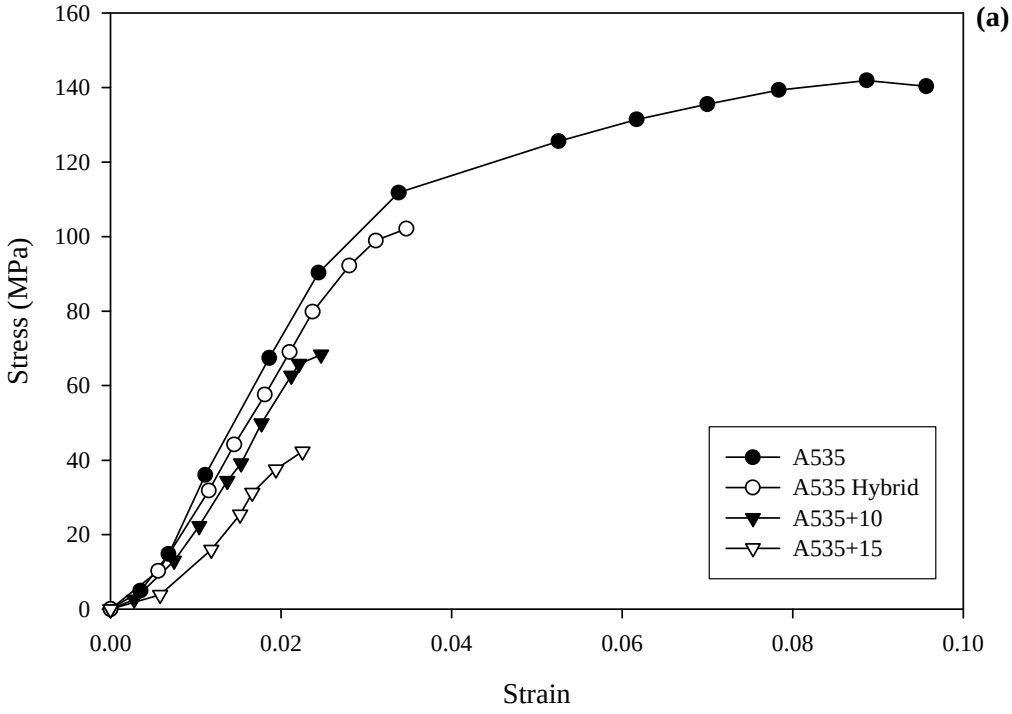
(a)
Stress (MPa)
Strain
A535
A535 Hybrid
A535+10
A535+15

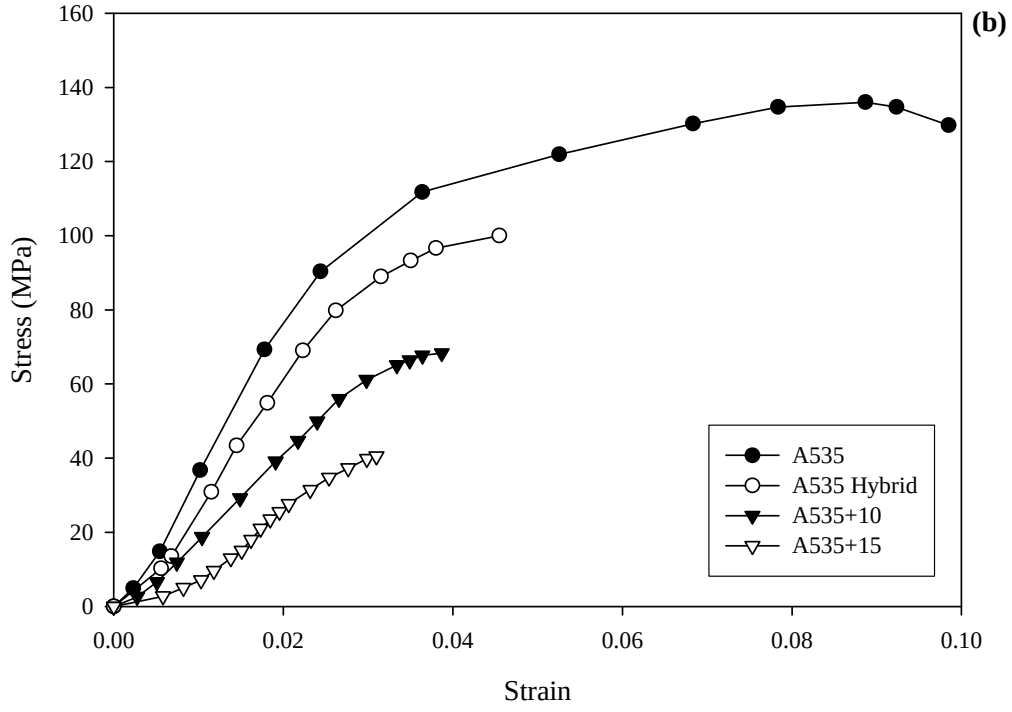
(b)
Stress (MPa)
Strain
A535
A535 Hybrid
A535+10
A535+15

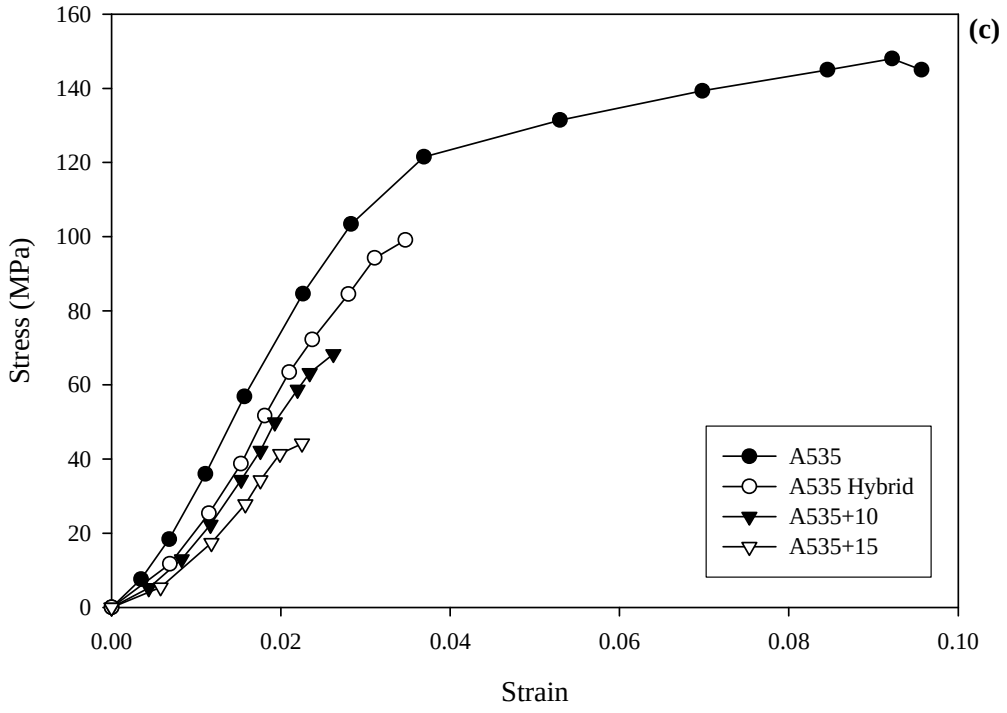

Figure C.6. (a) – (c) Stress versus strain curves obtained for test materials at 300 °C.